MEMBRANE ANCHORS FOR THE BACTERIAL TUBULIN FTSZ REGULATE CELL SHAPE DURING *CAULOBACTER CRESCENTUS* CELL DIVISION

By
Elizabeth L. Meier

A dissertation submitted to Johns Hopkins University in conformity with the requirements for the degree of Doctor of Philosophy

Baltimore, Maryland
June, 2017

ABSTRACT

Bacterial cell shape is genetically hardwired and critical for fitness as well as, in certain cases, pathogenesis. In most bacteria, a semi-rigid structure called the cell wall surrounds the inner membrane, offering protection against cell lysis while simultaneously maintaining cell shape. A highly dynamic macromolecular structure, the cell wall undergoes extensive remodeling as bacterial cells grow and divide. In the majority of bacteria, the tubulin-like GTPase FtsZ is essential for division and forms an annulus at midcell (the Z-ring) which recruits the division machinery and regulates cell wall remodeling. Although both activities require membrane attachment of FtsZ, few membrane anchors have been characterized. In the model α-proteobacterium *Caulobacter crescentus*, the division proteins FzlC and FtsEX arrive at midcell shortly after FtsZ and likely function as early FtsZ membrane anchors. As membrane attachment is important for FtsZ form and function, we sought to characterize the activities of FzlC and FtsEX toward FtsZ during cytokinesis. We demonstrate that FzlC associates with membranes directly *in vivo* and *in vitro* and recruits FtsZ to membranes *in vitro*. *In vivo*, overproduction of FzlC results in cytokinesis defects whereas deletion of *fzlC* causes synthetic defects with cell wall hydrolysis factors. Our characterization of FzlC as a novel membrane anchor for FtsZ expands our understanding of FtsZ regulators and establishes a role for membrane-anchored FtsZ in the control of cell wall hydrolysis.

We also investigated the membrane anchoring function of the broadly conserved complex, FtsEX, and demonstrate that in *C. crescentus* FtsEX relays signals from the cytoplasm to the cell wall to regulate key developmental shape changes. Consistent with

studies in diverse bacteria, we observe strong synthetic interactions between *ftsE* and cell wall hydrolytic factors, suggesting that regulation of cell wall remodeling is a conserved function of FtsEX. Intriguingly, without FtsE, cells frequently fail to separate and instead elaborate a thin, tubular structure between cell bodies, a growth mode observed in other α-proteobacteria. Overall, our results highlight the plasticity of bacterial cell shape and demonstrate how altering the activity of one morphogenetic program can produce diverse morphologies resembling those of other bacteria in nature.

Thesis Committee:

Professor Erin Goley, Advisor

Professor Jie Xiao, Chair

Professor Kumaran Ramamurthi, Reader

Professor Douglas Robinson

Professor Pierre Coloumbe

ACKNOWLEDGEMENTS

I have been extremely fortunate in my Ph.D. My decision to join Erin Goley's lab was of so much more importance than I could have possibly realized at the time. Erin was, and still is, kind, intelligent, supportive, and generous with her time and energy. She has taught me how to approach scientific questions critically, design experiments with foresight, and take pride in and ownership of my work. Her criticisms were always constructive and she frequently reminded me to bring enthusiasm to my research presentations because 'if you're not excited about your work, why would anyone else be?' Erin, thank you for accepting me as your first graduate student; it has been a pleasure to grow with the lab. Thank you also to my thesis committee for crucial support and guidance while navigating my PhD, which sometimes felt like very foreign territory.

For the past five years, I have been exceptionally grateful to not only have had an amazing mentor, but also the best colleagues: Kousik, Selam, PJ, Chris, Allison, Anant, and many other rotation, summer, and undergraduate students. DapK, you were my first successful recruit to the lab and I am so thankful that I peer pressured you endlessly. My hard work paid off. Swarmzzz, I am so lucky that I found the High Queen to my Trap Queen. I can't imagine what my life in Baltimore, and beyond, would be like if I hadn't met you. To all of my friends and classmates I met during my first year, thank you for making my time in Baltimore so memorable and worthwhile. A particular shoutout to Chris and Brian for putting up with me as their roommate for so many years. To my Baltimore wife, Adri, I'm so glad we exchanged rings on my rooftop. What better way to celebrate America's and our own independence? You have been a great friend and

support system and I am so thankful to have met you. Mallika, mi brujita, I am so sad that you decided to move to Baltimore just when I was wrapping up my PhD, but at least we overlapped for one year! I loved visiting you in D.C. and will continue to visit you regardless of location. You are my sister. Fran, I'm so glad you fell down my stairs and emailed me your number. I am so lucky to have spent the past two and a half years with you and want to thank you for always countering my pessimism with your dogged optimism. You have been incredibly supportive and have both pushed me and given me space to grow. Mil gracias franito. To my dad and brother, although we've been on opposite coasts I've still felt both of your love and support. My biannual trips to the West Coast were always a much-needed reprieve from my PhD and I can't wait to be living in the same time zone again. Finally, I want to thank both of my grandmas and my Virginia family. I love you all very much. A special thanks to Oma and my parents for sacrificing so much to help me succeed.

TABLE OF CONTENTS

LIST OF TABLES

LIST OF FIGURES

CHAPTER 1

GENERAL INTRODUCTION

Note: The majority of the information presented in this chapter was included in the publication:

Meier EL and Goley ED. Form and function of the bacterial cytokinetic ring. Curr Opin Cell Biol. 2014;26:19-27.

Bacterial cytokinesis is orchestrated by the divisome: a multiprotein complex composed of both essential and nonessential proteins. Foremost among the essential proteins is FtsZ, a conserved tubulin homolog that polymerizes into a ring-like structure (the Z-ring) at the incipient division site. The Z-ring acts as a scaffold for the recruitment of downstream division proteins which collectively coordinate peptidoglycan (PG) cell wall synthesis, membrane fission, and cell separation with other cell cycle events (Adams and Errington, 2009; Egan and Vollmer, 2013). The Z-ring has also long been hypothesized to generate constrictive force to direct envelope invagination during cytokinesis (Erickson *et al*., 2010).

Despite two decades of study, questions abound regarding the mechanisms of FtsZ function: What is the structure of the Z-ring *in vivo*? Does FtsZ generate constrictive force and, if so, how? How is assembly and constriction of the Z-ring coordinated with remodeling of PG? Here, we discuss recent work addressing these questions, with a focus on how new imaging technologies and biomimetic systems are driving the field forward.

Imaging the Z-ring in cells

Purified FtsZ assembles into linear protofilaments *in vitro* (Fig. 1.1A), but can form a variety of higher-ordered polymer species depending on the experimental conditions (Erickson *et al*., 2010). Although self-assembly of FtsZ is primarily mediated by the GTPase domain (Fig. 1.1B-C), the extreme C-terminus contributes to species-specific differences in FtsZ bundling (Buske and Levin, 2012) and the intrinsically disordered

variable linker between the GTPase domain and C-terminal tail is required for efficient polymerization (Buske and Levin, 2013; Gardner *et al*., 2013). In addition to intrinsic self-assembly of FtsZ, a growing list of binding partners organizes FtsZ polymers into diverse filament superstructures *in vitro* (Hale *et al*., 2000; Gueiros-Filho *et al*., 2002; Dajkovic *et al*., 2010; Goley *et al*., 2010b; Durand-Heredia *et al*., 2011; Gündoğdu *et al*., 2011; Hale *et al*., 2011; Durand-Heredia *et al*., 2012). A major obstacle to building testable models for mechanisms of Z-ring function and regulation *in vivo*, however, has been an inability to assign physiological relevance to the varied FtsZ polymer structures observed *in vitro*.

Conventional fluorescence microscopy depicts the Z-ring as a closed ring and does not permit visualization of individual protofilaments. In the first successful application of high resolution imaging to visualize FtsZ *in vivo*, Li *et al*. employed electron cryo-tomography (ECT) to image *Caulobacter crescentus* cells and observed a loosely scattered midcell band of FtsZ protofilaments, each 40-120 nm long and 16 nm from the inner membrane (IM) (Fig. 1.1D) (Li *et al*., 2007). Most of the arc-like filaments were gently curved, however straight filaments were also seen, perhaps reflecting FtsZ in different nucleotide-bound states as reported *in vitro* (Lu *et al*., 2000). ECT reconstructions also revealed FtsZ filaments that had clear connections with the IM, likely via association with other divisome proteins (Li *et al*., 2007).

Although ECT provides superior resolution, it is incompatible with specific labeling techniques and requires that cells be cryopreserved for imaging. ECT is also limited by

sample thickness, excluding high-resolution analysis of larger bacterial cells such as *Escherichia coli and Bacillus subtilis*. The use of super-resolution light microscopy allows for more complete visualization of fluorescently labeled FtsZ in live cells, albeit at lower resolution than ECT. In *E. coli*, photoactivated localization microscopy (PALM) of FtsZ-mEos2 revealed Z-rings ~100 nm wide, with packing densities of FtsZ molecules often greater than those predicted for a single layer of protofilaments (Fig. 1.1E) (Fu *et al*., 2010). Interestingly, increasing the concentration of FtsZ-mEos2 in the cell did not increase the width of the Z-ring, but rather increased the filament density, suggesting loose filament clustering with room to accommodate additional filaments in a ring of defined width (Fu *et al*., 2010). 3D-structured illumination microscopy (SIM) of FtsZ-GFP in *B. subtilis* and *Staphylococcus aureus* showed dynamic Z-rings composed of a heterogeneous distribution of FtsZ in a striking, bead-like arrangement, rather than a continuous ring (Fig. 1.1F) (Strauss *et al*., 2012). 3D super-resolution microscopy was also used to observe FtsZ-Dendra2 in *C. crescentus* cells at different cell cycle stages: Z-rings were dynamic over the cell cycle, adopting open conformations during the stalked stage and condensing into dense foci in pre-divisional cells (Fig. 1.1G) (Biteen *et al*., 2012).

Collectively, high-resolution images of FtsZ in four different organisms depict the Z-ring as a heterogeneous assembly of short (~100 nm) protofilaments underlying the IM at midcell, roughly perpendicular to the long axis of the cell. These clustered FtsZ polymers may make loose lateral contacts within a single layer or overlap to form loose bundles with a radial thickness (Fig. 1.1H). PALM imaging in *E. coli* and 3D super-

resolution data from *C. crescentus* favor a multi-layered Z-ring in the radial direction (Fu *et al*., 2010; Biteen *et al*., 2012), while ECT observations depict a single layer of protofilaments (Li *et al*., 2007). Additional technical advances, including continued improvement in the resolution achievable by light microscopy and methods for specific labeling of proteins for ECT, are necessary to clarify this model.

Advanced imaging technologies will also be central to determining the effects of FtsZ-binding proteins on Z-ring organization *in vivo*. Notably, no tight protofilament bundles such as those mediated by the Zaps, FzlA, SepF, or ZipA *in vitro* (Hale *et al*., 2000; Gueiros-Filho *et al*., 2002; Dajkovic *et al*., 2010; Goley *et al*., 2010b; Durand-Heredia *et al*., 2011; Gündoğdu *et al*., 2011; Hale *et al*., 2011; Durand-Heredia *et al*., 2012) have yet been observed in wild-type cells *in vivo*, nor have the actin-like FtsA filaments that are proposed to anchor FtsZ to the membrane (Szwedziak *et al*., 2012). In exciting initial work along these lines, Buss *et al.* applied PALM imaging to FtsZ in cells lacking the bundling protein, ZapA, or its binding partner, ZapB (Gueiros-Filho *et al*., 2002; Ebersbach *et al*., 2008). Surprisingly, multi-filament clusters still form in the absence of these factors, indicating that bundling and/or cross-linking of FtsZ polymers persists (Buss *et al*., 2013). Perhaps this should be unsurprising, given the growing list of non-essential and presumably redundant bundling factors described in *E. coli* (Gueiros-Filho *et al*., 2002; Durand-Heredia *et al*., 2011; Hale *et al*., 2011; Durand-Heredia *et al*., 2012).

Figure 1.1 The Z-ring is composed of dynamic clusters of short, overlapping protofilaments. (A) Transmission electron micrograph of polymers of purified *C. crescentus* FtsZ in the presence of GTP stained with uranyl acetate. Bar = 100 nm. (B) Domain organization of FtsZ. An N-terminal peptide of unknown function precedes the conserved GTPase domain. An intrinsically disordered variable linker (~25-400 residues, depending on the organism) separates the GTPase domain from the C-terminal peptide that binds membrane-tethering proteins like FtsA. (C) Molecular structure of FtsZ from *Pseudomonas aeruginosa* (PDB: 2VAW) colored from blue (N-terminus) to red (C-terminus). The variable linker and C-terminal peptide are not visible in the structure, but the C-terminus is facing away from the reader and into the page in this image. (D) Electron cryo-tomography (ECT) of a *Caulobacter crescentus* cell early in the constriction process (Li *et al*., 2007). (i) Low magnification cryo-electron micrograph (bar, 500 nm). (ii-iv) 3D segmentations of the division site from the cell in (i) viewed from different angles (pseudo-coloring: yellow-outer membrane, blue-inner membrane, red-FtsZ filaments). (v) Fluorescence and phase micrograph of FtsZ-YFP in a cell at an apparently analogous cell cycle stage to the images in i-iv. (E) (i) Brightfield, (ii) ensemble fluorescence and (iii) photoactivated light microscopy images of live *Escherichia coli* expressing FtsZ-mEos2 depict a ring of variable density, ~100 nm wide (Fu *et al*., 2010). Bar = 500 nm. (F) 3D-structured illumination microscopy images of FtsZ-GFP in *Bacillus subtilis* as viewed from the "top" of the cell (left) and through the cell down its long axis (right) illustrate the discontinuous nature of the Z-ring (arrowhead, gap in fluorescence intensity) (Strauss *et al*., 2012). (G) 2D projections of 3D super-resolution images of FtsZ-Dendra2 in *C. crescentus* as viewed from the "top" of the cell

(left) and through the cell down its long axis (right) show a ring 70-100 nm wide, extending radially into the cytoplasm (Biteen *et al*., 2012). Bar = 200 nm. (H) Model for organization of protofilaments in the Z-ring. Short (~100 nm long) protofilaments (red) are organized through loose lateral interactions into clusters ~100 nm wide that align at midcell with gaps between them (left). ECT suggests that the Z ring comprises a single layer of protofilaments (middle), whereas fluorescence super-resolution microscopy suggests a ring several filaments deep in the radial direction (right). Images in (D-G) are reproduced from (Li *et al*., 2007; Fu *et al*., 2010; Strauss *et al*., 2012; Biteen *et al*., 2012) with permissions when required.

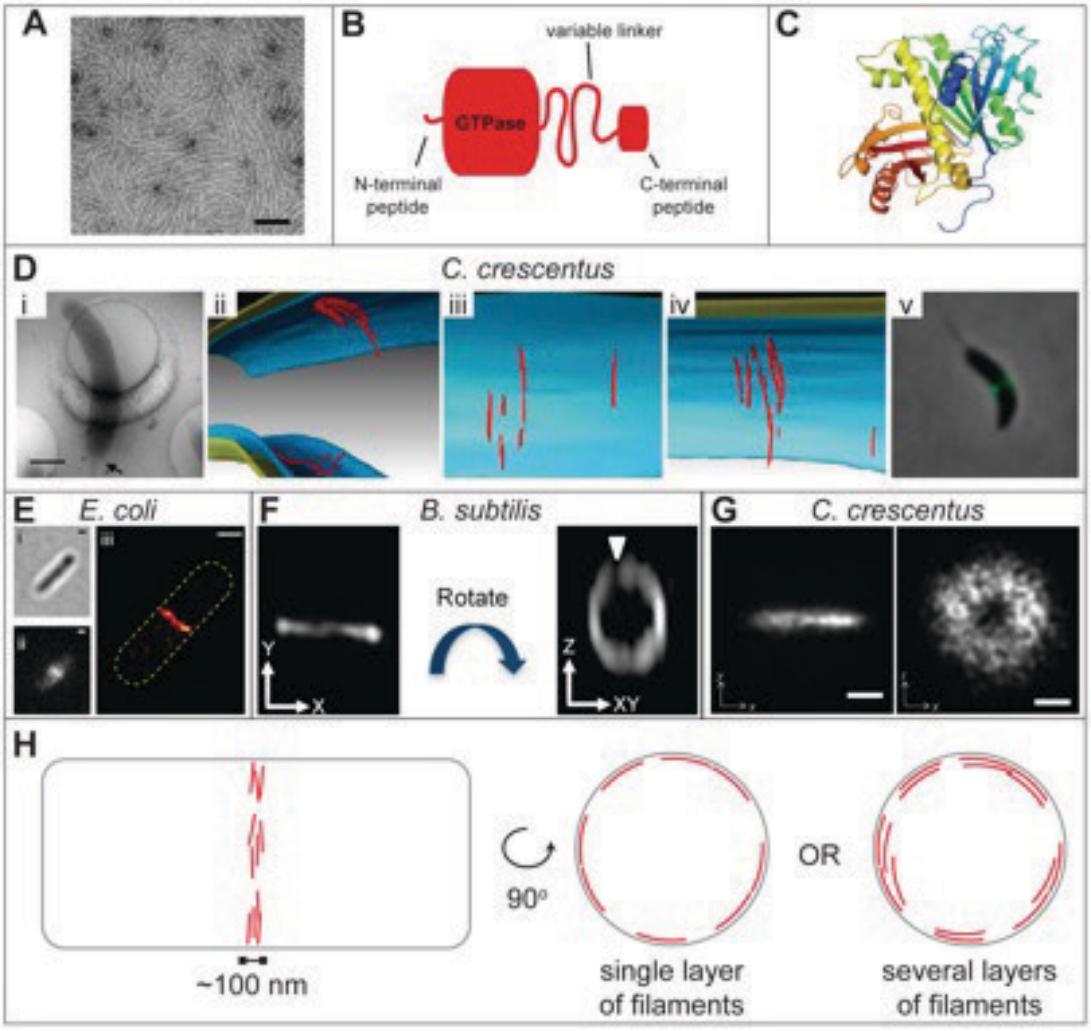

However, protofilament clusters do not align efficiently into a midcell ring without ZapA or ZapB, suggesting that this may be their primary function in promoting efficient cytokinesis (Buss *et al*., 2013) and one that cannot be fulfilled by other Zaps. This finding is consistent with the model proposed by Galli and Gerdes wherein a ZapB-ring underlies and stabilizes the Z-ring via interaction of each with ZapA (Galli and Gerdes, 2010). Importantly, the fact that ZapA, a protein routinely described as a bundling factor, is dispensable for clustering of FtsZ filaments *in vivo* highlights the necessity of correlating *in vitro* studies with *in vivo* structures and phenotypes to assign physiological relevance to FtsZ regulators.

From the work described above (Li *et al*., 2007; Strauss *et al*., 2012; Buss *et al*., 2013), it is clear that Z-rings comprise a heterogeneous arrangement of protofilament clusters rather than a continuous ring. This bears a striking resemblance to the recent discovery that the actin homolog, MreB, assembles into dynamic patches that move circumferentially, rather than into a large, continuous helix (Domínguez-Escobar *et al*., 2011; Gardner *et al*., 2011; van Teeffelen *et al*., 2011; Reimold *et al*., 2013). Like MreB, a variety of helical and other non-ring FtsZ structures have been reported (Ma *et al*., 1996; Sun and Margolin, 1998; Ben-Yehuda and Losick, 2002; Thanedar and Margolin, 2004; Thanbichler and Shapiro, 2006; Peters *et al*., 2007; Fu *et al*., 2010; Jennings *et al*., 2010; Reimold *et al*., 2013). Non-ring FtsZ localizations are not likely to constitute a continuous helix, but rather dynamic clusters of FtsZ filaments dispersed longitudinally (Jennings *et al*., 2010; Buss *et al*., 2013). The inherent twist of FtsZ filaments may contribute to the helical appearance of FtsZ structures *in vivo* (Arumugam *et al*., 2012;

Hsin *et al*., 2012; Li *et al*., 2013). Whether any aspects of non-ring FtsZ localization depend on its recently described interaction with MreB (Fenton *et al*., 2013) or whether, like MreB (Domínguez-Escobar *et al*., 2011; Gardner *et al*., 2011; van Teeffelen *et al*., 2011), the dynamics of FtsZ are directed by cell wall synthesis remain to be determined.

Z-ring formation in the test tube

Super-resolution technologies have provided initial glimpses of the *in vivo* structures adopted by FtsZ. However, the biochemical and biophysical complexity of live cells make *in vitro* reconstitutions with biomimetic membranes an important method for dissecting the regulation and function of membrane-bound FtsZ polymers (Fig. 1.2). In particular, reconstitution efforts have been central to asking if the Z-ring generates force and, if so, how it does so.

In a breakthrough study, Osawa *et al*. reconstituted Z-rings inside multilamellar liposomes (MLLs) using FtsZ with its C-terminal FtsA- and ZipA-binding peptide replaced with a membrane targeting sequence (MTS) (Osawa *et al*., 2008). When encapsulated in tubulated MLLs, FtsZ-YFP-MTS formed constricting Z-rings, demonstrating that membrane-associated FtsZ, alone, might generate force (Fig. 1.2a) (Osawa *et al*., 2008). Supporting this conclusion, FtsZ-YFP-MTS on the outside of liposomes induces concave depressions and membrane tubules (Fig. 1.2b) (Osawa *et al*., 2009; Arumugam *et al*., 2012). In a clever adaptation of their FtsZ-MTS system, the Erickson group implicated FtsZ filament curvature as driver of constriction by switching

the MTS to the N-terminus of FtsZ, which is on the opposite face of the molecule from the C-terminus: MTS-FtsZ-YFP induces convex bulges on the surface of spherical liposomes (Osawa *et al*., 2009; Arumugam *et al*., 2012) and forms "inside-out" Z-rings that squeeze tubulated MLLs from the outside (Fig. 1.2d-e) (Osawa and Erickson, 2011). These observations can be explained if filaments curve preferentially away from the C-terminal face of FtsZ, which is where native FtsZ is attached to the membrane, and force the membrane to follow along. Surprisingly, negative stain electron microscopy of inside-out Z-rings assembled on rigid lipid tubules unveiled filaments arranged in tightly packed ribbons (Milam *et al*., 2012), in sharp contrast to the beaded, loosely bundled Z-ring suggested from *in vivo* imaging. As Z-rings were "inside-out" and unable to constrict under the conditions used by Milam and coworkers, more work is needed to determine if they reflect a physiologically relevant structure.

Although artificial membrane targeting has proven incredibly fruitful, reconstitution using natural membrane anchors is ultimately necessary to understand the *in vivo* activity and regulation of FtsZ. The widely conserved actin homolog FtsA is thought of as the primary membrane tether during division (Pichoff and Luktenhaus, 2005). Progress in biochemical characterization of FtsA has been slow, as it is poorly behaved *in vitro* from most mesophilic organisms. Nevertheless, FtsAs from *B. subtilis* and *Thermotoga maritima* have been demonstrated to polymerize into actin-like filaments *in vitro* (Szwedziak *et al*., 2012; Singh *et al*., 2013) and *T. maritima* FtsA to recruit FtsZ to lipid vesicles (Szwedziak *et al*., 2012). In the most far-reaching work to date, Osawa and Erickson encapsulated *E. coli* FtsZ-YFP and a biochemically tractable hypermorph of

FtsA (FtsA-R286W, FtsA*) (Beuria *et al*., 2009; Pichoff *et al*., 2011) into unilamellar liposomes embedded in agarose (Fig. 1.2g). They observed partial constriction or complete fission of vesicles, although Z-rings formed at very low frequency (Osawa and Erickson, 2013). While both FtsZ-YFP-MTS and FtsZ-YFP:FtsA* formed Z-rings and generated a constriction force in this system, vesicle fission was only observed with FtsA* (Osawa and Erickson, 2013), implicating FtsA as an active player in membrane remodeling during division (Szwedziak *et al*., 2012; Osawa and Erickson, 2013).

This recent work with FtsA* must be reconciled with unexpected results from incorporation of *E. coli* FtsZ and wild-type FtsA into giant unilamellar inner membrane vesicles containing native *E. coli* inner membrane proteins (Fig. 1.2h). In that system, FtsA was dislodged from the membrane and preferentially associated with FtsZ polymers in the vesicle lumen (Jiménez *et al*., 2011). Important experimental differences exist between the work of Jiménez *et al.* and that of the Erickson group, including vesicle geometry, use of crowding agents, and presence or absence of other membrane proteins. Jimenez *et al.* also used wild-type FtsA that had been denatured and re-folded, as opposed to FtsA* purified in native form by Osawa and Erickson. It is relevant to bear in mind that FtsA* reportedly has reduced self-interaction as compared to wild-type (Pichoff *et al*., 2011). Clarifying which of these are the primary determinants of Z-ring formation and constriction is critical work for the future.

Figure 1.2. Biomimetic systems for studying FtsZ assembly and force generation on membranes *in vitro*. In all cases, *E. coli* proteins were used, except in Milam *et al*. (2012), where both *E. coli* MTS-FtsZ-YFP and *Mycobacterium tuberculosis* MTS-FtsZ-YFP were tested for assembly on lipid tubules. In graphical representations of outcomes, membranes are depicted in gray and FtsZ is depicted in red. FtsZΔC: FtsZ lacking its C-terminal FtsA-binding peptide; YFP: yellow fluorescent protein; MTS: membrane-targeting sequence (amphipathic α-helix from *E. coli* MinD); FtsA*: R286W hypermorph mutant of FtsA.

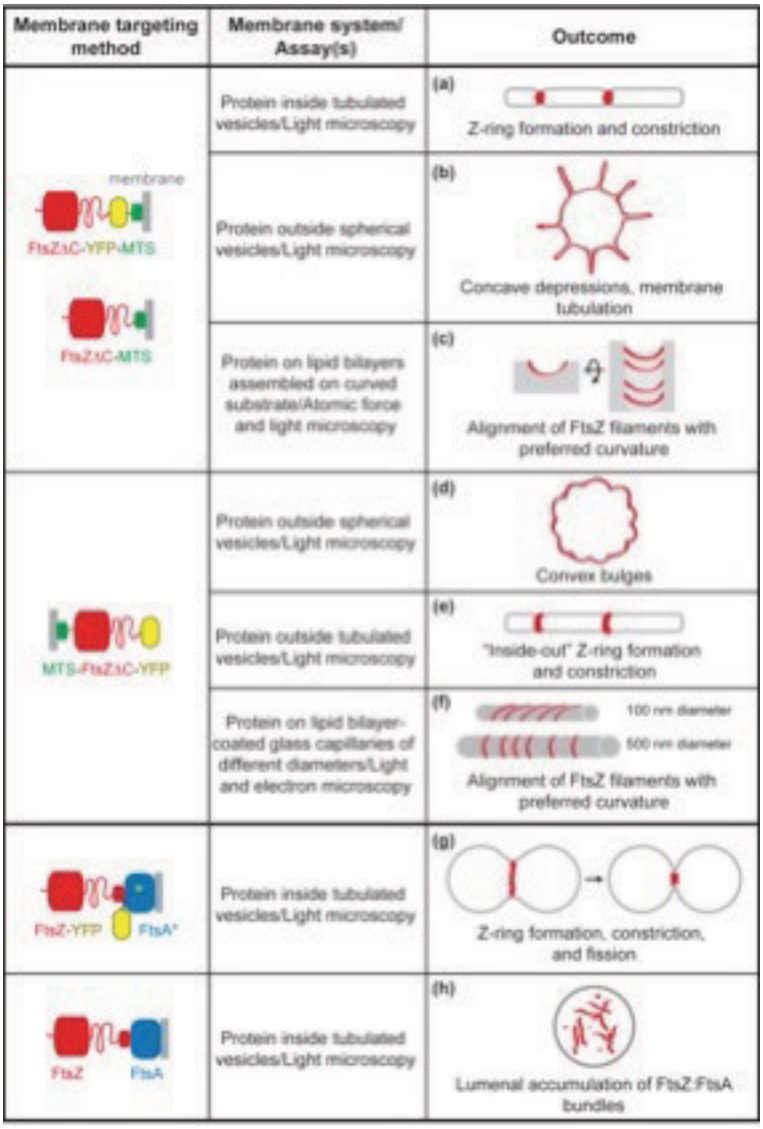

In vitro work with ZipA, a second membrane-tethering protein that is restricted to γ-proteobacteria (Hale and de Boer, 1997), serves as a useful point of comparison to work done with the more widely conserved FtsA. ZipA and FtsA have partially overlapping roles in stimulating Z-ring formation in *E. coli*, but ZipA has a specific function in promoting pre-septal FtsZ-directed PG synthesis (Potluri *et al*., 2012). Full-length ZipA, comprising a transmembrane anchor, intrinsically disordered P/Q-rich linker, and FtsZ-binding domain (ZBD), was demonstrated to recruit FtsZ to membrane nanodiscs (Hernández-Rocamora *et al*., 2012a) or supported lipid bilayers (Navajas *et al*., 2008). Similarly, a hexahistidine fusion to the ZBD (His_6-ZipA-ZBD) acts as a membrane-targeting factor for FtsZ when Ni-NTA phospholipids are incorporated into reconstituted membranes (Mateos-Gil *et al*., 2011; Hernández-Rocamora *et al*., 2012b; López-Montero *et al*., 2013). However, FtsZ targeted to membranes by ZipA has so far failed to produce Z-rings. When encapsulated in giant unilamellar vesicles composed of *E. coli* phospholipids doped with Ni-NTA phospholipids, FtsZ polymerization in the vesicle lumen in the absence of His_6-ZipA-ZBD resulted in vesicle dilation and rupture (López-Montero *et al*., 2013). In the presence of His_6-ZipA-ZBD, additional polymerization of FtsZ on the membrane increased membrane plasticity and prevented the vesicle rupture observed without the membrane tether (López-Montero *et al*., 2013). These results implicate membrane-associated FtsZ polymers in promoting membrane softening and plasticity. Employing a similar system, Cabre *et al.* incorporated soluble ZipA in permeablized, FtsZ-containing vesicles and reported GTP-dependent vesicle shrinkage which, they argue, resembles constriction of the cytoplasmic membrane (2013). It remains to be seen whether ZipA-mediated attachment of FtsZ is insufficient for Z-ring

formation and constriction of the type seen with FtsA, or if the requisite experimental conditions have simply not yet been met.

Mechanisms of FtsZ-generated force

The evidence that FtsZ is capable of generating constrictive force *in vitro* is now quite convincing. How it does so, and whether FtsZ-mediated force generation is required for division in cells, are important next questions. Existing data mostly favor a model where bending of membrane-attached FtsZ filaments away from the membrane towards their preferred radius of curvature (~100 nm for GTP-bound or ~12 nm for GDP-bound FtsZ) generates a pulling force (Erickson, 1997; Lu *et al*., 2000; Li *et al*., 2007; Osawa *et al*., 2009; Osawa and Erickson, 2011). If this model is correct, the gently curved GTP-bound state must be sufficient to drive initial constriction, as GTP hydrolysis was not required for inside-out Z-ring constriction (Osawa and Erickson, 2011). Theoretical modeling indicates that either curved state of FtsZ filaments (GTP-bound or GDP-bound) could generate enough force to constrict the inner membrane (Ghosh and Sain, 2008; Allard and Cytrynbaum, 2009; Ghosh and Sain, 2011; Hsin *et al*., 2012; Li *et al*., 2013). However, without GTP hydrolysis, MTS-FtsZ-YFP Z-rings stop constricting and become stabilized, indicating that filament turnover is necessary for persistent constriction (Osawa and Erickson, 2011). Filament disassembly may generate gaps in the Z-ring, such as those observed by 3D-SIM in *B. subtilis* (Strauss *et al*., 2012), to allow continued constriction without filaments annealing into closed circles that are unable to constrict (Osawa and Erickson, 2011).

Surprisingly, by assembling MTS-FtsZ-YFP filaments on lipid bilayer-coated glass capillaries of different diameters, Arumugam *et al.* found that FtsZ filaments align preferentially to match a radius of curvature of ~250–500 nm (2012). This argues against the ability of filament curvature, alone, to drive constriction to smaller diameters (Arumugam *et al*., 2012) and may explain the requirement of FtsA* for complete vesicle fission (Osawa and Erickson, 2013). Elaboration of the biomimetic systems developed thus far to include additional regulatory proteins will help refine models for how FtsZ generates force, and may lead to tools that specifically disengage FtsZ-mediated force generation to address its relevance *in vivo*.

Z-ring pulling versus PG pushing

While it is clear that FtsZ is capable of membrane deformation *in vitro*, there is no evidence that FtsZ-mediated force generation is required for cytokinesis *in vivo*. We can imagine at least three scenarios for the origins of the forces necessary for cytokinesis in bacteria (Fig. 1.3). In an FtsZ-centric model, all of the force required to overcome turgor pressure and constrict the IM comes from the Z-ring (Fig. 1.3b-i). Z-ring pulling on the IM opens up space for, or otherwise activates, ingrowth of PG mediated by enzymes recruited to the division site by FtsZ, and PG synthesis follows behind an ever-constricting Z-ring. In a second, PG-centric model, the Z-ring serves simply to recruit PG-remodeling enzymes to the division site (Fig. 1.3a, b-ii). These enzymes shape the PG such that it pushes against the IM, driving invagination. Our favored model envisions contributions both from Z-ring pulling and PG pushing (Fig. 1.3b-iii). The force generated by the Z-ring may contribute directionality and/or efficiency to the constriction

process, as was recently suggested for the actomyosin contractile ring in *Schizosaccharomyces pombe* (Proctor *et al*., 2012), or it could mechanically regulate the kinetics of PG remodeling, as has been proposed for crescentin-mediated cell curvature in *C. crescentus* (Cabeen *et al*., 2009). In each of these force-generation scenarios, rapid assembly and disassembly of FtsZ polymers (Stricker *et al*., 2002) must be coordinated with cell wall synthesis and hydrolysis in an iterative constriction process (Fig. 1.3c).

The road ahead: new assays for old questions

Even after decades of dedicated study, the form and function of FtsZ in cells remains largely enigmatic. The two approaches focused on here, advanced imaging and *in vitro* reconstitution, will continue to be of critical importance to resolving the structure of FtsZ in the cell and understanding its mechanism of action. We now envision the Z-ring as a heterogeneous collection of short FtsZ filaments at midcell undergoing continuous, dynamic rearrangement. Application of currently available high-resolution and single molecule imaging technologies to monitor FtsZ in cells lacking different FtsZ regulators will clarify their individual and/or collective contribution(s) to Z-ring organization. A comprehensive, detailed picture of the FtsZ polymer structures present in the cell, however, awaits development of imaging techniques that achieve the resolution of ECT with the specificity of fluorescent protein fusions.

Figure 1.3. Models for the contributions of Z-ring constriction and PG synthesis to the generation of force during cytokinesis. We envision at least three possible scenarios for the source of the forces required to invaginate the cell envelope during cytokinesis. In each case, the Z-ring is required to localize PG remodeling enzymes (green) to the incipient division site (A). In an FtsZ-centric model (Bi, Z-ring pulling), the Z-ring generates constrictive force that pulls on the IM. This opens up space for PG remodeling enzymes to build the cell wall radially inward and follow behind the constricting Z-ring. In a PG-centric model (Bii, PG pushing), FtsZ acts as a passive scaffold, localizing PG enzymes to the division site, where they build a cell wall that pushes the IM inward. A third model depicts contributions from both FtsZ-based pulling and PG-based pushing (Biii, concerted constriction): FtsZ generates a constrictive force that contributes to the efficiency, directionality, and/or mechanical regulation of the synthesis of PG, which also pushes on the IM. For each of these mechanisms, FtsZ turnover accompanies an iterative constriction process, cell wall hydrolases contribute to appropriate shaping of the cell wall and cell separation, and in Gram-negative organisms, PG-outer membrane (OM) attachments draw the OM inward (C). The models presented are overly simplified to convey general concepts. They are not meant to depict the detailed mechanisms of constriction or PG remodeling or to suggest significant temporal separation of the activities depicted in A, B, and C. Indeed, these events are certainly tightly coupled in both time and space.

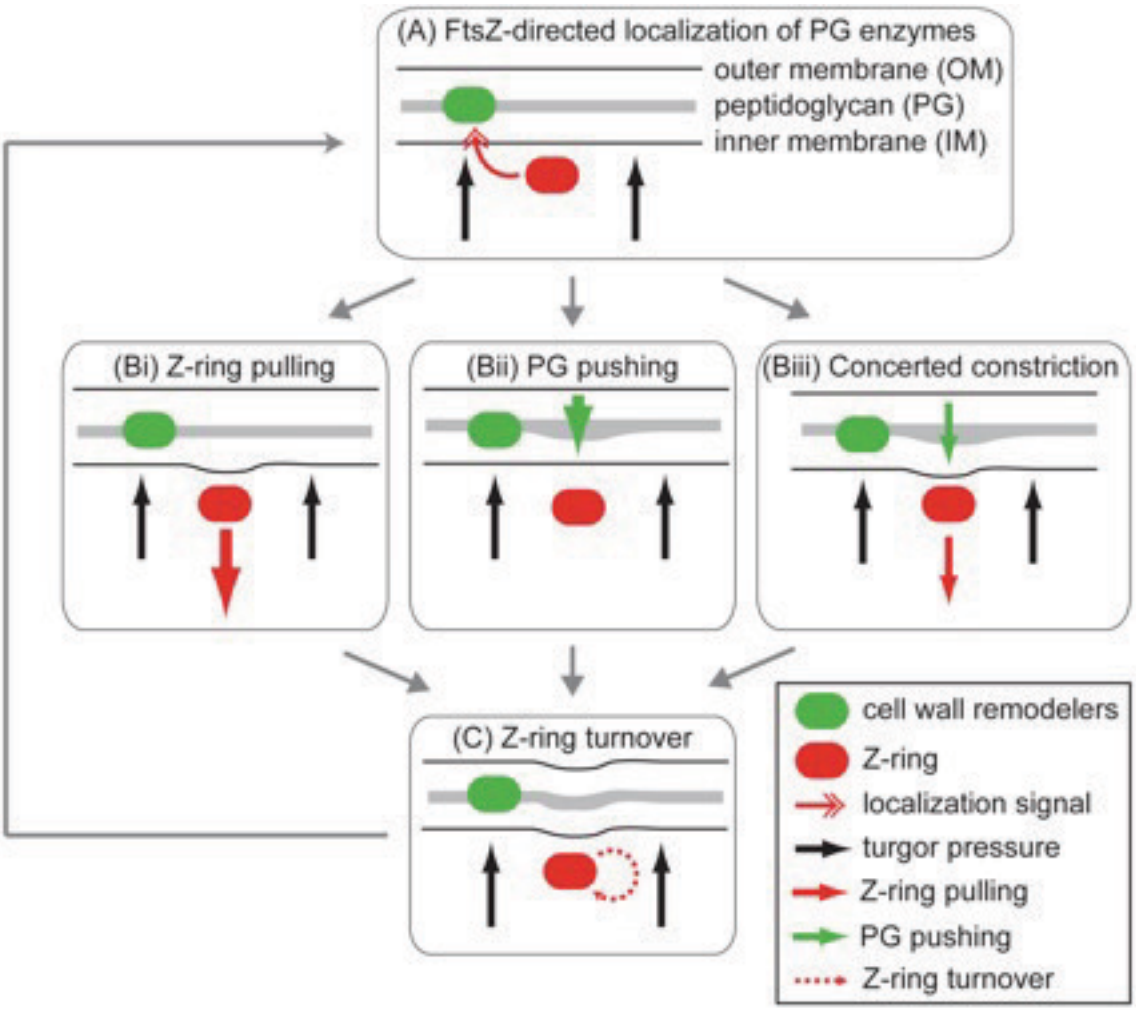
(A) FtsZ-directed localization of PG enzymes
outer membrane (OM)
peptidoglycan (PG)
inner membrane (IM)
(Bi) Z-ring pulling
(Bii) PG pushing
(Biii) Concerted constriction
(C) Z-ring turnover
cell wall remodelers
Z-ring
localization signal
turgor pressure
Z-ring pulling
PG pushing
Z-ring turnover

Complementing the imaging work performed *in vivo*, the use of biomimetic membrane systems has demonstrated that membrane-targeted FtsZ has the ability to form a ring and constrict. Recent efforts to reconstitute physiologically relevant forms of FtsZ membrane attachment with FtsA and ZipA hint that not all membrane-associated FtsZ behaves the same: efficient Z-ring constriction and membrane fission may require active input from the membrane tether. The utility of the current approaches for generating Z-rings *in vitro* is limited, however, by the difficulty of working with FtsA biochemically and the low frequency of Z-rings typically observed. The field awaits robust, efficient assays for reconstituting FtsZ on membranes that will allow elucidation of the requirements for and mechanisms of Z-ring formation and constriction, and the regulation of these activities by binding partners. Additional tools to monitor and perturb FtsZ-mediated force, beyond using membrane deformation as a read-out, are also necessary to unequivocally determine if and how FtsZ generates constrictive force *in vitro* and *in vivo*. Ultimately, pairing assays for FtsZ-mediated force generation with probes for cell wall remodeling enzymes, their substrates, and the cell wall, itself, will be required to resolve the questions of where and how the cytokinetic force originates in bacteria.

Caulobacter crescentus **as a model for bacterial cell biology**

Caulobacter crescentus is a Gram-negative, α-proteobacterium which inhabits oligotrophic aquatic environments. Known for its obligate dimorphism and clear cell polarity, vibrioid *C. crescentus* is an ideal model organism for studying developmentally regulated changes in cell shape (Woldemeskel and Goley, 2017). Every division event in *C. crescentus* produces two distinct daughter cell types: a flagellated, motile ‘swarmer’

cell and a sessile, 'stalked' cell (Fig. 1.4). The swarmer cell has a polar flagellum surrounded by adhesive pili and is unable to replicate its DNA. To progress through the cell cycle, the swarmer cell must differentiate into a stalked cell by ejecting its flagellum, retracting its pili, and protruding a thin, cylindrical extension of its cell envelope called a stalk at the same pole (Curtis and Brun, 2010; Woldemeskel and Goley, 2017). The stalked cell matures into a predivisional cell by elongating its cell body, duplicating its DNA, and extending a flagellum at the pole opposite its stalk (Curtis and Brun, 2010; Woldemeskel and Goley, 2017). At the end of division, the morphologically and biochemically distinct daughter cells have different fates: the stalked cell enters another round of the cell cycle while the swarmer cell must first differentiate into a stalked cell (Curtis and Brun, 2010; Woldemeskel and Goley, 2017). Due to differences in density, swarmer and stalked cells can easily be separated, allowing for the study of cell cycle-dependent morphological changes in a synchronized population.

In most bacteria, including *C. crescentus*, cytoskeletal proteins are important regulators of cell cycle progression and developmental changes in cell morphology (Sundararajan and Goley, 2017). To affect such diverse processes as polarity establishment, DNA segregation, and cell division and elongation, cytoskeletal proteins must spatially and temporally regulate remodeling of the peptidoglycan (PG) cell wall. Perhaps the most extensively studied cytoskeletal protein is FtsZ, a tubulin homolog which regulates PG remodeling and is essential for division in most bacteria (Fig. 1.4). In *C. crescentus*, a negative regulator of FtsZ assembly, MipZ, coordinates chromosome segregation with cell division through its association with the chromosomal centromere, a locus near the

origin of replication. The centromere is the first region of the chromosome to be replicated and is quickly translocated to the new pole by dedicated DNA segregation machinery. Thus, bipolarization of MipZ directs FtsZ polymers and consequently Z-rings to midcell where MipZ concentration is the lowest (Thanbichler and Shapiro, 2006).

For cytokinesis to occur, FtsZ must recruit numerous downstream division proteins to midcell. Some of these proteins directly regulate FtsZ structure, dynamics, and/or membrane attachment while others reside in the periplasm and influence cell wall metabolism (Goley *et al*., 2011; Sundararajan and Goley, 2017). Interestingly, beyond functioning as a passive scaffold for the division machinery, Sundararajan *et al*. ascribe a more active role to FtsZ, via its long, disordered C-terminal linker, in robust cell wall metabolism during division in *C. crescentus* (2015). In addition to its role in division specific cell wall remodeling, *C. crescentus* FtsZ also directs midcell localized cell wall synthesis prior to the onset of constriction through MreB, an actin homolog that directs elongation-specific PG synthesis, and MurG, an important player in the PG precursor synthesis pathway (Fig. 1.4; Aaron *et al*., 2007, Goley *et al*., 2011; Kuru *et al*., 2012). While FtsZ is involved in cell length maintenance, MreB is important for maintaining proper cell width in most bacilli; however, in *C. crescentus*, MreB also plays a role in promoting cell curvature, likely through the intermediate filament-like protein crescentin (Fig 1.4; Sundararajan and Goley, 2017). Additionally, in what has been described as a specialized form of cell elongation, MreB has been implicated in the maintenance of cell polarity as well as the specification of stalk width and morphology (Wagner *et al*., 2005). Overall, there are still significant knowledge gaps regarding the molecular mechanisms

by which cytoskeletal proteins regulate developmental shape changes in bacteria; however, the uniquely dimorphic and morphologically tractable life cycle of *C. crescentus* makes it an ideal system to tackle these open questions moving forward.

Figure 1.4. *C. crescentus* cell shape is dynamically regulated through cytoskeletal proteins. (A) *C. crescentus* undergoes changes in morphology as well as localization of cytoskeletal proteins, FtsZ, MreB, crescentin, and bactofilins over the cell cycle (Woldemeskel and Goley, 2017).

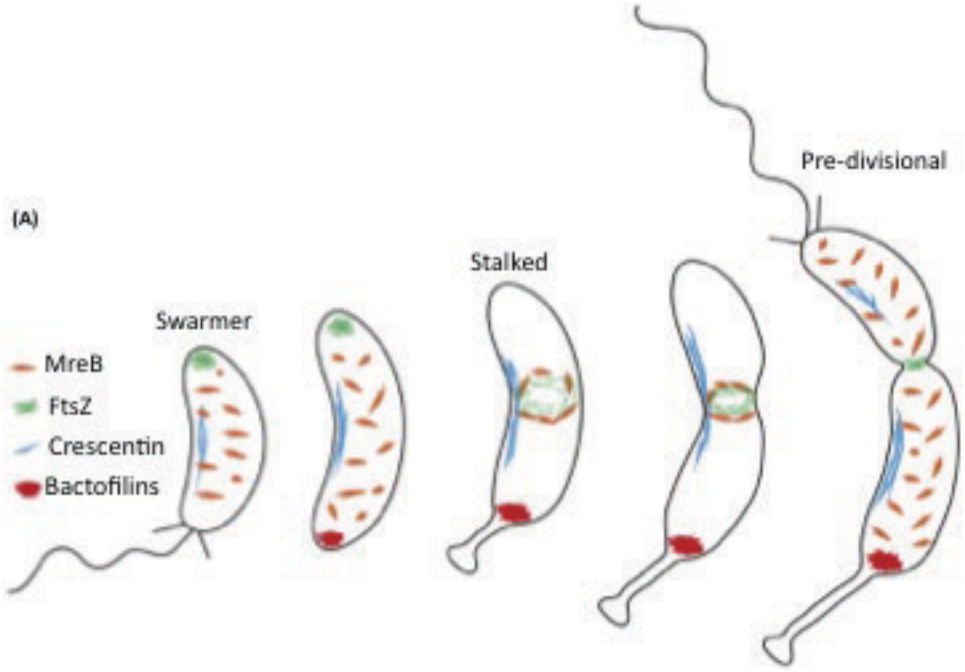

Woldemeskel and Goley, 2017

CHAPTER 2

A novel membrane anchor for FtsZ is linked to cell wall hydrolysis in *Caulobacter crescentus*

Note: The majority of the information presented in this chapter was included in the publication:

Meier EL, Razavi S, Inoue T, Goley ED. A novel membrane anchor for FtsZ is linked to cell wall hydrolysis in *Caulobacter crescentus*. Mol Microbiol. 2016;101(2):265-80.

Introduction

Bacterial cytokinesis is a multi-step process that couples dramatic reorganization of the cell envelope with faithful nucleoid replication and segregation. The tubulin-like GTPase FtsZ plays an essential role in bacterial cell division as a scaffold for the assembly of the division machinery (divisome) and, possibly, as a source of constrictive force (Osawa *et al*., 2008; Osawa *et al*., 2013). FtsZ forms a ring-like structure (the Z-ring) under the membrane at midcell and is thought to constrict to initiate cell division (Erickson *et al*., 2010; Meier *et al*., 2014). All downstream components of the divisome require FtsZ for enrichment at midcell, including cell wall remodeling enzymes. A subset of divisome proteins interacts directly with and regulates FtsZ assembly, activity, and structure.

One poorly understood class of FtsZ regulators mediates its membrane association. Most of what is known about FtsZ's membrane association comes from work in *Escherichia coli*. In that organism, inactivation of both of the known membrane anchors, FtsA and ZipA, destabilizes preformed Z-rings and blocks *de novo* Z-ring assembly (Pichoff *et al*., 2002). This inspired a model wherein FtsZ must be tethered to the membrane to form a stable Z-ring. Moreover, transmission of constrictive force and communication with the cell wall remodeling machinery intuitively require membrane attachment of the Z-ring. In *E. coli* cells, FtsA and ZipA perform unique roles beyond promoting Z-ring formation: FtsA recruits downstream division proteins and ZipA mediates pre-septal peptidoglycan synthesis (Pichoff *et al*., 2012; Potluri *et al*., 2012; Pichoff *et al*., 2015). These functional differences are borne out *in vitro* where each membrane anchor confers distinct dynamic properties to the membrane-associated FtsZ assemblies they mediate (Loose *et al*., 2014).

However, the mechanisms by which these membrane-anchoring proteins differentially direct the function of FtsZ are poorly understood.

FtsA is considered the primary membrane tether for FtsZ in bacteria as it is broadly distributed and a gain-of-function mutation in FtsA renders ZipA non-essential in *E. coli* (Hale *et al*., 1997; Geissler *et al*., 2003). However, FtsA is not essential in *Bacillus subtilis*, where SepF, and potentially EzrA, also function as membrane anchors (Beall *et al*., 1992; Jensen *et al*., 2005; Singh *et al*., 2007; Duman *et al*., 2013). FtsA is entirely absent in some bacteria, including *Mycobacterium tuberculosis*, where SepF and FtsW are postulated to play membrane-tethering roles (Datta *et al*., 2002; Gupta *et al*., 2015). The diversity of membrane anchors across bacteria suggests unique, though poorly understood, roles in regulating FtsZ dynamics and activity during division.

FtsA is essential in the Gram-negative α-proteobacterium *Caulobacter crescentus*, known for its obligate asymmetric division and ease of synchronization (Osley *et al*., 1977; Ohta *et al*., 1997; Christen *et al*., 2011). However, FtsA arrives at the division site after stable Z-ring assembly and early, FtsZ-directed cell wall synthesis (Moll *et al*., 2009; Goley *et al*., 2011). If membrane tethering is, indeed, required for Z-ring formation, the late arrival of FtsA in *C. crescentus* implies the existence of additional membrane anchors that tether FtsZ to the membrane early in the cell cycle. *In vivo* and *in vitro* characterization of the FtsZ-binding protein FzlC suggests that it is one such candidate membrane tether. FzlC, a hypothetical protein with limited sequence similarity to heparinase II/III family proteins, is predicted to be cytoplasmic and is widely conserved

in α-proteobacteria (Goley *et al*., 2010b). FzlC binds directly to FtsZ polymers *in vitro* and requires FtsZ for its early recruitment to midcell *in vivo* (Goley *et al*., 2010b). Interestingly, despite lacking a predicted membrane-binding domain, in cells depleted of FtsZ, FzlC has a patchy localization pattern that is reminiscent of membrane-associated proteins (Fig. 2.1A; Goley *et al*., 2010b).

Based on its early recruitment to midcell, direct binding to FtsZ polymers, and potential membrane localization, we hypothesized that FzlC could be an early membrane anchor for FtsZ before the arrival of FtsA. We pursued this hypothesis biochemically and found that FzlC indeed binds to membranes *in vivo* and *in vitro* and recruits FtsZ to membranes *in vitro*. *fzlC* overexpression led to impaired division while *fzlC* deletion caused synthetic cytokinesis defects in genetic backgrounds lacking other non-essential division genes implicated in cell wall hydrolysis. We postulate that FzlC is a redundant membrane anchor for FtsZ early in the cell cycle and improves the efficiency of cytokinesis through the regulation of cell wall hydrolysis.

Results

FzlC associates with membranes *in vivo* and *in vitro*

The localization of an mCherry-FzlC fluorescent fusion in *C. crescentus* cells depleted for FtsZ provided us with our first hint as to the role of FzlC during division (Fig. 2.1A; Goley *et al*., 2010b). Under these conditions, FzlC appeared to associate with the cell membrane similar to the transmembrane fluorescent fusion, mCherry-FtsW (Fig. 2.1A). To support this observation, we took advantage of *E. coli* as a heterologous expression system for investigating FzlC association with membranes in cells. CFP-FzlC localized primarily to the periphery in *E. coli* cells, indicating that FzlC interacts with membranes in *E. coli* (Fig. 2.1B).

In order to biochemically test if FzlC associates with membranes *in vivo*, we fractionated wild-type (WT) *C. crescentus* cells into membrane and soluble fractions and probed for FzlC by immunoblotting. Consistent with our fluorescence microscopy findings, FzlC was enriched in the pellet with the transmembrane protein control, SpmX, indicating association with membranes *in vivo* (Fig. 2.2A). We also fractionated *C. crescentus* cells expressing *yfp-fzlC* as the only copy of *fzlC*, since we used purified YFP-FzlC for most of the *in vitro* analyses described below. We found that YFP-FzlC was also enriched in the membrane fraction in this assay (Fig. 2.2A). Since the primary sequence of FzlC lacks any predicted membrane binding motifs, we next asked if it could interact with membranes directly. The composition of *C. crescentus* membranes is ~90-95% phosphatidylglycerol (PG) and 5% cardiolipin (Contreras *et al*., 1978). We therefore performed copelleting assays with purified FzlC and sucrose-loaded unilamellar vesicles.

The vesicles contained a range of molar percentages of PG, which is anionic, and phosphatidylcholine (PC), which is net neutral and not found in *C. crescentus* membranes. FzlC copelleted with vesicles in a PG dose-dependent manner and did not bind to 100% PC vesicles (Fig. 2.2 B and C). Thus, FzlC is a novel *C. crescentus* membrane-associated protein that binds the physiologically relevant lipid, PG, *in vitro*.

Figure 2.1. FzlC localizes to membranes in *C. crescentus* and *E. coli* cells. (A) Fluorescence and merged micrographs of cells depleted of FtsZ for 3 h and expressing mCherry fusions to the indicated proteins induced with vanillate for 2 h. FzlA is diffuse in the cytoplasm (top row) while FtsW and FzlC display a patchy peripheral localization typical of membrane-associated proteins (middle and bottom rows). (B) Fluorescence and merged micrographs of cells producing CFP-FzlC after 2 h induction with 1% L-arabinose in *E. coli*. CFP-FzlC localizes to the periphery, indicating membrane association. Scale bars = 2 μm.

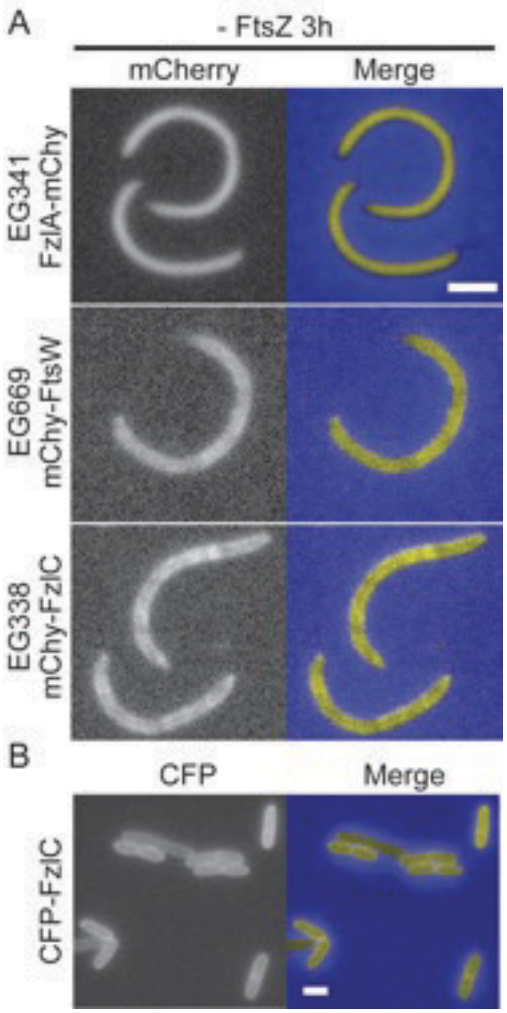

Figure 2.2 FzlC binds to membranes *in vivo* and *in vitro*. (A) WT (EG864) or cells expressing *yfp-fzlC* as the only copy of *fzlC* (EG1445) were lysed and centrifuged to separate soluble (supernatant) and membrane (pellet) protein fractions. Whole cell lysate/input (I), soluble (S), and membrane (P) fractions were probed by immunoblotting for FzlC, as well as for SpmX (transmembrane protein) and HU (DNA-binding protein) as controls for membrane and soluble fractions, respectively. (B) Coomassie stained gels of supernatant (S) and pellet (P) fractions after copelleting of FzlC with sucrose loaded unilamellar vesicles with the indicated molar percentages of phosphatidylglycerol (PG) and phosphatidylcholine (PC). Abundance of FzlC in the pellet indicates degree of binding to vesicles. (C) Quantification of FzlC lipid binding shown in (B). % FzlC in pellet was calculated by dividing the FzlC pellet band intensity by the total FzlC band intensity (pellet and supe) for each reaction. Error bars represent mean ± standard error of the mean (SEM) from three experimental replicates.

FzlC brings FtsZ to membranes

Since FzlC binds both to FtsZ filaments and membranes *in vitro*, we hypothesized that FzlC could function as a membrane anchor for FtsZ. The precedence of encapsulating bacterial proteins, including FtsZ membrane tethers, inside giant unilamellar vesicles (GUVs) inspired us to employ this minimal system for assaying FtsZ recruitment to membranes by FzlC (Cabre *et al*., 2013; Osawa and Erickson, 2013). We used the inverted emulsion method to encapsulate YFP-FzlC and/or FtsZ-CFP +/- GTP inside GUVs with outer leaflets composed of 4:1 PC:phosphatidylserine (PS) and inner leaflets composed of 1:1 PG:PC (Pautot *et al*., 2003; Luo *et al*., 2014). YFP-FzlC alone localized robustly to the membrane while FtsZ-CFP alone remained lumenal under polymerizing (+GTP) and non-polymerizing (-GTP) conditions (Fig. 2.3A). When we combined YFP-FzlC and FtsZ-CFP +/- GTP, YFP-FzlC invariably localized to the membrane and it recruited FtsZ-CFP to the membrane in a GTP-dependent manner (Fig. 2.3B). Since FtsZ was recruited to the membrane only in the presence of FzlC and GTP, we conclude that FzlC can act as a membrane anchor for FtsZ polymers *in vitro*. We did not observe Z-ring assembly or FtsZ-dependent membrane deformation as reported for *E. coli* FtsZ-YFP-MTS or FtsZ and FtsA encapsulated inside liposomes (Osawa *et al*., 2008; Osawa and Erickson, 2013). However, GUVs containing FzlC and FtsZ polymers were less stable than any of our other GUV preparations, and we occasionally observed vesicle shrinkage under these conditions.

Since many FtsZ-binding proteins regulate the localization or activity of FtsZ by altering its superstructure or assembly dynamics, we assessed whether FzlC affected FtsZ

polymer structure and/or GTPase activity. At equimolar concentrations of purified proteins, FzlC did not have any obvious effect on FtsZ filament organization, as visualized using negative stain transmission electron microscopy (Fig. 2.4A). Although filament architecture was not appreciably affected, additional densities were observed along FtsZ filaments in the presence of FzlC, likely reflecting FzlC bound to filaments. The GTPase activity of FtsZ was also unaffected in the presence of FzlC, even when FzlC was added in molar excess (Fig. 2.4B). These data indicate that the primary biochemical activity of FzlC towards FtsZ is to serve as a membrane anchor.

FzlC and FtsZ interact in a CTC-dependent manner

The membrane anchoring proteins FtsA, ZipA, and SepF all bind to the C-terminal conserved peptide (CTC) of FtsZ, which is highly conserved across bacteria (Vaughan *et al*., 2004; Erickson *et al*., 2010; Duman *et al*., 2013). We sought to test if, like other canonical membrane tethers, FzlC interacts with FtsZ *via* the CTC using purified proteins *in vitro.* We first measured the polymerization activity of FtsZΔCTC-CFP and observed indistinguishable GTPase activity and only mildly reduced light scattering when compared to full length FtsZ-CFP (Fig. 2.5A and B). To test if FzlC binds to the CTC, we encapsulated FtsZΔCTC-CFP +/- YFP-FzlC inside GUVs identical to those used for full length FtsZ as described above. Unlike full length FtsZ, under polymerizing conditions FtsZΔCTC-CFP remained completely luminal +/- YFP-FzlC (Fig. 2.3C and D). These data suggest that FzlC interacts with FtsZ by binding to the CTC.

Figure 2.3. YFP-FzlC recruits FtsZ-CFP polymers to membranes inside giant unilamellar vesicles (GUVs). (A-D) Fluorescence micrographs of representative GUVs containing the indicated proteins ± GTP. In (A, C, and D), normalized fluorescence intensities from lines scans across the representative GUVs are shown, as localizations were uniform for each of these GUV populations. In (B), the mean normalized fluorescence intensities of line scans across 18 GUVs for each condition (± GTP) are presented, and error bars (thin lines above and below middle line) represent standard deviation. Proteins were used at 2 μM, $MgCl_2$ was present at 2.5 mM in all FtsZ-containing reactions and, where indicated, GTP was used at 2 mM. Scale bars = 5 μm.

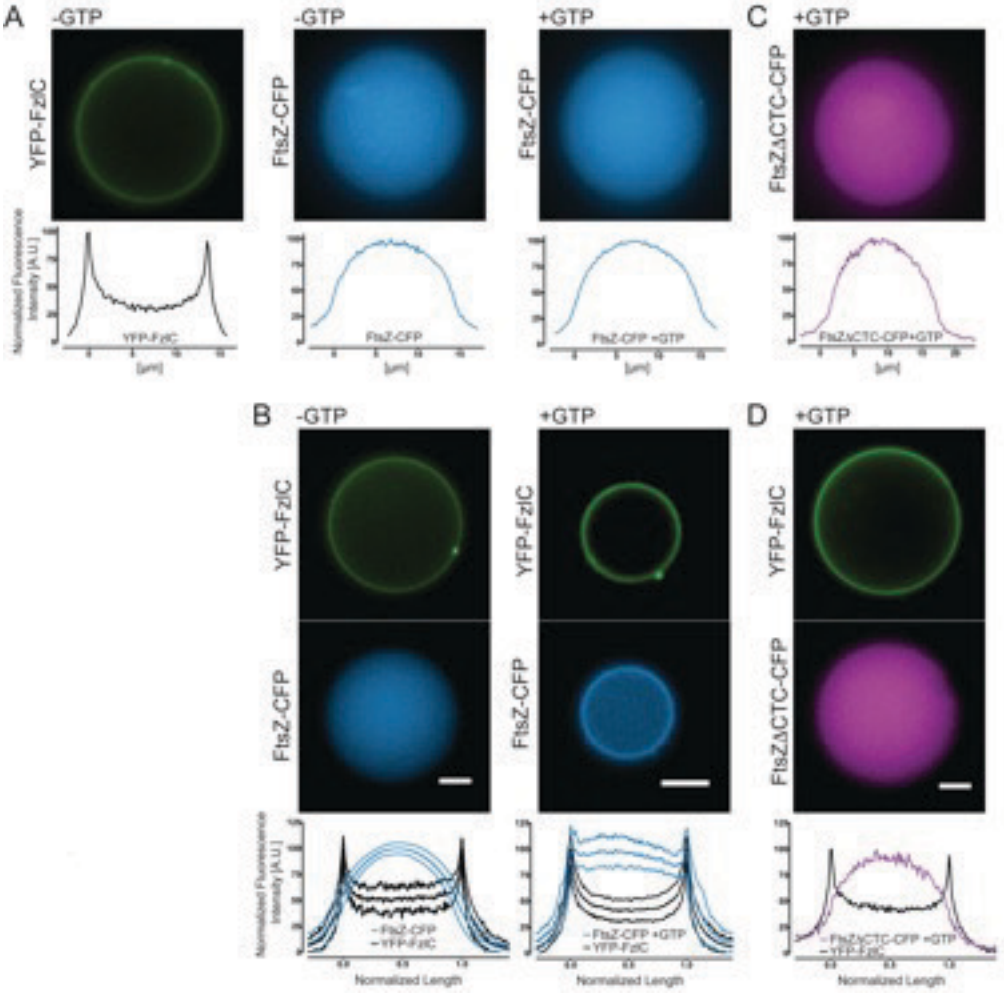

Figure 2.4. FzlC does not affect FtsZ polymer structure or GTPase activity. (A) Electron micrographs of purified FtsZ, YFP-FzlC, or FtsZ and YFP-FzlC. All reactions contained 4 μM protein, 2 mM GTP (in reactions containing FtsZ), and 2.5 mM $MgCl_2$. Scale bar = 100 nm (B) GTPase rate measured as the amount of inorganic phosphate released over time by 3 μM FtsZ as a function of increasing FzlC concentration. Error bars represent mean GTPase rate ± standard error of the mean (SEM) from three experimental replicates taken from two experiments performed on separate days.

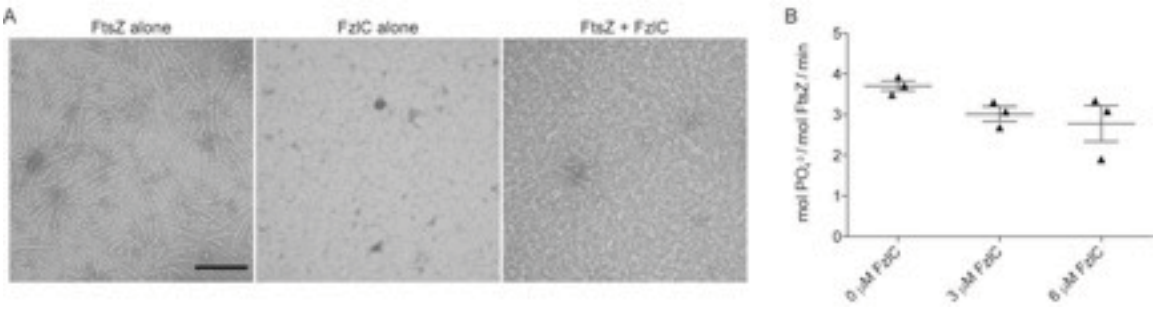

Figure 2.5. FtsZ-CFP and FtsZΔCTC-CFP display similar polymerization activities. (A) Right angle light scattering over time for solutions of 2 μM FtsZ-CFP or FtsZΔCTC-CFP. GTP was added to 2 mM to induce polymerization when indicated with the arrow. Mean ± SEM for three replicates is shown. (B) Inorganic phosphate concentration over time for solutions of 2 μM FtsZ or FtsZΔCTC. Mean ± SEM is shown for three replicates. Lines are linear regressions fit to the data.

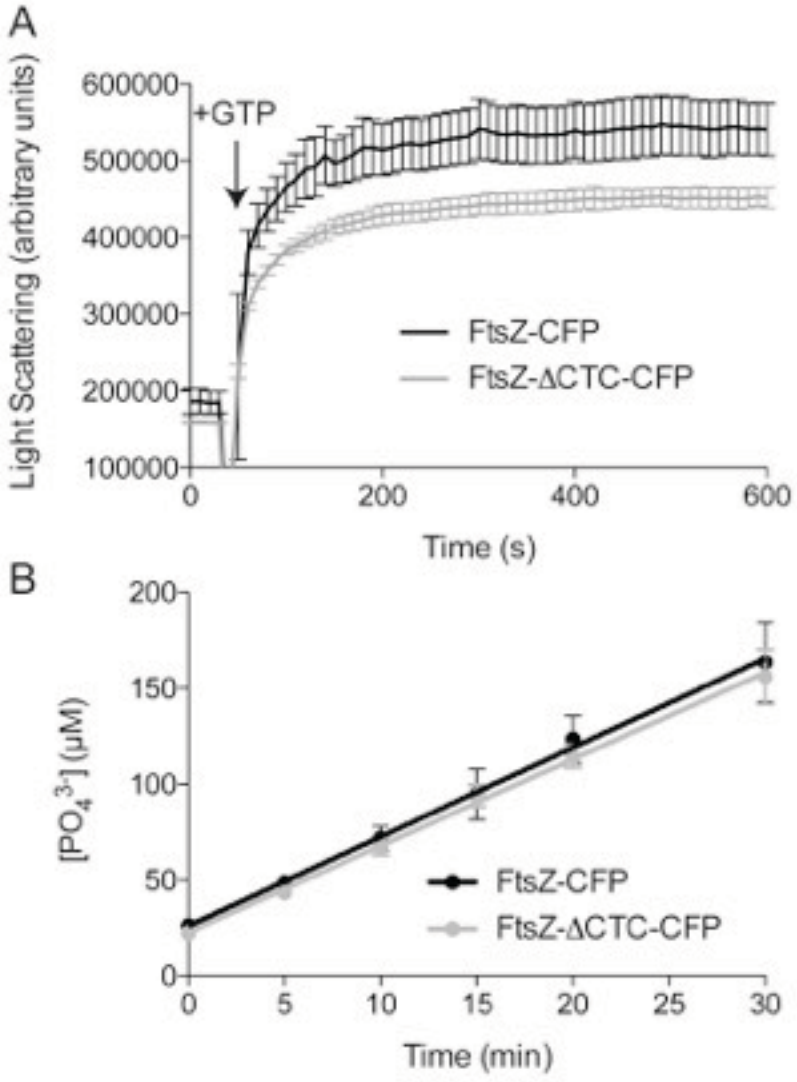

To further validate the CTC dependence of FzlC-FtsZ association on membranes, we used an *in vitro* fluorescence resonance energy transfer (FRET) approach. When we combined purified YFP-FzlC and full-length FtsZ-CFP and excited at the CFP excitation wavelength, we observed minimal emission at the YFP wavelength, indicating a low basal level of FRET (Fig. 2.6). Addition of either GTP to induce FtsZ polymerization, or PG vesicles to induce membrane association did not change the FRET observed. However, we observed an increase in the FRET emission at 527 nm and corresponding decrease in the CFP emission at 475 nm leading to an increased FRET/CFP ratio - hallmarks of FRET indicating close proximity of FzlC and FtsZ - when YFP-FzlC and FtsZ-CFP were incubated in the presence of both GTP and PG vesicles (Fig. 2.6). This result suggested that we could use this FRET assay to ask if the CTC is required for the interaction of FtsZ polymers with FzlC on vesicles. When we combined YFP-FzlC with FtsZ lacking its CTC and fused to CFP (FtsZΔCTC-CFP), we saw complete abrogation of the GTP- and PG vesicle-induced FRET increase observed for full-length FtsZ-CFP (Fig. 2.6). Corroborating our GUV results, we conclude that recruitment of FtsZ polymers to membranes by FzlC *in vitro* requires the CTC.

Figure 2.6. FzlC and full length FtsZ, but not FtsZΔCTC, display FRET with GTP and PG vesicles *in vitro*. (A, B) Emission profiles of YFP-FzlC and FtsZ-CFP or FtsZΔCTC-CFP ± GTP in the presence (A) or absence (B) of PG vesicles after excitation at 435 nm. (C) FRET/CFP ratios of YFP-FzlC and FtsZ-CFP or FtsZΔCTC-CFP ± GTP in the presence or absence of PG vesicles. Error bars represent the mean FRET/CFP ratio ± SEM from three experimental replicates for reactions containing FtsZ-CFP and from two experimental replicates for reactions containing FtsZΔCTC-CFP, *** = $p < 0.001$, one-way ANOVA. Labels: ZC = FtsZ-CFP/YFP-FzlC, ΔZC = FtsZΔCTC-CFP/YFP-FzlC

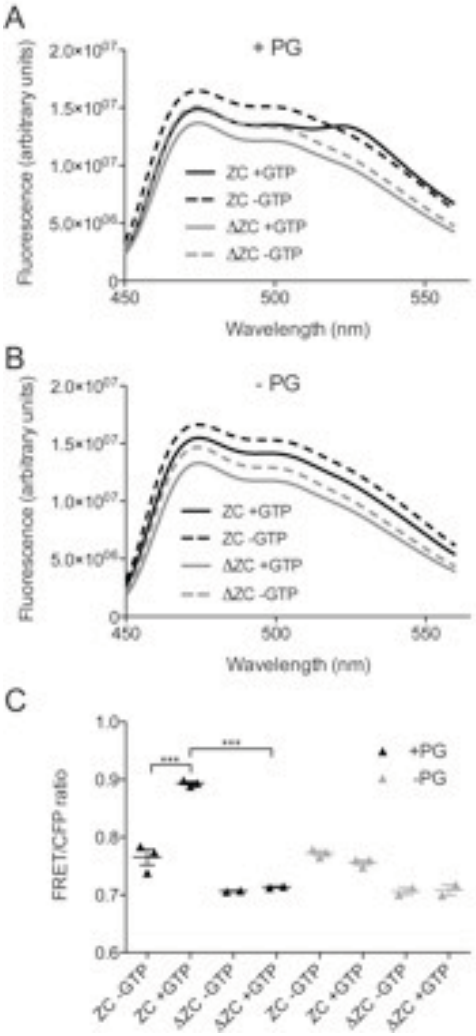

To complement our *in vitro* analyses, we investigated whether FzlC requires the CTC to localize *in vivo* by imaging Venus-FzlC in a strain with vanillate-driven induction of the only copy of full-length *ftsZ* and xylose-driven induction of *ftsZΔCTC*. The localization of FtsA-Venus and ZapA-Venus were assessed in the same strain background as controls for proteins that do or do not require the CTC for localization, respectively. After depleting full-length FtsZ and producing FtsZΔCTC for 6.5 h, ZapA-Venus localized to prominent, wide Z-rings. In contrast, FtsA-Venus and Venus-FzlC were both diffuse with only occasional, weak localization (Fig. 2.7). The loss of localization of FzlC upon depletion of full length FtsZ and production of FtsZΔCTC suggests that, like FtsA, it requires the CTC to associate with Z-rings *in vivo* (Din *et al*., 1998).

fzlC overexpression causes a cell division defect

Having validated FzlC as a novel membrane anchor for FtsZ in *C. crescentus*, we next sought to elucidate its role during cell division. To this end, we constructed a strain containing a high copy plasmid for vanillate-inducible *fzlC* overexpression (EG891). We observed that, when compared to the empty vector control (EG890), cells overproducing FzlC were mildly elongated, with extended division sites, more pointed cell poles and longer doubling times (Fig. 2.8A and B; Table 1). We used principle component analysis (PCA) to quantify modes of variation in cell shape after FzlC overproduction (Pincus *et al*., 2007). Seven shape modes captured 99% of the variance in the data set of cells bearing the empty vector or vanillate-inducible *fzlC* grown with vanillate for 2, 6, 8 or 24 h. Shape modes 1 (roughly corresponding to cell length), 2 (cell curvature), and 6 (shape of the poles) were of particular interest as they most closely reflected the changes noted

by manual inspection of cells upon *fzlC* overexpression. Indeed, at the 8 and 24 h time points, *fzlC* overexpressing cells (EG891) were significantly longer, more curved, and had narrower cell poles compared to cells containing an empty vector (EG890), validating our qualitative observations of cell morphology (Fig. 2.8C-E). As cell poles are derived from cell division events, these FzlC-induced shape changes indicate aberrant cytokinesis in cells with excess FzlC.

Figure 2.7. FzlC requires the CTC to localize to Z-rings *in vivo*. (A) Merged fluorescent (yellow) and phase contrast (blue) micrographs of cells with vanillate inducible *ftsZ* and xylose inducible *ftsZΔCTC* expressing either *ftsA-venus* (EG1048), *zapA-venus* (EG1049), or *venus-fzlC* (EG1054) on a low copy replicating plasmid under the control of its own promoter grown with the indicated inducers for 6.5 h. The white asterisks denote localization to focused Z-rings, the white arrowheads denote localization to wider Z-rings, and # denotes weak localization. Scale bar = 2 µm. (B) Immunoblot of FtsZ or FtsZΔCTC levels in the strains from (A). FtsZΔCTC was present at much higher levels than FtsZ, presumably because it lacks the C-terminal degradation sequence recognized by the ClpXP protease. V = vanillate; X = xylose; G = glucose.

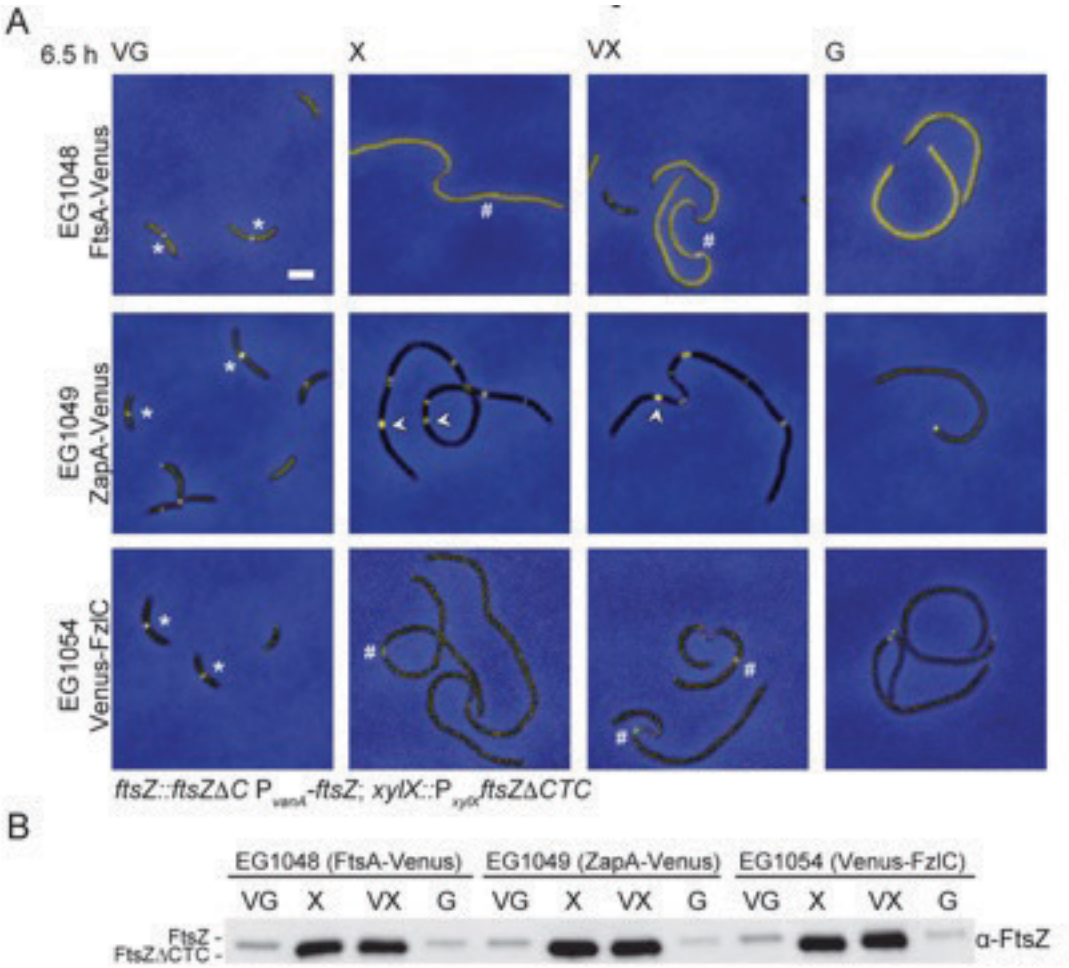

Figure 2.8. High levels of FzlC interfere with efficient cytokinesis. (A,B) Phase contrast micrographs of cells containing empty vector (EG890) or vanillate-inducible *fzlC* overexpression vector (EG891) grown for 8 or 24 h in the presence of vanillate. The black arrows denote pointy poles (shape mode 6). Scale bar = 2 μm. (C-E) PCA of EG890 and EG891 produced seven different shape modes. Shown are scatter plots of shape modes 1, 2 and 6, which roughly correspond to length, curvature, and pole shape, respectively. Contours reflecting the mean shape and ± 1 or 2 standard deviations (s.d.) from the mean in each shape mode are shown to the left of the corresponding scatter plot. The differences between EG890 (n = 582 and 752 cells at 8 and 24 h, respectively) and EG891 (n = 658 and 817 cells at 8 and 24 h, respectively) were statistically significant for these three shape modes (*** = $p < 0.001$, Bonferroni's Multiple Comparison Test).

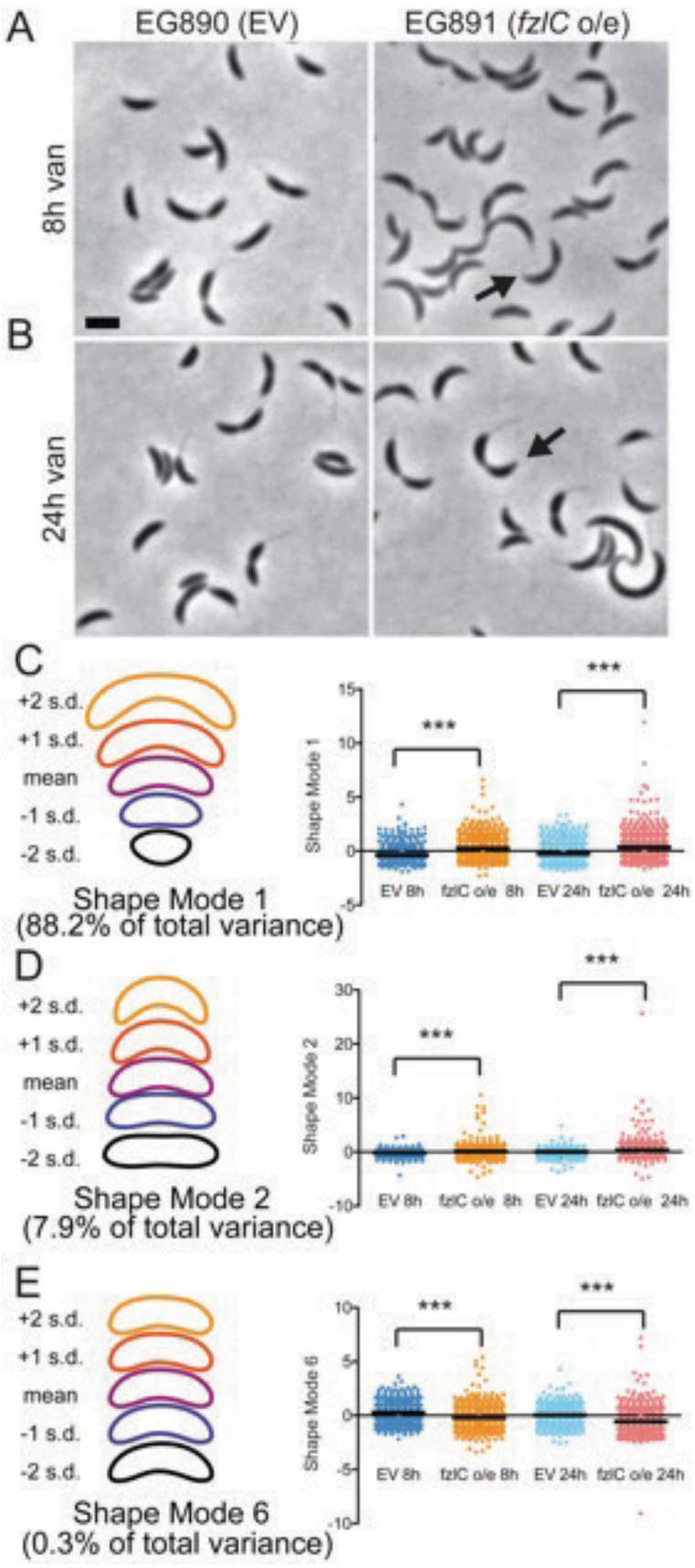
A
EG890 (EV)
EG891 (fzlC o/e)
8h van
B
24h van
C
+2 s.d.
+1 s.d.
mean
-1 s.d.
-2 s.d.
Shape Mode 1
(88.2% of total variance)
Shape Mode 1
***
***
EV 8h
fzlC o/e 8h
EV 24h
fzlC o/e 24h
D
+2 s.d.
+1 s.d.
mean
-1 s.d.
-2 s.d.
Shape Mode 2
(7.9% of total variance)
Shape Mode 2
***
***
EV 8h
fzlC o/e 8h
EV 24h
fzlC o/e 24h
E
+2 s.d.
+1 s.d.
mean
-1 s.d.
-2 s.d.
Shape Mode 6
(0.3% of total variance)
Shape Mode 6
***
***
EV 8h
fzlC o/e 8h
EV 24h
fzlC o/e 24h

Table 1. Growth rate and cell length of strains in Figs. 2.8 and 2.10

Strain	**Description (24 h o/e)**	**Doubling time ± SEM (hr)***	**Mean cell length ± SEM (μm)†**	**N**
EG890	Empty vector	1.94 ± 0.01	2.42 ± 0.02	800
EG891	*fzlC* o/e vector	2.07 ± 0.01	2.98 ± 0.04	800
EG1405	Empty vector; *xylX::*P_{xyl}-*ftsZ-yfp*	ND	2.95 ± 0.04	490
EG1406	*fzlC* o/e vector; *xylX::*P_{xyl}-*ftsZ-yfp*	ND	3.79 ± 0.05	578

* EG890 vs EG891 = $p < 0.001$ unpaired t test, two-tailed

† EG890 vs EG891, EG1405 vs EG1406 = $p < 0.001$ unpaired t test, two-tailed; N refers to sample size for cell length analysis.

Tagged variants of FzlC exhibit different phenotypes and localization ability

Interestingly, we found that when we replaced the native copy of *fzlC* with an N-terminal *mChy-fzlC* fusion (EG653), the phenotype was similar to *fzlC* overexpression. This cell division defect was specific to the N-terminal mCherry tag, as cells expressing C-terminal *fzlC-mChy* (EG859) or N-terminal *yfp-fzlC* (EG1445) fusions as the only copies of *fzlC* had morphologies and growth rates resembling WT (EG864) (Fig. 2.9A and C; Table 2). mChy-FzlC and YFP-FzlC localized to midcell with dynamics similar to FtsZ-YFP, while FzlC-mChy appeared more diffuse with only occasional midcell localization (Fig. 2.9A; Goley *et al*., 2011). These data suggest that the C-terminus of FzlC is important for robust midcell localization.

Immunoblotting revealed FzlC to be present at very low levels in WT cells but to markedly increase after inducing *fzlC* expression with vanillate for 24 h (Fig. 2.9D). To ask whether differences in protein levels contributed to the phenotypes of the fluorescent FzlC fusions, we probed for FzlC by immunoblotting in cells with native *fzlC* replaced with *mChy-fzlC* (EG653), *fzlC-mChy* (EG859), or *yfp-fzlC* (EG1445). Cells with *mChy-fzlC* as the only copy of *fzlC* had strikingly higher levels of FzlC compared to cells with *fzlC-mChy* or *yfp-fzlC* (Fig. 2.9D), reinforcing our conclusion that excess FzlC impairs cytokinesis efficiency.

High levels of FzlC broaden the Z-ring in constricting cells

Since overexpressing *fzlC* produced a cytokinesis defect and FzlC tethers FtsZ polymers to membranes, we hypothesized that Z-ring structure may be affected in these cells. To

address this hypothesis, we integrated a xylose-inducible copy of *ftsZ-yfp* at the *xylX* locus in cells containing a high copy plasmid for vanillate-inducible *fzlC* overexpression (EG1406) or an empty vector (EG1405). After growth with vanillate for 24 h, many *fzlC* overexpressing cells (EG1406) formed apparently normal Z-rings. In constricting cells, however, FtsZ was present in wider bands compared to the focused rings seen in cells containing an empty vector (EG1405) (Fig. 2.10A). To quantify this effect, we determined the full width at half maximum (FWHM) of FtsZ-YFP intensity along the long cell axis in cells with visible constrictions. Cells overexpressing *fzlC* had statistically higher FWHM values compared to the empty vector control, reflecting wider Z-rings in predivisional cells with excess FzlC (Fig. 2.10B). FtsZ localization was even more obviously affected in cells expressing the *mChy-fzlC* fusion as the only copy of *fzlC* at its native locus (EG1404). Z-rings were wider and more dispersed, with patches of FtsZ occasionally observed on one side of the cell (Fig. 2.9B). We attribute this synthetic cell division defect to the combination of mild overexpression of *ftsZ-yfp* with high cellular levels of FzlC and/or the N-terminal mCherry tag affecting FzlC function (Fig. 2.9B; Table 2). We conclude that overproducing FzlC alters Z-ring organization in a manner consistent with the observed moderate reduction in cytokinesis efficiency.

As a point of comparison, we assessed Z-ring organization and cell morphology in cells overproducing the only other known membrane anchor in *C. crescentus*, FtsA. We integrated a vanillate-inducible copy of *ftsZ-cfp* at the *vanA* locus in cells containing an empty vector (EG1284) or a high copy plasmid for xylose inducible *ftsA* overexpression (EG1302). After inducing *ftsA* overexpression for 4 h, cells were filamentous and had

multiple Z-rings with a range of widths, as well as patchy and diffuse FtsZ localization (Fig. 2.10C). The unique effects on cellular and Z-ring morphology upon overexpression of *fzlC* versus *ftsA* indicate distinct roles for these FtsZ membrane anchors *in vivo*.

Figure 2.9. Differentially tagging FzlC affects FzlC localization, cellular morphology and FzlC protein levels. (A) Phase contrast and merged micrographs (phase contrast in blue and fluorescence in yellow) of cells with *mChy-fzlC* (EG653), *fzlC-mChy* (EG859), or *yfp-fzlC* (EG1445) at the native *fzlC* locus as the only copy of *fzlC* or of xylose inducible *ftsZ-yfp* at the *xylX* locus in a WT background (EG444). Demographs (far right) represent normalized signal profiles of fluorescent fusions to FzlC or FtsZ in cells arranged by increasing cell length. White asterisks denote focused FzlC or Z-rings and the white arrowheads denote more diffuse FzlC or Z-rings. Scale bar = 2 μm. (B) Phase contrast, fluorescence, and merged micrographs (phase contrast in blue and fluorescence in red (FzlC) or green (FtsZ)) of cells with *mChy-fzlC* at the native *fzlC* locus as the only copy of *fzlC* and xylose-inducible *ftsZ-yfp* (EG1404). Demographs represent normalized signal profiles of fluorescent fusions to FzlC or FtsZ in cells arranged by increasing cell length. (C) Cell lengths of strains in (A) (see Table 2 for sample sizes). Error bars represent the mean cell length ± SEM, *** = $p < 0.001$, one-way ANOVA. (D) Immunoblots of cell lysates from strains from (A) and Fig. 2.8 probed for FzlC and, when appropriate, RFP (EG653 and EG859) or GFP (EG1445). SpmX was used as a loading control. Two different exposure times for the α-FzlC immunoblot (2 sec or 10 sec) are presented for better visualization of FzlC levels in the different strains.

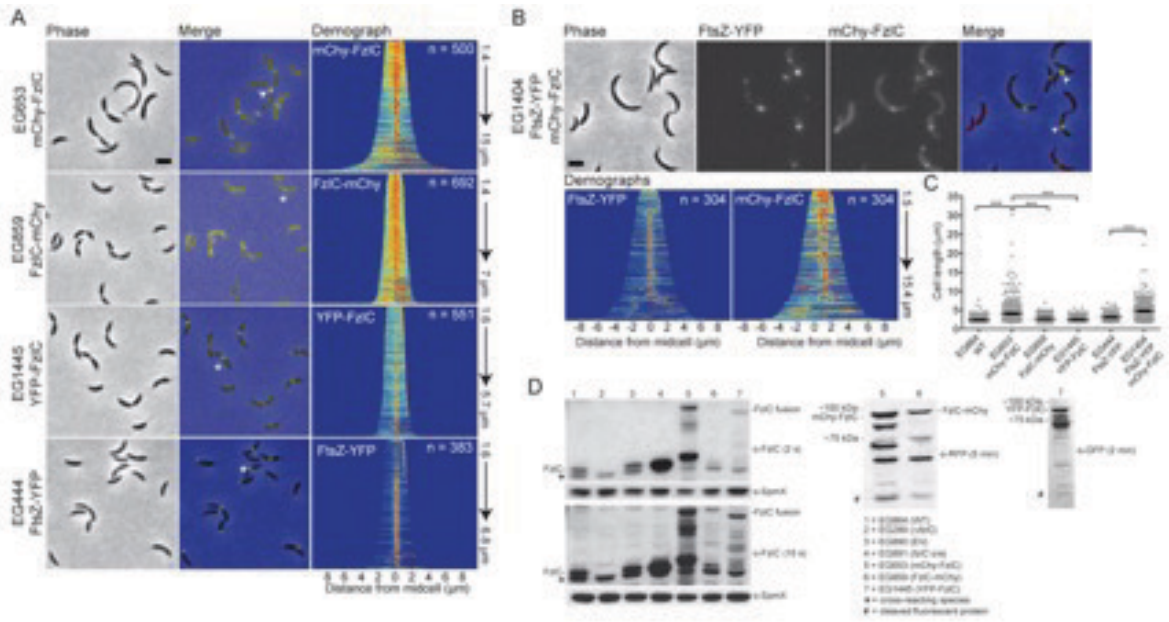
A
Phase
Merge
Demograph
EG653 mChy-FzlC
EG859 FzlC-mChy
EG1445 YFP-FzlC
EG444 FtsZ-YFP
mChy-FzlC
n = 500
FzlC-mChy
n = 692
YFP-FzlC
n = 551
FtsZ-YFP
n = 383
Distance from midcell (μm)
B
Phase
FtsZ-YFP
mChy-FzlC
Merge
EG1404 FtsZ-YFP mChy-FzlC
Demographs
FtsZ-YFP
n = 304
mChy-FzlC
n = 304
Distance from midcell (μm)
C
D

Table 2. Growth rate and cell length of strains in Fig. 2.9

Strain	Description	Doubling time ± SEM (hr)*	Mean cell length ± SEM (μm)†	N
EG864	WT	1.85 ± 0.004	2.46 ± 0.03	614
EG653	*fzlC::mChy-fzlC*	3.37 ± 0.2	4.03 ± 0.12	503
EG859	*fzlC::fzlC-mChy*	ND	2.73 ± 0.03	692
EG1445	*fzlC::yfp-fzlC*	1.95 ± 0.01	2.58 ± 0.03	551
EG444	*xylX::* P_{xyl}*-ftsZ-yfp*	ND	3.10 ± 0.04	383
EG1404	*fzlC::mChy-fzlC*; *xylX::* P_{xyl}*-ftsZ-yfp*	ND	4.78 ± 0.14	305

* EG864 vs EG653, EG1445 vs EG653 = $p < 0.001$; EG864 vs EG1445 = not significant (ns) ANOVA Tukey's Multiple Comparison Test

† EG864 vs EG653, EG859 vs EG653, EG1445 vs EG653 = $p < 0.001$; EG864 vs EG859 = $p < 0.01$; EG864 vs EG1445, EG859 vs EG1445 = ns ANOVA Tukey's Multiple Comparison Test; EG444 vs EG1404 = $p < 0.001$ unpaired t test, two-tailed; N refers to sample size for cell length analysis.

Figure 2.10. High levels of FzlC broaden the Z-ring in constricting cells. (A) Phase contrast and merged fluorescent micrographs of cells containing xylose inducible *ftsZ-yfp* with an empty vector (EG1405) or vanillate-inducible *fzlC* overexpression vector (EG1406) grown in the presence of vanillate for 24 h and xylose for 1 h. The white asterisks denote focused Z-rings and white arrowheads denote more broad Z-rings at extended division sites. (B) Merged fluorescent micrographs from (A) with representative line scan full width half maximum (FWHM) measurements. Scatter plot shows the FWHM of Z-rings in cells with visible constrictions for EG1405 (n = 163) and EG1406 (n = 262) (*** = $p < 0.001$, unpaired t-test). (C) Phase contrast and merged micrographs of cells containing vanillate inducible *ftsZ-cfp* with empty vector (EG1285) or xylose-inducible *ftsA* overexpression vector (EG1302) grown in the presence of xylose for 4 h and vanillate for 1 h. The white asterisks denote focused Z-rings, the black arrowhead denotes deeply constricted sites, and the white arrowheads denote a more diffuse Z-ring. Scale bars = 2 μm.

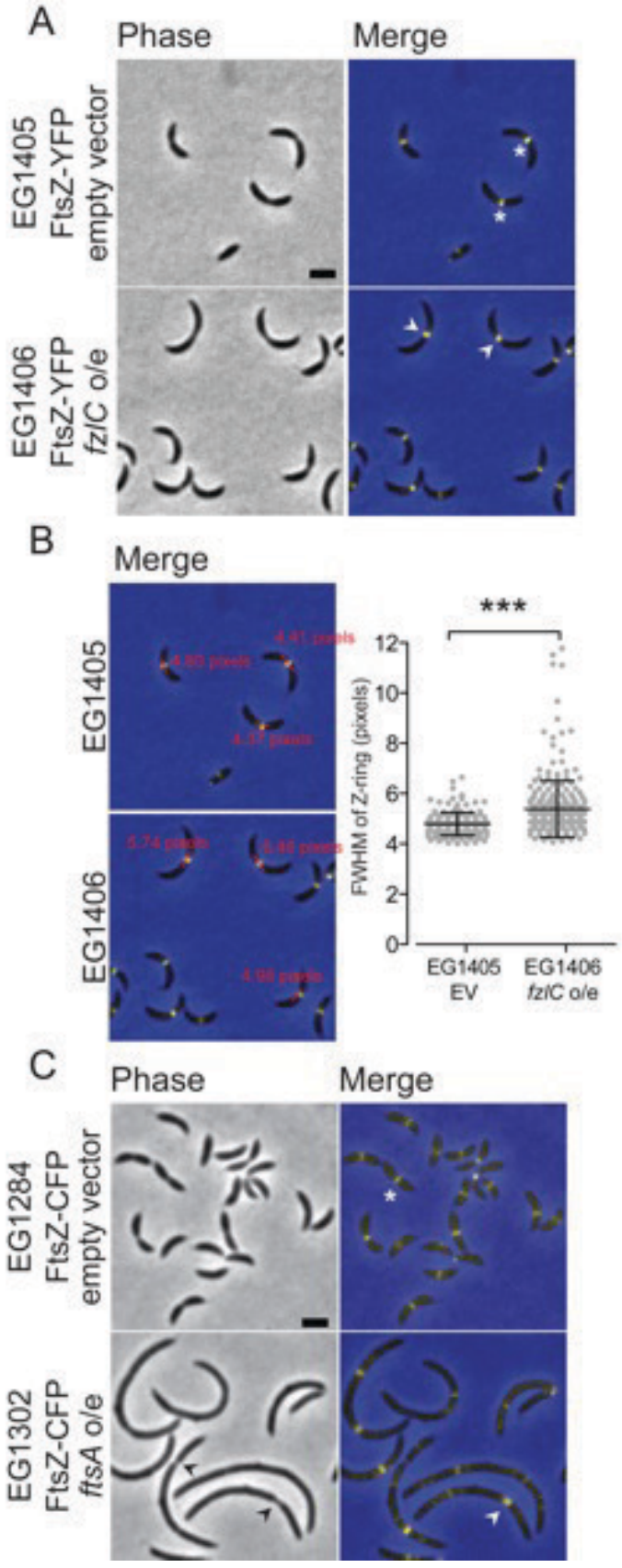
A
Phase
Merge
EG1405
FtsZ-YFP
empty vector
EG1406
FtsZ-YFP
fzlC o/e
B
Merge
EG1405
EG1406
***
FWHM of Z-ring (pixels)
0
2
4
6
8
10
12
EG1405
EV
EG1406
fzlC o/e
C
Phase
Merge
EG1284
FtsZ-CFP
empty vector
EG1302
FtsZ-CFP
ftsA o/e

fzlC has synthetic interactions with other non-essential division genes

To further define the role of FzlC in cell division, we next assessed the consequences of deleting *fzlC*. We found that *fzlC* was not essential: *ΔfzlC* (EG289) cells had WT morphology, growth rate, and Z-ring organization (Figs. 2.11A, 2.12A and 2.13A; Table 3; Goley *et al*., 2010b). To test if *fzlC* had synthetic interactions with other non-essential division genes, we deleted *fzlC* in Δ*dipM* (EG1242), Δ*ftsE* (EG1162), Δ*zapA* (EG1232), Δ*tipN* (EG1299), Δ*kidO* (EG1298), Δ*ftsB* (EG1307), *Δpbp1aΔpbpYΔpbpCΔpbpZΔmtgA* ("*Δ5pbp"* a quintuple mutant lacking five of the six bifunctional PBPs encoded in *C. crescentus*) (Yakhnina *et al*., 2013) (EG1509), or Δ*amiC* (EG1771) strain backgrounds (Figs. 2.11B-D and 2.13A-F; Tables 3 and 4).

We looked for synthetic interactions wherein a mutant combination yielded statistically significant differences in growth rate and/or cell length between the double mutant and each of the corresponding single mutants. Of the genes tested, we found such interactions only with *dipM*, a peptidoglycan-binding putative endopeptidase; *ftsE*, the ATP-binding component of the ABC-transporter FtsEX complex; and the peptidoglycan amidase *amiC*. The synthetic double mutants (EG1242, EG1162, EG1771) had significantly longer doubling times and/or cell lengths compared to either single mutant alone (Fig. 2.11, Table 3). Furthermore, all of the synthetic double mutants displayed, to different degrees, a chaining phenotype indicative of a late stage cell separation defect frequently associated with factors involved in cell wall hydrolysis (Fig. 2.11). In *E. coli*, *Streptococcus pneumoniae*, *B. subtilis*, and *M. tuberculosis* FtsEX has been shown to activate peptidoglycan hydrolysis (Sham *et al*., 2011; Yang *et al*., 2011; Meisner *et al*., 2013;

Mavrici *et al*., 2014). Thus, the synthetic division defects upon deletion of *fzlC* in cells lacking DipM, FtsE, or AmiC suggest that *fzlC* is specifically implicated in the regulation of cell wall hydrolysis. This synthetic relationship appears specific for cell wall hydrolysis, as opposed to synthesis, as no genetic interaction was observed with the quintuple glycosyltransferase mutant ("Δ*5pbp*"), nor was any effect observed on the location or timing of cell wall synthesis in cells lacking *fzlC* (Fig. 2.14). Moreover, deleting *fzlC* had no effect on the sensitivity of β-lactamase deficient *C. crescentus* to mecillinam and cephalexin, inhibitors of the transpeptidases, PBP2 and PBP3, respectively (Fig. 2.13G and H).

fzlC* overexpression partially rescues the cytokinesis defects of Δ*ftsE

The synthetic interaction between *fzlC* and *ftsE* was of particular interest to us since, beyond regulating cell wall hydrolysis, FtsEX hypothetically could function as a membrane tether for FtsZ (Goley *et al*., 2011). In *E. coli* FtsE is proposed to bind FtsZ while FtsX is embedded in the inner membrane (Corbin *et al*., 2007); this topology would allow for recruitment of FtsZ to membranes. Moreover, FtsE is among the first proteins recruited to the incipient division site (Goley *et al*., 2011). Consistent with Δ*fzlC* cells' lack of morphological and growth defects, Z-ring assembly was similarly unaffected in Δ*fzlC* cells compared to WT (Fig. 2.12A). In contrast, we observed striking mislocalization of FtsZ in Δ*ftsE* cells: FtsZ was more diffuse and frequently formed clusters of puncta instead of focused Z-rings (Fig. 2.12B). The mislocalization of FtsZ was even more pronounced in Δ*ftsE*Δ*fzlC* cells as demonstrated by the mostly diffuse FtsZ-CFP signal in cells and in the corresponding demograph (Fig. 2.12B). We hypothesized that the synthetic effect on FtsZ

localization in Δ*ftsE*Δ*fzlC* cells was due to partially redundant functions of FtsE and FzlC as membrane tethers. To test this hypothesis, we overexpressed *fzlC* in Δ*ftsE* cells for 24 h and observed partial rescue of growth rate and cell length compared to the empty vector control (Fig. 2.15A-C; Table 5). Correspondingly, overproducing FzlC in Δ*ftsE* cells largely restored the focused, midcell localization of FtsZ (Fig. 2.15D). The ability of high levels of FzlC to partially rescue Z-ring localization and function in Δ*ftsE* cells suggests FzlC and FtsEX, in addition to regulating cell wall hydrolysis, may function as redundant membrane anchors for FtsZ during division.

Figure 2.11. Deletion of *fzlC* has synthetic interactions with non-essential division genes *dipM*, *ftsE*, and *amiC*. (A-D) Phase contrast micrographs of cells with or without *fzlC* in WT, Δ*dipM*, Δ*ftsE*, or Δ*amiC* backgrounds. (Ai-Di) Cell length of strains in (A-D) (see Table 3 for sample sizes). Error bars represent the mean cell length ± SEM, *** = $p < 0.001$, one-way ANOVA. (Aii-Dii) Growth curves of strains shown in (A-D). Scale bars = 2 μm.

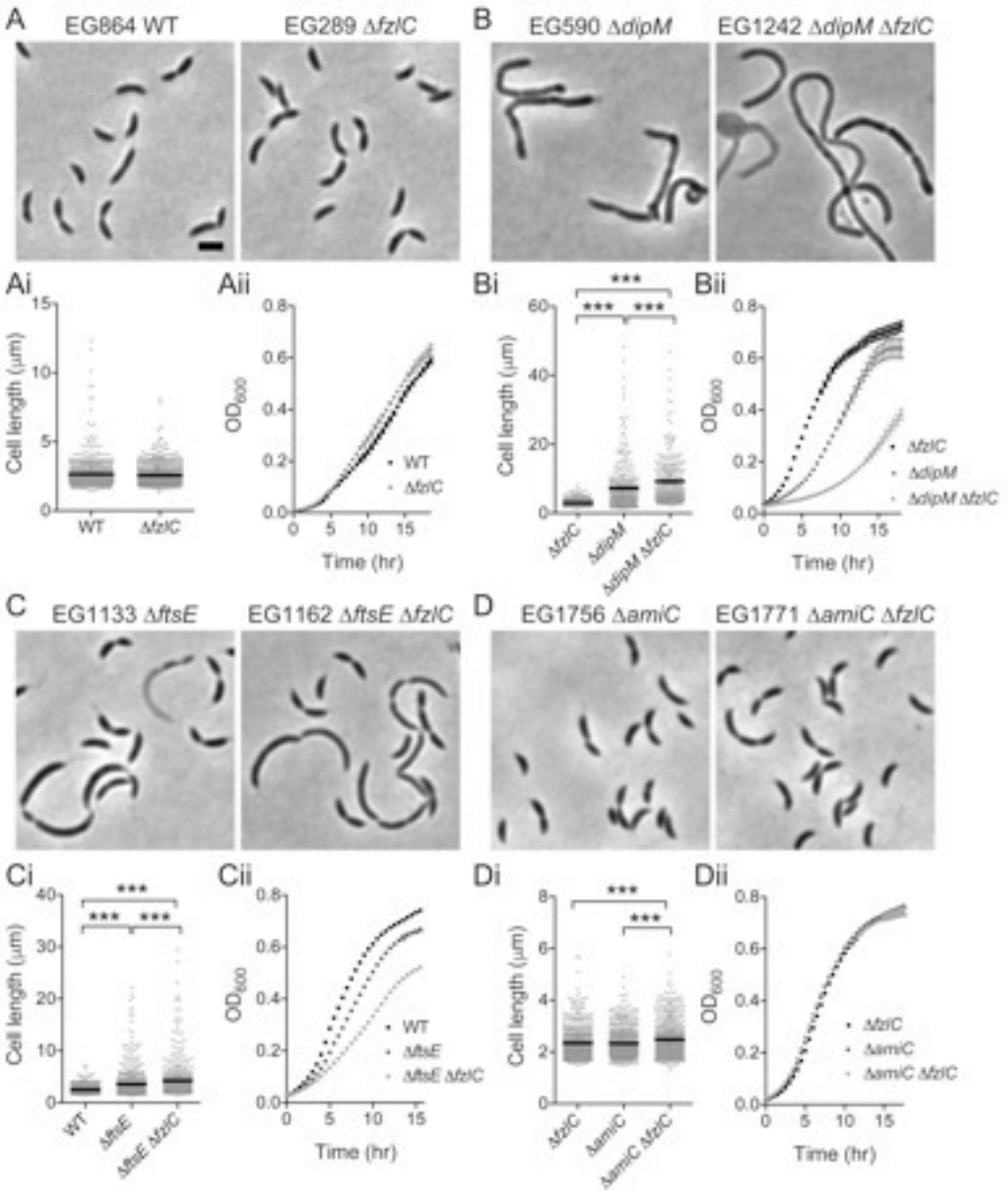

Table 3. Growth rate and cell length of strains in Fig. 2.11

Strain	Description	Doubling time ± SEM (hr)*	Mean cell length ± SEM (μm)†	N
Fig. 2.11A				
EG864	WT	2.14 ± 0.06	2.66 ± 0.04	700
EG289	Δ*fzlC*	2.08 ± 0.05	2.57 ± 0.03	700
Fig. 2.11B				
EG289	Δ*fzlC*	1.59 ± 0.01	3.03 ± 0.03	645
EG590	Δ*dipM*	2.93 ± 0.02	7.29 ± 0.36	347
EG1242	Δ*dipM*Δ*fzlC*	4.51 ± 0.17	9.25 ± 0.39	300
Fig. 2.11C				
EG864	WT	1.65 ± 0.004	2.52 ± 0.03	632
EG1133	Δ*ftsE*	1.88 ± 0.005	3.51 ± 0.10	655
EG1162	Δ*ftsE*Δ*fzlC*	2.60 ± 0.007	4.20 ± 0.13	585
Fig. 2.11D				
EG289	Δ*fzlC*	1.54 ± 0.05	2.34 ± 0.02	600
EG1756	Δ*amiC*	1.59 ± 0.01	2.32 ± 0.02	600
EG1771	Δ*amiC*Δ*fzlC*	1.53 ± 0.03	2.48 ± 0.03	600

* Fig. 2.11A: EG864 vs EG289 = ns; Fig. 2.11B: EG289 vs EG590, EG289 vs EG1242, EG590 vs EG1242 = $p < 0.001$; Fig. 2.11C: EG864 vs EG1133, EG864 vs EG1162, EG1133 vs EG1162 = $p < 0.001$; Fig. 2.11D: EG289 vs EG1756, EG289 vs EG1771, EG1756 vs EG1771 = ns ANOVA Tukey's Multiple Comparison Test

† Fig. 2.11A: EG864 vs EG289 = ns Mann Whitney test; 2.11B: EG289 vs EG590, EG289 vs EG1242, and EG590 vs EG1242 = $p < 0.001$; Fig. 2.11C = EG864 vs EG1133, EG864 vs EG1162, and EG1133 vs EG1162 = $p < 0.001$; Fig. 2.11D = EG289 vs EG1756 = ns, EG289 vs EG1771 and EG1756 vs EG1771 = $p < 0.001$ ANOVA Tukey's Multiple Comparison Test; N refers to sample size for cell length analysis.

Figure 2.12. Z-ring assembly is unaffected in Δ*fzlC* cells but aberrant in Δ*ftsE* cells. (A) Merged fluorescent (yellow) and phase contrast (blue) micrographs of cells with xylose-inducible *ftsZ-yfp* at the *xylX* locus in a WT (EG444) or Δ*fzlC* (EG1062) background. Demographs represent normalized signal profiles of FtsZ-YFP in cells arranged by increasing cell length. (B) Merged fluorescent (yellow) and phase contrast (blue) micrographs of cells with vanillate-inducible *ftsZ-cfp* at the vanillate locus in a WT (EG1215), Δ*ftsE* (EG1148), or Δ*ftsE*Δ*fzlC* (EG1168) background. Demographs represent signal profiles of FtsZ-CFP in cells arranged by increasing cell length. Scale bar = 2 μm.

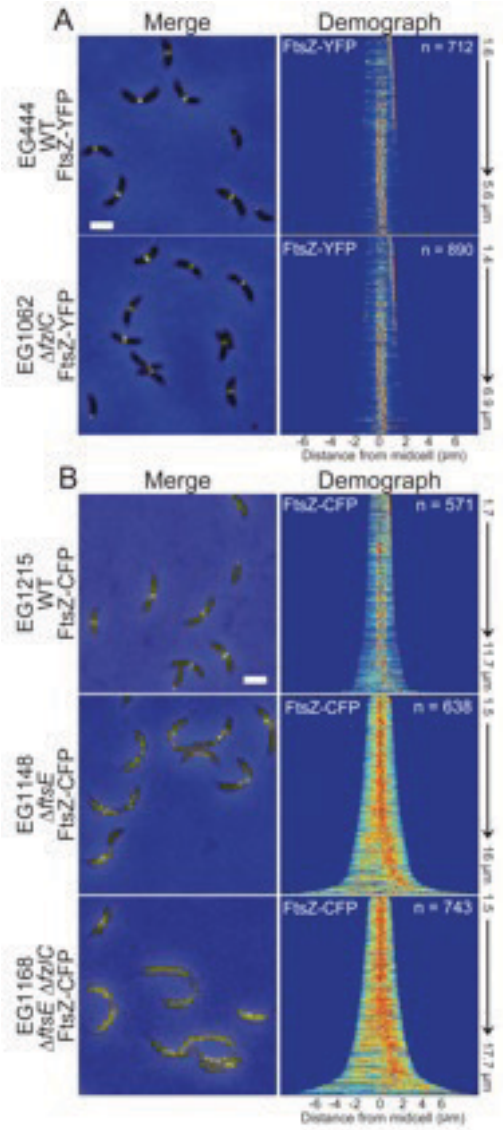

Figure 2.13. *fzlC* does not interact genetically with many non-essential division genes. (A-F) Phase contrast micrographs of cells with or without *fzlC* in WT and in non-essential gene mutant backgrounds. Scale bar = 2 μm. "Δ*5pbp*" = Δ*pbp1a*Δ*pbpY*Δ*pbpC*Δ*pbpZ*Δ*mtgA* (G) Growth curves of Δ*βla* (EG1121, lacking the primary β-lactamase) and Δ*βla*Δ*fzlC* (EG1504) cells treated with cephalexin at sublethal (1.25 μg/mL (C1.25)) or lethal (2 μg/mL (C2)) concentrations. (H) Growth curves of EG1121 and EG1504 treated with mecillinam at sublethal (12 μg/mL (M12)) or lethal (18 μg/mL (M18)) concentrations.

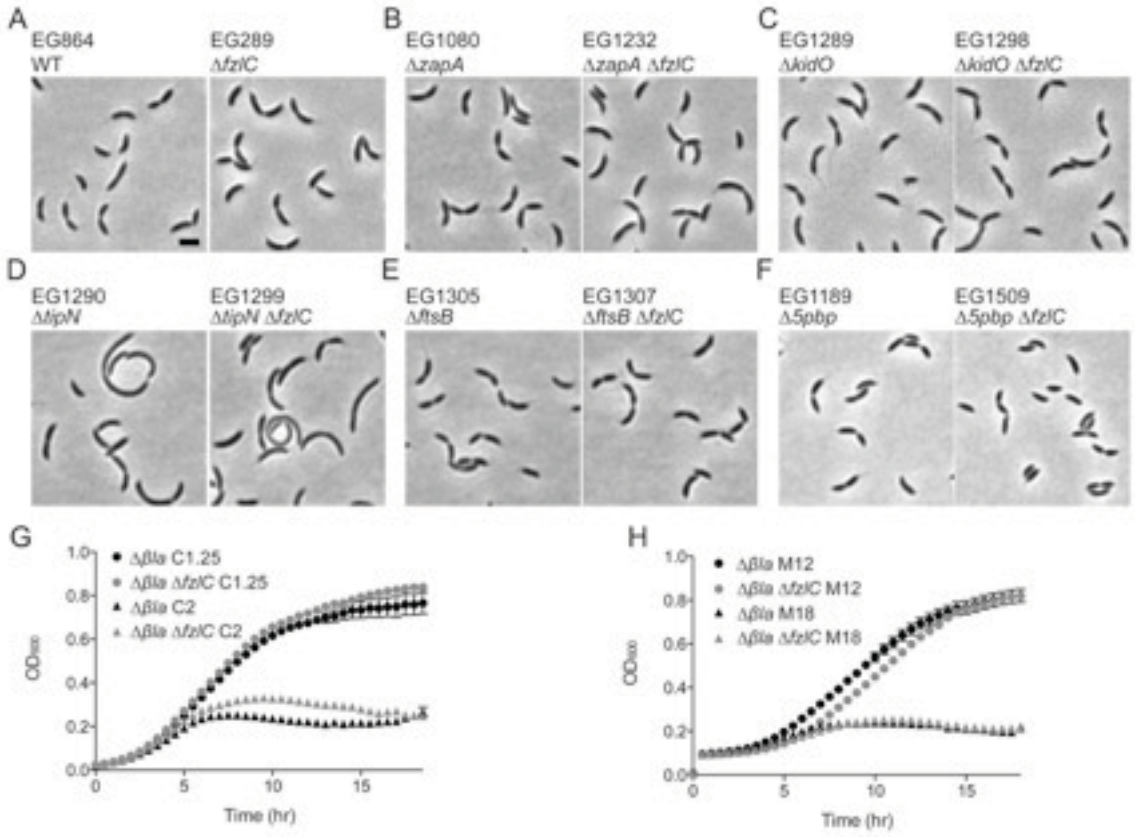

Table 4. Growth rate and cell length of strains in Fig. 2.13

Strain	Description	Doubling time ± SEM (hr) *	Mean cell length ± SEM (μm) †	N
Fig. 2.13B				
EG289	Δ*fzlC*	1.59 ± 0.01	3.02 ± 0.04	600
EG1080	Δ*zapA*	1.82 ± 0.01	2.79 ± 0.04	600
EG1232	Δ*zapA*Δ*fzlC*	1.74 ± 0.01	3.20 ± 0.05	600
Fig. 2.13C				
EG289	Δ*fzlC*	1.55 ± 0.06	2.62 ± 0.03	600
EG1289	Δ*kidO*	1.66 ± 0.04	2.99 ± 0.06	600
EG1298	Δ*kidO*Δ*fzlC*	1.56 ± 0.07	3.08 ± 0.06	600
Fig. 2.13D				
EG289	Δ*fzlC*	1.78 ± 0.05	2.85 ± 0.03	600
EG1290	Δ*tipN*	2.26 ± 0.02	4.37 ± 0.13	600
EG1299	Δ*tipN*Δ*fzlC*	2.26 ± 0.04	4.19 ± 0.11	600
Fig. 2.13E				
EG289	Δ*fzlC*	1.78 ± 0.05	2.85 ± 0.03	600
EG1305	Δ*ftsB*	2.03 ± 0.01	3.02 ± 0.04	600
EG1307	Δ*ftsB*Δ*fzlC*	2.14 ± 0.02	2.83 ± 0.03	600
Fig. 2.13F				
EG289	Δ*fzlC*	1.55 ± 0.005	2.32 ± 0.02	600
EG1189	*Δ5pbp*	1.76 ± 0.02	2.49 ± 0.02	600
EG1509	*Δ5pbpΔfzlC*	1.89 ± 0.03	2.25 ± 0.02	600

* Fig. 2.13B: EG289 vs 1080, EG289 vs EG1232 = p <0.001, EG1080 vs EG1232 = p <0.01; Fig. 2.13C: all strain combinations were ns; Fig. 2.13D: EG289 vs EG1290, EG289 vs EG1299 = p <0.001, EG1290 vs EG1299 = ns; Fig. 2.13E: EG289 vs 1305 = p <0.01, EG289 vs EG1307 = p <0.001, EG1305 vs EG1307 = ns; Fig. 2.13F: EG289 vs EG1189, EG289 vs EG1509 = p <0.001, EG1189 vs EG1509 = p <0.01 ANOVA Tukey's Multiple Comparison Test

† Fig. 2.13B: EG289 vs EG1080, EG1080 vs EG1232 = $p < 0.001$, EG289 vs EG1242 = ns; Fig. 2.13C: EG289 vs EG1289, EG289 vs EG1298 = $p < 0.001$, EG1289 vs EG1298 = ns; Fig. 2.13D: EG289 vs EG1290, EG289 vs EG1299 = $p < 0.001$, EG1290 vs EG1299 = ns; Fig. 2.13E: EG289 vs EG1305, EG1305 vs EG1307 = $p < 0.01$, EG289 vs EG1307 = ns; Fig. 2.13F: EG289 vs EG1189, EG1189 vs EG1509 = $p < 0.001$, EG289 vs EG1509 = ns, ANOVA Tukey's Multiple Comparison Test; N refers to sample size for cell length analysis.

Figure 2.14. Z-rings still assemble and direct new cell wall synthesis in Δ*fzlC* cells. Phase contrast, fluorescent and merged micrographs of cells with xylose-inducible *ftsZ-yfp* at the *xylX* locus in a WT (EG444) or Δ*fzlC* (EG1062) background that were synchronized, pulse-labelled with HADA for 5 min at 30 min post-synchrony, and imaged. In the merged image, FtsZ-YFP is in red and HADA is in green. Demographs represent signal profiles of FtsZ-YFP or HADA in cells arranged by increasing cell length. Scale bar = 2 μm.

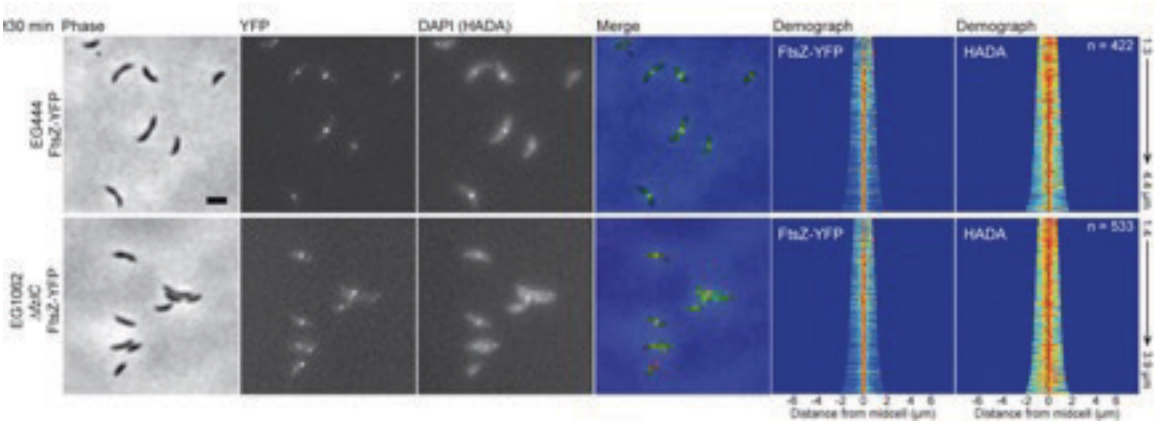

Figure 2.15. High levels of FzlC partially rescue the morphological, growth, and Z-ring structure defects in Δ*ftsE* cells. (A) Phase contrast micrographs of Δ*ftsE* cells with an empty vector (EG1357) or vanillate-inducible *fzlC* overexpression vector (EG1346) grown in the presence of vanillate for 24 h. (B,C) Growth curves and cell lengths of EG1357 and EG1346 cells shown in (A) (*** = $p < 0.001$, one-way ANOVA). (D) Xylose-inducible *ftsZ-yfp* at the *xylX* locus in an EG1357 or EG1346 background. Demographs represent normalized signal profiles of FtsZ-YFP in cells arranged by increasing cell length Scale bars = 2 μm.

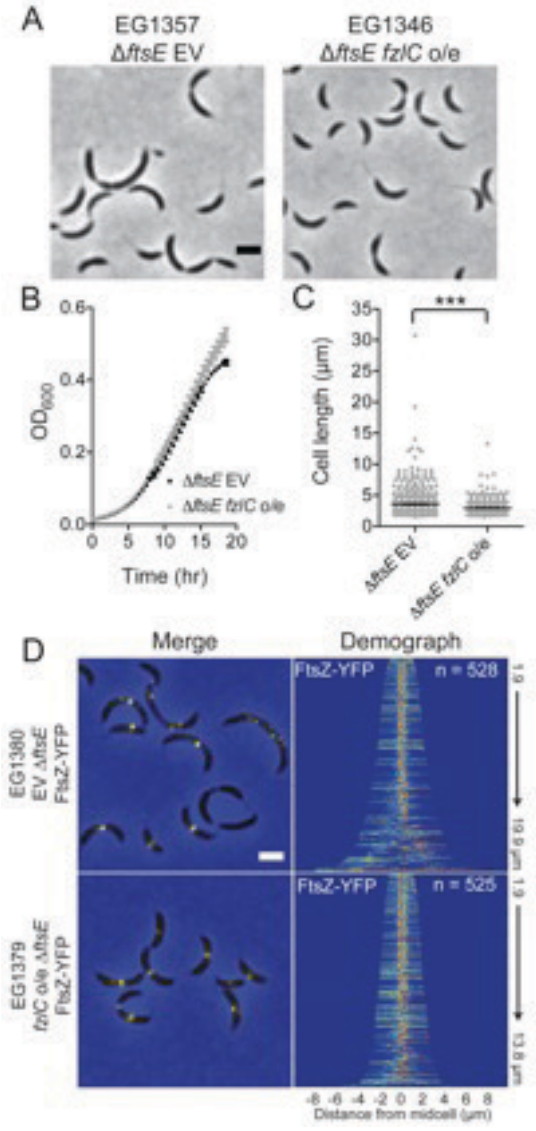

Table 5. Growth rate and cell length of strains in Fig. 2.15

Strain	**Description (24 h o/e)**	**Doubling time ± SEM (hr)***	**Mean cell length ± SEM (μm)†**	**N**
EG1357	Empty vector; Δ*ftsE*	2.91 ± 0.04	3.55 ± 0.08	650
EG1346	*fzlC* o/e vector; Δ*ftsE*	2.84 ± 0.04	2.94 ± 0.04	650
EG1380	Empty vector; Δ*ftsE* *xylX::* P_{xyl}-*ftsZ-yfp*	ND	5.17 ± 0.12	528
EG1379	*fzlC* o/e vector; Δ*ftsE* *xylX::* P_{xyl}-*ftsZ-yfp*	ND	4.02 ± 0.06	525

* EG1357 vs EG1346 = ns unpaired t test, two-tailed

† EG1357 vs EG1346, EG1380 vs EG1379 = *p* value < 0.001 unpaired t test, two-tailed; N refers to sample size for cell length analysis.

Discussion

It is becoming increasingly apparent that the mode of membrane attachment of FtsZ defines a control point for the assembly and function of the Z-ring. Our discovery that FzlC binds and recruits FtsZ to membranes *in vivo* and *in vitro* fulfills the necessary requirements to define it as a new membrane anchor for FtsZ. FzlC recruits FtsZ polymers to membranes in a CTC-dependent manner, placing it in the company of FtsA, ZipA, and SepF in ensuring that FtsZ is positioned with its flexible C-terminal linker separating the polymerizing GTPase domain from the membrane attachment point (Erickson *et al*., 2010; Duman *et al*., 2013). *In vivo*, high levels of FzlC cause defects in growth rate and morphology as well as a moderate alteration in Z-ring structure in constricting cells. Although non-essential, *fzlC* has synthetic interactions with a subset of other non-essential division genes, *dipM*, *ftsE*, and *amiC*: these synthetic effects suggest that FzlC, like these other factors, acts in the regulation of peptidoglycan hydrolysis.

In light of the late arrival of FtsA to the division plane in *C. crescentus*, we originally set out to answer the question of how FtsZ is tethered to the membrane early in the cell cycle. Although we proposed FzlC as an attractive candidate for mediating membrane attachment of FtsZ before the arrival FtsA, Δ*fzlC* cells still assemble Z-rings with localized new cell wall synthesis early in the cell cycle (Figs. 2.12A and 2.14). Moreover, we did not observe a synthetic defect with Δ*fzlC* and loss of *zapA*, an FtsZ-binding protein important for assembly of focused Z-rings (Fig. 2.13B; Buss *et al*., 2013), as would be predicted if FzlC were important for early Z-ring assembly. This implies either that FzlC acts redundantly with another membrane anchor or that membrane

attachment of FtsZ is not strictly required for Z-ring assembly and activity. If the former is true, the most likely candidate is the highly conserved FtsEX ABC transporter complex (Goley *et al*., 2011). The synthetic interaction between *fzlC* and *ftsE* (Figs. 2.11, 2.12, 2.15) further supports the possibility that FtsEX plays a redundant membrane-anchoring role with FzlC and FtsA in *C. crescentus*. Likewise, the ability of FzlC to positively regulate Z-ring assembly in the absence of FtsE underscores FzlC's role as a physiologically relevant membrane anchor. However, the putative activity of FtsEX as an early membrane anchor awaits biochemical and cytological confirmation.

Overproduction of FzlC led to broader Z-rings, especially at extended division sites, and morphological defects consistent with a slowed constriction rate (Figs. 2.8 and 2.10). This phenotype is markedly different from overproduction of FtsA, which causes filamentation and formation of Z-rings that are non-functional for constriction (Fig. 2.10C). These observations reinforce the idea that all membrane anchors are not functionally equivalent, even if they bind FtsZ and membranes in similar ways. Depletion of FtsA causes cells to grow into filaments with deep, broad constrictions similar in morphology to those in FzlC-overproducing cells (Martin *et al*., 2004). We postulate that excess FzlC, which is normally present at very low levels, competes with FtsA for binding to the CTC of FtsZ, titrating away FtsZ that is normally free to bind FtsA and complete constriction. Interestingly, replacing the native copy of *fzlC* with an N-terminal *mChy-fzlC* fusion increases FzlC levels and mimics the overexpression phenotype (Fig. 2.9). This mCherry tag could potentially mask an N-terminal degron sequence, which normally promotes high turnover of FzlC and contributes to the low WT protein levels. It

is possible that FzlC is upregulated or stabilized to control cytokinesis under particular environmental conditions. However, a survey of common stresses including temperature, osmotic stress, oxidative stress, and starvation has not revealed a condition under which FzlC is upregulated or essential.

The specific synthetic interactions between deletion of *fzlC* and loss of *dipM*, *ftsE*, and *amiC* implicate FzlC in pathways impinging on cell wall hydrolysis. Cell wall hydrolase activity is particularly important in the late stages of cytokinesis, where hydrolases are required to split the peptidoglycan that holds the two daughter cells together (Lee *et al*., 2013). Though incompletely understood, coupling between Z-ring constriction and cell wall hydrolase activity was first proposed in *E. coli*. In that organism, local activation of the cell wall amidases, AmiA and AmiB, at the division site requires EnvC (Uehara *et al*., 2010), which is in turn activated by FtsX (Meisner *et al*., 2013). The activity of FtsX is proposed to be regulated by its partner, FtsE. Since FtsE is thought to directly interact with FtsZ, this series of interactions may transmit information about the state of the Z-ring to cell wall hydrolases in the periplasm, allowing for coordinated membrane and cell wall invagination (Yang *et al*., 2011).

Though the details of these interactions differ from organism to organism, activation of cell wall hydrolysis by FtsX appears to be a conserved mechanism for regulating envelope constriction (Sham *et al*., 2011; Meisner *et al*., 2013; Mavrici *et al*., 2014). In *C. crescentus*, splitting of septal peptidoglycan occurs synchronously with peptidoglycan synthesis and inner membrane constriction, rather than being delayed, as it is in *E. coli*

and *B. subtilis* (Judd *et al*., 2005). However, relatively little is known about the molecular mechanisms regulating these processes. In particular, the identity of the hydrolase regulated by FtsX in *C. crescentus*, if it exists, is unknown: there are no clear homologs of AmiA, AmiB, or EnvC encoded in its genome. Complicating matters further, DipM is a LytM family protein similar to *E. coli* NlpD, which activates the amidase, AmiC, yet DipM does not activate AmiC in *C. crescentus* (Goley *et al*., 2010a; Moll *et al*., 2010). The phenotypes associated with loss of DipM, AmiC, or FtsE are dissimilar (Fig. 2.11), suggesting that these factors act in distinct, though perhaps partially redundant, pathways in this organism. While our genetic interaction analyses did not reveal which hydrolase(s) FzlC may ultimately activate, its synthetic interactions reinforce the concept of coordination between Z-ring activity and cell wall splitting and identify a novel route from FtsZ to the cell wall via FzlC membrane attachment.

It has long been hypothesized that in *E. coli* FtsZ must be attached to the membrane to assemble stable Z-rings (Pichoff *et al*., 2002). At least in *C. crescentus*, however, the CTC appears to be dispensable for Z-ring formation as Z-rings still form in cells expressing FtsZΔCTC and depleted of full-length FtsZ (Fig. 2.7; Sundararajan *et al*., 2015). As all known membrane-tethering proteins bind FtsZ through the CTC, these observations indicate that membrane attachment is not strictly necessary for Z-ring assembly. However, in *C. crescentus*, Z-rings containing FtsZΔCTC were non-functional and dominant negative, indicating loss of essential CTC binding partners and/or an important role for membrane attachment beyond stable Z-ring assembly (Fig. 2.7). The transduction of FtsZ-based constrictive force to the inner membrane and/or the coupling

of Z-ring structure and dynamics with cell wall remodeling are likely candidates for downstream events requiring membrane-tethered FtsZ. Further supporting the connection between membrane-associated FtsZ and the cell wall, the SepF homolog recently identified in *M. tuberculosis* was reported to bind not only FtsZ and membranes, but also MurG, an essential enzyme in the synthesis of the lipid II peptidoglycan precursor (Gupta *et al*., 2015). Our data demonstrate that the function of FzlC similarly transcends passive membrane anchoring, as it helps to translate "inside" Z-ring dynamics to "outside" cell wall remodeling events. These findings support a paradigm in which membrane anchors for FtsZ are key regulators in the coordinated constriction of the cell envelope during bacterial cytokinesis.

Materials and Methods

Bacterial strains and growth conditions

C. crescentus NA1000 strains were grown in peptone yeast extract (PYE) medium at 30^{o}C (Sundararajan *et al*., 2015). Additives and antibiotics were used at the following concentrations in liquid (solid) media for *C. crescentus*: xylose 0.3 (0.3)%, glucose 0.2 (0.2)%, vanillate 0.5 (0.5) mM, gentamycin 1 (5) μg ml^{-1}, kanamycin 5 (25) μg ml^{-1}, spectinomycin 25 (100) μg ml^{-1}, streptomycin (5 μg ml^{-1}), cephalexin 1.25 and 2 μg ml^{-1} and mecillinam 12 and 18 μg ml^{-1}. Before changes in induction conditions, cells were washed two to three times in plain media. Growth rate analyses were performed in 96-well plates with shaking at 30^{o}C using a Tecan Infinite 200 Pro plate reader. *E. coli* strain BL21-Gold(DE3) was grown in Luria-Bertani (LB) broth at 30^{o}C. Antibiotics were used at the following concentrations for *E. coli*: ampicillin 50 μg ml^{-1} and tetracycline 12 μg ml^{-1}. Small-scale synchrony of *C. crescentus* cells was performed as in (Goley *et al*., 2011).

Heterologous E. coli expression system

E. coli strain BL21-Gold(DE3) was transformed with a plasmid for arabinose inducible expression of *cfp-fzlC* (pEG908). To continuously maintain the cultures in log phase, a single colony was inoculated into fresh LB in the morning and grown at 30^{o}C until the OD_{600} reached ~0.1. *cfp-fzlC* expression was then induced with 1% L-arabinose for 2 h at 30^{o}C and imaged.

Light microscopy and image analysis

Cells were imaged during the log phase of growth after immobilization on 1% agarose pads. Light microscopy was performed on a Nikon Eclipse Ti inverted microscope equipped with a Nikon Plan Fluor x 100 (numeric aperture 1.30) oil Ph3 objective and Photometrics CoolSNAP HQ cooled CCD (charge-coupled device) camera. Chroma filter cubes were used as follows: ET-EYFP for YFP and ET-ECFP for CFP, ET-dsRED for mCherry and rhodamine and ET-DAPI for HADA. Images were processed in Adobe Photoshop. Automated cell length analysis was performed using MicrobeTracker (Sliusarenko *et al*., 2011). Algorithm 4 was used for determining cell outlines, with the following parameter change: areaMin=150. Principal component analysis was performed using CellTool (Pincus *et al*., 2007). Binary masks of phase contrast images were generated in ImageJ and manually curated in Adobe Photoshop to remove signal from incomplete cells at the edges of the field, from cells that were touching, or from debris. The shape model was built to capture 99% of the variation in the *fzlC*-overexpressing and empty vector populations. FWHM of Z-ring width in cells overexpressing *fzlC* was determined by manually drawing a line through Z-rings in constricted cells in ImageJ and using an ImageJ macro to fit a Gaussian to the intensity profile and calculate the FWHM of the Gaussian.

Antibodies and immunoblotting

Purified *C. crescentus* His_6-FzlC was used to immunize a rabbit for antibody production (Josman, LLC). To affinity purify the antibody, His_6SUMO-FzlC was coupled to Affigel 10 resin and incubated with serum. FzlC-specific antibodies were serially eluted with 0.2 M glycine pH 2.5 and 6 M guanidine, and dialyzed into Tris-buffered saline. The

guanidine elution had higher specificity and was used for all future immunoblots. Specificity for FzlC was demonstrated by immunoblotting lysates from strains with *fzlC* deleted or overexpressed and observing elimination or amplification, respectively, of the signal at the expected molecular weight of FzlC (predicted 61 kDa; for example, Fig. 2.2 and 2.9). For immunoblotting against whole-cell lysates, cells were harvested in the log phase of growth and lysed in SDS-PAGE loading buffer by boiling for 5 min. SDS-PAGE and transfer of protein to nitrocellulose membrane were performed using standard procedures. FtsZ antiserum was used at 1:20,000 dilution (Sundararajan *et al*., 2015). FzlC antibody was used at 1:2,000 or 1:5,000 dilutions. SpmX antiserum was used at 1:50,000 dilution (Radhakrishnan *et al*., 2008). HU antiserum was used at 1:5,000 dilution (Bowman *et al*., 2010).

Protein purification

FtsZ and FtsZ variants were overproduced and purified as described previously (Goley *et al*., 2010b) with slight modifications. Rosetta (DE3) pLysS *E. coli* cells bearing constructs for expression of FtsZ (pEG012), His_6-FtsZ-CFP (pEG448), or His_6-FtsZΔCTC-CFP (pEG1170) were grown in LB at 37°C to OD_{600} of 0.8-1.0 before induction with 0.5 mM isopropylthiogalactoside (IPTG) for 3-4 h. Cells were harvested by centrifugation at 6,000*g* for 10 min at 4°C, resuspended in 30 mL Buffer QA (50 mM Tris-HCl pH 8.0, 50 mM KCl, 1 mM EDTA, 1 mM β-mercaptoethanol and 10% glycerol) per 0.5 to 1 liter of culture, snap-frozen in liquid nitrogen and stored at -80°C until purification. Cell suspensions were thawed at 37°C, one Mini Complete Protease Inhibitor tablet (Roche) was added per 30 mL, lysozyme was added to 1 μg ml^{-1},

phenylmethyl sulphonyl fluoride (PMSF) was added to 2 mM and DNase I (New England Biolabs) was added to 2 units ml^{-1} final concentrations. Cell suspensions were incubated for 30-60 min at room temperature or 4°C, sonicated, and centrifuged at 15,000*g* for 30 min at 4°C. Supernatant was filtered and loaded on two HiTrap Q HP 5 mL columns (GE Life Sciences) joined in tandem and equilibrated in Buffer QA. Protein was eluted using a linear KCl gradient from 50 to 500 mM over 20 column volumes. Peak fractions containing FtsZ were combined and ammonium sulfate was added to 20% saturation. Ammonium sulfate precipitate was recovered with centrifugation at 10,000*g* for 10 min at 4°C. Precipitates were either stored on ice overnight or immediately resuspended in FtsZ Storage Buffer (50 mM HEPES-KOH pH 7.2, 50 mM KCl, 0.1 mM EDTA, 1 mM β-mercaptoethanol and 10% glycerol) and consequently applied to a Superdex 200 10/300 GL (GE Life Sciences) equilibrated in FtsZ Storage Buffer. Peak fractions were combined, concentrated if necessary, snap-frozen in liquid nitrogen, and stored at -80°C.

To purify His_6-SUMO-FzlC, Rosetta (DE3) pLysS *E. coli* cells bearing plasmid pEG605 were grown at 30°C to OD_{600} of 0.8-1.0 before induction with 30 μM IPTG overnight at 15°C (Guo *et al*., 2007). Cells were harvested by centrifugation at 6,000*g* for 10 min at 4°C, resuspended in 30 mL FzlC Column Buffer A (50 mM Tris-HCl pH 8.0, 1 M KCl, 20 mM imidazole, 1 mM β-mercaptoethanol, and 20% glycerol) per 0.5 to 1 liter of culture, snap-frozen in liquid nitrogen and stored at -80°C until purification. Cell suspensions were thawed at 37°C and lysozyme was added to 1 μg ml^{-1}, $MgCl_2$ was added to 2.5 mM and DNase I (New England Biolabs) was added to 2 units ml^{-1} final

concentrations. Cell suspensions were incubated for 30-60 min on ice, sonicated, and centrifuged at 15,000*g* for 30 min at 4°C. Supernatant was filtered and supplemented with 3 mM ATP before loading on a HisTrap FF 1 mL column (GE Life Sciences) equilibrated in FzlC Column Buffer A. Protein was eluted at 30% FzlC Column Buffer B (same as Column Buffer A except 1 M imidazole). Peak fractions containing His_6-SUMO-FzlC were combined and His_6-Ulp1 (SUMO-protease) was added at 1:100 (protease:His_6-SUMO-FzlC) molar ratio. The His_6-SUMO tag was cleaved while dialyzing into FzlC Column Buffer A overnight at 4°C. Cleaved FzlC was incubated with Ni^{2+} Sepharose (GE Healthcare) for 1h at 4°C after which the flow-through was collected. The Ni^{2+} Sepharose was then washed 3 times with 1 mL FzlC Column Buffer A. The flow-through and wash fractions containing FzlC were dialyzed overnight at 4°C in FzlC Storage Buffer (50 mM Tris-HCl pH 8.0, 300 mM KCl, 0.1 mM β-mercaptoethanol, and 10% glycerol), concentrated if necessary, snap-frozen in liquid nitrogen, and stored at -80°C.

To purify His_6-YFP-FzlC, Rosetta (DE3) pLysS *E. coli* cells were transformed with pEG420. The induction, harvesting, and lysis were the same as for His_6-SUMO-FzlC. After centrifugation, the cleared supernatant was filtered and loaded on a HisTrap FF 1 mL column (GE Life Sciences) equilibrated in FzlC Column Buffer A. Protein was eluted with a linear gradient (1-100%) of FzlC Column Buffer B (same as Column Buffer A except 1 M imidazole). Peak fractions containing His_6-YFP-FzlC were combined and applied to a Superdex 200 10/300 GL column (GE Life Sciences) equilibrated in FzlC

Storage Buffer. Peak fractions were combined, concentrated if necessary, snap-frozen in liquid nitrogen, and stored at -80^{o}C.

Cell fractionation

C. crescentus cells were fractionated as described previously (Jenal *et al*., 1994) with slight modifications. 10 mL cultures of EG864 and EG1445 were grown in PYE to log phase and cells were centrifuged at 3,500*g* for 10 min. The pellets were resuspended in 1 mL Tris-HCl pH 7.5 and spun at maximum speed on a tabletop centrifuge for 2 min at 4^{o}C. The pellets were resuspended in 1 mL lysis buffer (10 mM Tris-HCl pH 7.5, 1 mM EDTA, 250 μg ml^{-1} lysozyme) and incubated at room temperature for 10 min. 8 μl of DNase was added and the cells were sonicated on ice. After centrifugation at 4,000*g* for 10 min at 4^{o}C to remove intact cells, the supernatants were harvested and incubated on ice for 1h. The lysates were centrifuged at 150,000*g* for 2h at 4^{o}C. The supernatants were collected as the soluble "cytoplasmic fractions" and the pellets were subsequently washed twice with 10 mM Tris-HCl pH 7.5. The final pellets were resuspended in SDS-PAGE loading buffer with the same volumes as the soluble fractions and treated as the "membrane fractions."

Liposome preparation and sedimentation assay

Phosphatidylglycerol (PG) and/or L-α-phosphatidylcholine (Egg, Chicken PC) (Avanti Polar Lipids) in chloroform were transferred to glass tubes, dried under nitrogen gas, and placed under vacuum for at least 1h to remove residual chloroform. The lipids were resuspended in TK300 buffer (50 mM Tris-HCl pH 8.0, 300 mM KCl) and, if sucrose-

loading the liposomes, sucrose was added to 170 mM final concentration. The glass tubes with resuspended lipids were covered in parafilm to prevent evaporation, incubated for at least 30 min at 42^{o}C and sonicated and vortexed briefly every 10 min until the resuspended lipids appeared completely uniform. The multilamellar vesicles were then extruded with a 100 nm pore membrane. Sucrose-loaded vesicles were diluted at least 5X with non-sucrose containing TK300 buffer and centrifuged at 90,000*g* in a Beckman TLA-55 rotor in a table-top ultracentrifuge for 1h at 25^{o}C. The supernatant was discarded and the pellet containing the sucrose-loaded liposomes was resuspended in the appropriate volume of TK300. The resuspended liposomes were stored at 4^{o}C for up to 2 weeks.

Sucrose-loaded liposomes (100 nm) of different percentages of PG and PC were prepared as described above in TK300 buffer. FzlC was quickly thawed and spun at 115,000*g* at 4^{o}C for 15 min in a Beckman TLA-100 rotor and TL-100 ultracentrifuge to remove aggregates. FzlC (2 μM) was added to a suspension of 400 μM sucrose-loaded liposomes in TK300 buffer. Reactions were incubated at room temperature for 15 min. Sucrose-loaded vesicles were sedimented by centrifugation at 115,000*g* for 30 min at 25 ^{o}C. 90% of the supernatant was collected and 4X SDS-PAGE loading buffer was added to make a 1X mixture. The pellet was resuspended in 1X SDS-PAGE loading buffer to the same volume as the supernatant brought to 1X. The fraction of FzlC in the pellet was determined by running the samples on a SDS-PAGE gel, staining with Coomassie blue, and performing densitometry on the bands.

Lipid preparation and GUV fabrication

Giant unilamellar vesicles were fabricated using the inverted emulsion technique (Pautot *et al*., 2003; Luo *et al*., 2014). For the inside monolayer 1-palmitoyl-2-oleoyl-*sn*-glycero-3-phosphocholine (POPC) and 1-hexadecanoyl-2-(9Z-octadecenoyl)-*sn*-glycero-3-phospho-(1'-*rac*-glycerol) (POPG) at a 1:1 (wt:wt) ratio, and for the outer layer L-α-phosphatidylcholine (Egg, Chicken PC) and 1-palmitoyl-2-oleoyl-*sn*-glycero-3-phospho-L-serine (POPS) at a 4:1 (wt:wt) ratio were aliquoted. All lipids were purchased from Avanti in their chloroform-solubilized form. Chloroform was evaporated overnight and the lipids were dissolved in hexadecane at 65 °C for 3 hours to obtain a 1 mg/ml stock solution. A 100 µl reaction containing YFP-FzlC, CFP-FtsZ, FtsZΔCTC-CFP or a combination of YFP-FzlC with either of the other two proteins were mixed with 10 mM phosphate-buffered saline (PBS) pH 7.6 and sucrose to obtain a 2 µM final concentration of each protein. $MgCl_2$ and GTP were added depending on the experimental condition. This solution was mixed with the inner leaflet-lipids and agitated for aqueous droplet formation. This phase was centrifuged (2500*g* for 6 min) over a stabilized monolayer of outer lipids that formed on top of a glucose solution. The GUVs were collected by punching a hole in the bottom of the centrifuge tube. Matching molar concentrations of glucose and sucrose were used to balance the osmotic pressure.

GUV imaging and image analysis

100 µl of GUVs were transferred to an 8-well plate and the GUVs were imaged with an inverted epi-fluorescence microscope (Axiovert135TV, ZEISS) using a 40X oil objective. QIClick charge-coupled camera (QImaging) was used to collect the

fluorescence images. Exposure time was 10-50 ms depending on the channel and the intensity of the detected signal.

Image analysis was performed using MetaMorph®. Background fluorescent signal was subtracted from each GUV. A line scan was used to measure the fluorescent intensity across the diameter of each GUV. For YFP-FzlC and FtsZ-CFP +/- GTP conditions, this value was normalized based on the maximum signal intensity detected for each vesicle to enable comparison of signal between GUVs of different sizes. To determine the variation in protein co-localization across different GUV populations statistical analysis in *Prism*® was performed. The length and fluorescence intensity of each GUV was normalized. A cubic spline function was used to fit a fluorescent intensity curve for each vesicle. Standard deviation of this intensity was then calculated among a population of 18 GUVs.

FRET

FtsZ-CFP or FtsZΔCTC-CFP and/or YFP-FzlC (2 μM final concentration) were added to TK300 buffer. $MgCl_2$ was used at 2.5 mM, GTP was used at 2 mM and PG vesicles were used at 1 mg/mL. A Fluoromax-3 spectrofluorometer (Jobin Yvon Inc.) was used for fluorescence measurements. The solution was excited at 435 nm (CFP excitation) and scanned for emission from 450-560 nm. FRET/CFP ratios were determined by dividing peak YFP emission (523-528 nm) by peak CFP emission (472-477 nm).

FtsZ activity assays

FtsZ GTPase activity assay was performed in HEK50 buffer (50 mM HEPES-KOH pH 7.2, 300 mM KCl, and 0.1 mM EDTA). GTPase activity was assayed using the SensoLyte MG Phosphate Assay Kit (AnaSpec) following the manufacturer's protocol. The GraphPad Prism software was used to fit curves and determine GTPase rates.

Right angle light scattering was performed as described previously (Sundararajan *et al.*, 2015).

TEM was performed as in (Sundararajan *et al*., 2015) with the following modifications: FtsZ and/or YFP-FzlC were used at 4 μM and the reaction buffer was TK300.

HADA labeling

Cells from strains EG444 and EG1062 were grown for 1 h in PYE with xylose to induce *ftsZ-yfp* expression, synchronized, and the swarmers were released in fresh PYE. HADA (Kuru *et al*., 2012) was added to 0.41 mM after 30 min and cells were fixed and imaged as in (Sundararajan *et al*., 2015).

CHAPTER 3

FtsEX-mediated regulation of the late stages of cell division reveals morphogenetic plasticity in *Caulobacter crescentus*

Note: The majority of the information presented in this chapter was included in the publication:

Meier EL, Daitch AK, Yao Q, Jensen GJ, Goley ED. FtsEX-mediated regulation of the late stages of cell division reveals morphogenetic plasticity in *Caulobacter crescentus*. PLOS Genetics. 2017; In review.

Introduction

Bacteria are capable of adopting an impressive array of shapes exquisitely tuned for their particular environmental niches. Underpinning these shapes is the bacterial cell wall, which plays an essential role in specifying and maintaining diverse morphologies (Jiang *et al*., 2015). The cell wall consists of a layer of peptidoglycan (PG) composed of glycan strands of repeating disaccharide subunits crosslinked by pentapeptide bridges. In addition to adapting to changing environments, the PG also undergoes dynamic remodeling to drive shape changes during dedicated cellular processes such as division (Typas *et al*., 2011; Woldemeskel and Goley, 2017).

The α-proteobacterium *Caulobacter crescentus* is an ideal model organism for the study of cell shape as it undergoes a series of coordinated morphogenetic changes during its cell cycle. After every division event, *C. crescentus* produces two distinct daughter cell types. One is a flagellated, motile swarmer cell, which contains a flagellum and pili at one cell pole (Curtis and Brun, 2010). The other is a sessile stalked cell, where the polar flagellum has been replaced by a thin, tubular extension of the cell envelope known as a stalk (Curtis and Brun, 2010). Unable to replicate its chromosome or initiate cell division, a swarmer cell differentiates into a stalked cell by ejecting its flagellum, disassembling its pili, and growing a stalk at the same pole (Curtis and Brun, 2010). A stalked cell then elongates its cell body, replicates and segregates its DNA, and produces a flagellum at the pole opposite its stalk prior to cytokinesis. The asymmetric polarization of distinct organelles imparts *C. crescentus* with a highly tractable dimorphic life cycle ideally suited for studying developmental shape changes.

One cell cycle event that requires obvious reshaping of the cell envelope is cell division, which, in nearly all bacteria, requires the conserved tubulin homolog FtsZ. A GTPase, FtsZ polymerizes into a patchy annular structure (the Z-ring) at the incipient division site and recruits the downstream division machinery or divisome. Together, FtsZ and proteins of the divisome coordinate invagination and fission of the membrane(s) with extensive cell wall remodeling (Meier and Goley, 2014). A number of division proteins are known to interact directly with FtsZ. For many of these regulators, however, their mechanism of action toward FtsZ and physiological role in division remain to be discovered. One division complex that has been particularly enigmatic is the ATP-binding cassette (ABC) transporter family complex FtsEX, which is widely conserved in bacteria and functions as a heterodimer with FtsE in the cytoplasm and FtsX in the inner membrane. In *Escherichia coli*, FtsEX localizes to the septum and contributes to the efficiency of cell division, particularly in salt-free media (Schmidt *et al*., 2004). There is no evidence that FtsEX acts as a transporter, however, and recent studies from a wide range of bacteria have instead implicated FtsEX in the activation of cell wall hydrolysis (Sham *et al*., 2011; Sham *et al*., 2013; Yang *et al*., 2011; Meisner *et al*., 2013; Mavrici *et al*., 2014). Septal PG material needs to be split to allow for outer membrane constriction and ultimately for separation of the two new daughter cells. In high salt media, *E. coli* Δ*ftsEX* cells exhibit a phenotype similar to cell wall hydrolysis mutants, i.e. cells are chained and mildly filamentous, suggesting a common genetic pathway (Yang *et al*., 2011).

In addition to its involvement in cell wall hydrolysis, in *E. coli*, FtsEX is important for the recruitment of late division proteins and the assembly and/or stability of the septal ring (Schmidt *et al*., 2004). Interestingly, *E. coli ftsE* mutants impaired for ATP binding and hydrolysis support Z-ring assembly, but constrict poorly (Arends *et al*., 2009). Since FtsE interacts with FtsZ in *E. coli*, one possibility is that FtsEX functions as a membrane anchor for FtsZ and utilizes ATP binding and hydrolysis to regulate Z-ring constriction (Schmidt *et al*., 2004; Corbin *et al*., 2007).

In this study, we were originally motivated to characterize FtsEX as a novel membrane anchor for FtsZ in *C. crescentus* since FtsE is one of the first proteins recruited to the nascent division site and is important for efficient cell separation and Z-ring assembly and/or stability (Goley *et al*., 2011; Meier *et al*., 2016). Considering the conserved function of FtsEX as a modulator of cell wall remodeling, we asked whether FtsEX, in addition to promoting Z-ring structure, regulates cell wall cleavage in *C. crescentus*. We find that *ftsE* has strong synthetic cell separation defects with cell wall hydrolytic factors. Interestingly, however, deleting *ftsE* produces chains of cell bodies connected by thin, tube-like connections that contain all layers of the cell envelope. This is in stark contrast to the thick, uncleaved septa and compartmentalized cytoplasms observed in hydrolysis mutants from *E. coli* and other organisms. The cell-cell connections of Δ*ftsE* cells are, instead, morphologically and topologically similar to *C. crescentus* stalks. In accordance with their shared morphological features, the stalk proteins StpX and PbpC localize to both the skinny connections and stalks of Δ*ftsE* cells, indicating that stalk formation may be mechanistically similar to the elaboration of the extended constriction sites. Our data

reveal unanticipated morphogenetic plasticity in *C. crescentus*, with a stalk-like program taking over at failed division sites in the Δ*ftsE* mutant to yield novel cell morphology.

Results

Δ*ftsE* cells form chains connected by skinny constrictions

To begin to address the role of FtsEX in *C. crescentus*, we first attempted to make *ftsE* and *ftsX* deletion strains. Although *ftsE* is annotated as essential (Christen *et al*., 2011; Goley *et al*., 2011), we successfully made several independent Δ*ftsE* clones (Meier *et al*., 2016). *ftsX* is also annotated as essential (Christen *et al*., 2011), but unlike *ftsE*, we were unable to make an *ftsX* deletion, depletion, or overexpression strain, suggesting that *C. crescentus* cells are highly sensitive to changes in FtsX levels. To understand the role of the FtsEX complex in *C. crescentus* morphogenesis, we focused on characterizing the *ftsE* mutant in detail. Δ*ftsE* cells displayed a striking division phenotype consisting of chained cells with skinny, extended connections between cell bodies. Consistent with the chaining phenotype, Δ*ftsE* cells are longer and grow more slowly than WT (Meier *et al*., 2016). Transmission electron microscopy (TEM) offered us better resolution of cells lacking FtsE (Fig. 3.1). Δ*ftsE* cell bodies were heterogeneous in length, but overall appeared elongated compared to WT, which suggests a delay or inefficiency in the initiation of constriction. The thin connections between Δ*ftsE* cell bodies were also heterogeneous in length, with some extending hundreds of nanometers, and had dimensions qualitatively similar to those observed for stalks (Fig. 3.1B). Overall, the Δ*ftsE* phenotype supports a role for FtsE both in the initiation of constriction and in late stage cell separation.

Figure 3.1. Transmission electron microscopy (TEM) of chained Δ*ftsE* cells with thin, extended connections between cell bodies. (A) Micrograph of WT cells. (B) Micrographs of Δ*ftsE* cells. * = stalk; # = skinny connection. Scale bar = 2 um.

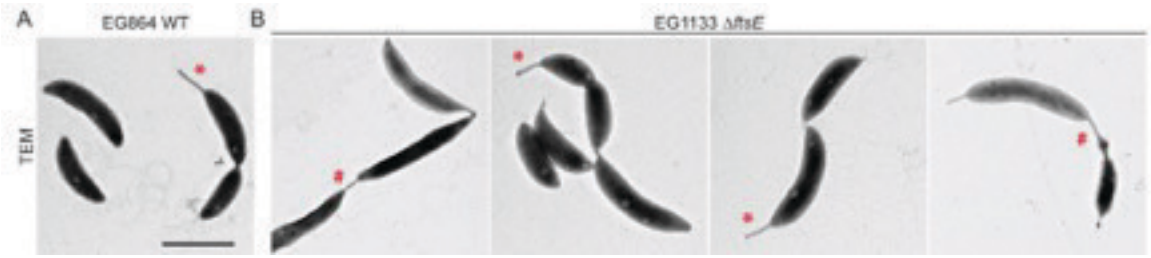

FtsE promotes focused Z-ring organization

FtsE has been reported to bind FtsZ in *E. coli*, is one of the first division proteins to localize to midcell after FtsZ in *C. crescentus*, and *C. crescentus* Δ*ftsE* cells have aberrant Z-rings (Corbin *et al*., 2007; Goley *et al*., 2011; Meier *et al*., 2016). Specifically, in Δ*ftsE* cells FtsZ is more diffuse and often localizes as clusters of puncta instead of focused Z-rings (Fig. 3.2) (Meier *et al*., 2016). These data suggest that FtsE may regulate early Z-ring structure and/or assembly. Consequently, we tested if *ftsE* interacted genetically with the positive Z-ring regulator *zapA*, which, like FtsE, is also recruited early to midcell by FtsZ in *C. crescentus* (Goley *et al*., 2011; Buss *et al*., 2013). Δ*zapA*Δ*ftsE* cells displayed mild synthetic growth and cell length defects, but had severely disrupted, diffuse Z-ring structures (Fig. 3.2). We also observed that Δ*zapA*Δ*ftsE* cells were very sensitive to even slight increases in FtsZ-CFP levels and were noticeably filamentous after only one hour of *ftsZ-cfp* expression (Fig. 3.2D). We conclude that FtsE contributes to proper Z-ring focusing at midcell and that the elongated cell bodies in Δ*ftsE* are likely due to inefficient initiation of constriction by the aberrant FtsZ structures.

Figure 3.2. *ftsE* has synthetic growth, cell length, and Z-ring structural defects with Z-ring regulator *zapA*. (A) Phase contrast micrographs of Δ*ftsE*, Δ*zapA*, and Δ*ftsE*Δ*zapA* cells. (B) Growth curves of strains in (A). Doubling time (h) ± SEM: EG1080 = 1.78 ± 0.01; EG1133 = 1.81 ± 0.02; EG1745 = 1.86 ± 0.02. Differences between strain doubling times were ns by one-way ANOVA. (C) Cell length analyses of strains in (A). Mean cell length (μm) ± SEM: EG1080 = 2.54 ± 0.03; EG1133 = 3.50 ± 0.11; EG1745 = 3.94 ± 0.10. All pairwise comparisons of mean cell lengths yielded p values < 0.01 by one-way ANOVA. (D) FtsZ-CFP localization after 1 h of induction in WT, Δ*ftsE*, Δ*zapA*, and Δ*ftsE*Δ*zapA* cells. # = focused Z-ring; * = diffuse, punctate Z-ring. Scale bars = 2 μm.

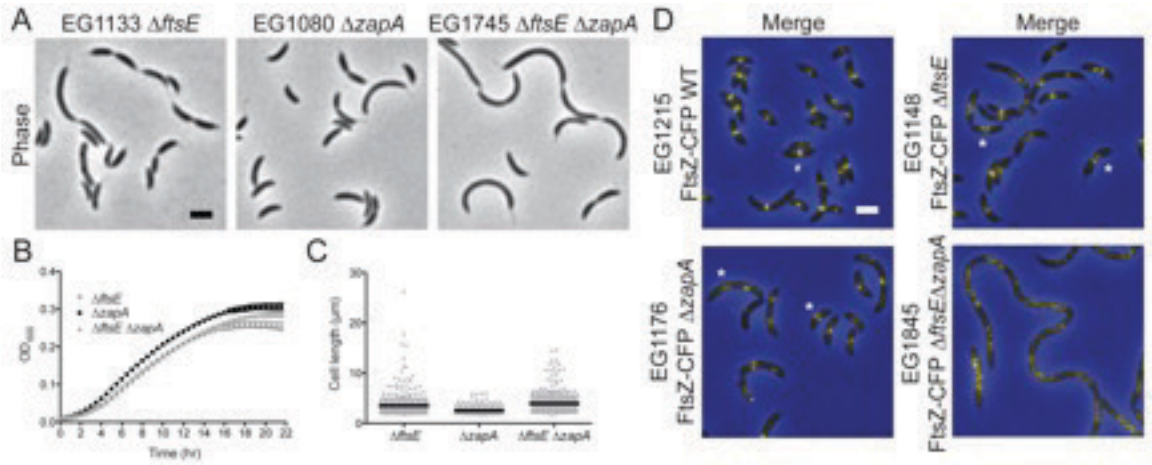

Excess FtsE or FtsEX alters the localization of FtsZ and new cell wall synthesis

Because cells lacking FtsE have perturbed Z-ring organization, we hypothesized that overproducing FtsE would affect Z-ring structure, particularly if FtsE binds directly to FtsZ. Overexpression of either *ftsE* or *ftsEX* caused dramatic filamentation, and overexpression of *ftsE* alone also caused ectopic poles to form (Fig. 3.3). After four hours of FtsE overproduction, instead of Z-rings, FtsZ-CFP formed discrete puncta along the length of the filamentous cells (Fig. 3.3A). Interestingly, when we overproduced FtsEX, FtsZ-CFP localized in a drastically different pattern, as multiple wide bands (Fig. 3.3A). *C. crescentus* Z-ring positioning is in part dictated by a negative regulator of FtsZ assembly called MipZ, which forms a complex near the origin of replication (Thanbichler and Shapiro, 2006). After the polar origin region is duplicated, the second copy is quickly transported to the opposite cell pole. Bipolar MipZ thereby directs Z-ring assembly at midcell by inhibiting FtsZ polymerization at the poles (Thanbichler and Shapiro). MipZ-YFP localized at the poles and as fairly regularly spaced puncta in cells overproducing FtsE or FtsEX, but its localization was more diffuse in cells overproducing FtsEX (Fig. 3.3B). We interpret the MipZ localization data as evidence that chromosomal replication and segregation still occur in cells overproducing FtsE despite the inhibition of division; however high levels of FtsEX may interfere with levels or localization of MipZ.

In *C. crescentus*, FtsZ directs new cell wall synthesis at midcell even before the onset of division (Fig. 3.3C) (Aaron *et al*., 2007). To determine if the FtsZ structures in FtsE or FtsEX overproducing cells were competent to localize new cell wall synthesis, we pulse-

labeled cells with the fluorescent D-amino acid hydroxycoumarin-carbonyl-amino-D-alanine (HADA), which can replace D-Ala^4 or D-Ala/Gly^5 in the lipid II peptide side chain, to track the incorporation of newly synthesized PG (Kuru *et al*., 2012). High levels of FtsE resulted in diffuse HADA labeling which closely resembled the pattern of HADA incorporation in FtsZ-depleted cells (Fig. 3.3C). This result suggests that the FtsZ puncta associated with *ftsE* overexpression are unable to direct local cell wall metabolism. Cells overexpressing *ftsEX,* however, had discrete, wide bands of new PG incorporation, likely directed by the similarly organized Z-ring structures (Fig. 3.3C). Thus, high levels of FtsE or FtsEX not only differentially affect Z-ring organization, but also affect FtsZ's ability to locally incorporate new cell wall material at midcell. Specifically, the intact FtsEX complex is required both for formation of Z-rings and downstream communication with PG synthetic machinery.

Figure 3.3. Overproducing FtsE or FtsEX causes filamentation and affects the localization of FtsZ and new PG. (A) FtsZ-CFP localization after 1 h of induction in cells bearing an empty vector (EV) or overexpressing *ftsE* or *ftsEX* for 4 h. (B) MipZ-YFP localization in cells bearing and EV or overexpressing *ftsE* or *ftsEX* for 4 h. (C) HADA labeling of cells depleted for FtsZ for 4 h, bearing an EV, or overexpressing *ftsE* or *ftsEX* for 4 h. * = ectopic poles. Scale bars = 2 μm.

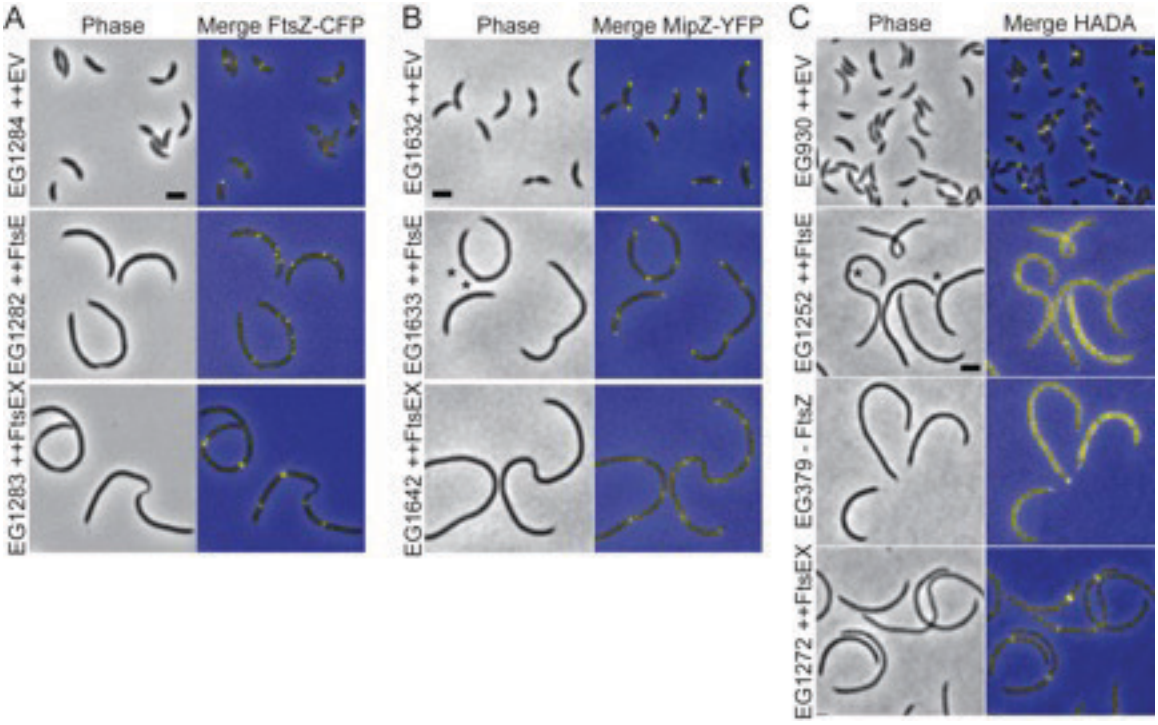

ftsE interacts genetically with PG hydrolytic factors and a regulator of stalked pole development

Since FtsEX has been implicated in cell wall hydrolysis in numerous bacteria and Δ*ftsE* cells displayed a cell chaining phenotype, we asked whether FtsEX, in addition to promoting Z-ring structure, regulates *C. crescentus* cell wall hydrolysis. In *E. coli*, periplasmic *N*-acetylmuramyl-$_L$-alanine amidases AmiA/B/C are responsible for cleaving bonds that link stem peptides to glycan strands at the septum (Heidrich *et al*., 2001). The amidases require activation by the LytM domain containing proteins EnvC, which stimulates AmiA/B, and NlpD, which stimulates AmiC, to split apart septal PG (Uehara *et al*., 2009; Uehara *et al*., 2010). FtsEX directly recruits EnvC to the septum via the periplasmic extracellular loop (ECL) of FtsX and the coiled coil (CC) domain of EnvC (Yang *et al*., 2011). *C. crescentus* possesses a limited number of lytic enzymes involved in peptidoglycan remodeling, with only a single *N*-acetylmuramyl-$_L$-alanine amidase, most similar to *E. coli* AmiC (Nierman *et al*., 2001; Moll *et al*., 2010). There are at least seven genes coding for putative LytM domain containing proteins; however, the only characterized protein in the *C. crescentus* LytM family is DipM, which participates in cell wall remodeling and coordinated constriction of the cell envelope layers at the division plane (Goley *et al*., 2010a; Moll *et al*., 2010; Pogglio *et al*., 2010). To determine whether the FtsEX PG hydrolysis paradigm applies to *C. crescentus*, we performed a BLAST search for *E. coli* EnvC homologues and found CCNA_03547, which we will hereafter refer to as *L*ytM *d*omain *p*rotein *F* (LdpF) (Martin Thanbichler, personal communication). Like EnvC, LdpF is a LytM domain containing protein with a signal peptide, two N-terminal CC domains, and a C-terminal LytM domain (Fig. 3.4A). We

hypothesized that *C. crescentus* FtsEX-LdpF-AmiC may function in an activation pathway analogous to *E. coli* FtsEX-EnvC-AmiA/B.

We first adopted a genetic approach to investigate the role of FtsEX in cell wall hydrolysis during division. In *E. coli*, FtsEX is required for EnvC's localization at midcell (Yang *et al*., 2011). However, LdpF-mCherry is diffuse, and we did not observe differences in its localization between WT and Δ*ftsE* cells (Fig. 3.4B). Although *E. coli* cells lacking EnvC or AmiA/B are not as sick as cells lacking FtsEX, part of the division defect associated with loss of FtsEX may be due to EnvC inactivation (Yang *et al*., 2011). Consistent with this reasoning, in *C. crescentus*, cells lacking LdpF or AmiC had mild chaining and growth defects compared to Δ*ftsE* cells (Fig. 3.5). Depleting AmiC in Δ*ftsE* or Δ*ldpF* backgrounds caused strong synthetic cell separation and growth defects, accompanied by noticeable lengthening of the skinny connections between cell bodies, particularly in the *ftsE* mutant (Fig. 3.5). Combining Δ*ldpF* with loss of FtsE produced only mild synthetic growth and chaining defects, which is consistent with them acting in a common pathway (Fig. 3.5).

Figure 3.4. *In vivo* LdpF-mCherry has a diffuse, patchy localization in WT and Δ*ftsE*. (A) Predicted domain organization of *E. coli* EnvC and *C. crescentus* LdpF. (B) Localization of LdpF-mCherry induced for 4 h in WT or Δ*ftsE*. Abbreviations are as follows: SS = signal sequence; CC = coiled coil domain; LytM = LytM domain. Scale bar = 2 μm.

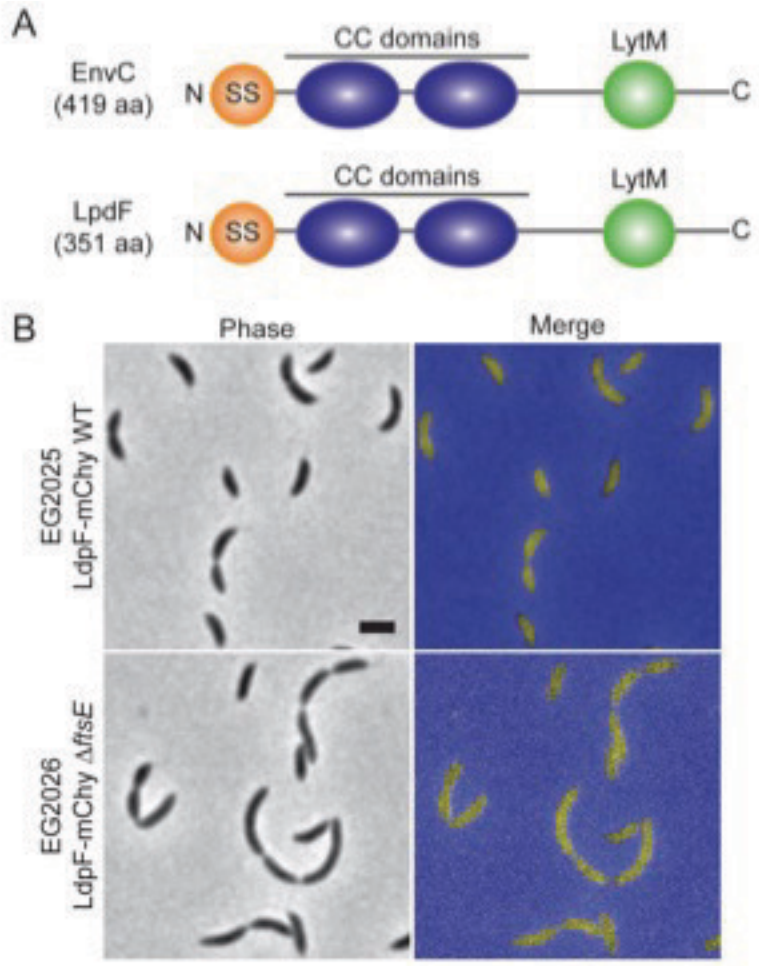

Figure 3.5. Synthetic genetic interactions between *amiC*, *ftsE*, and *ldpF*.

Phase contrast micrographs and serial spot dilutions of (A) WT, Δ*ftsE*, and Δ*ldpF*; (B) WT and Δ*ftsE* cells depleted for AmiC for 24 h; (C) WT and Δ*ldpF* cells depleted for AmiC for 24 h; (D) WT and Δ*ldpF* cells depleted for FtsE for 24 h. Scale bar = 2 μm.

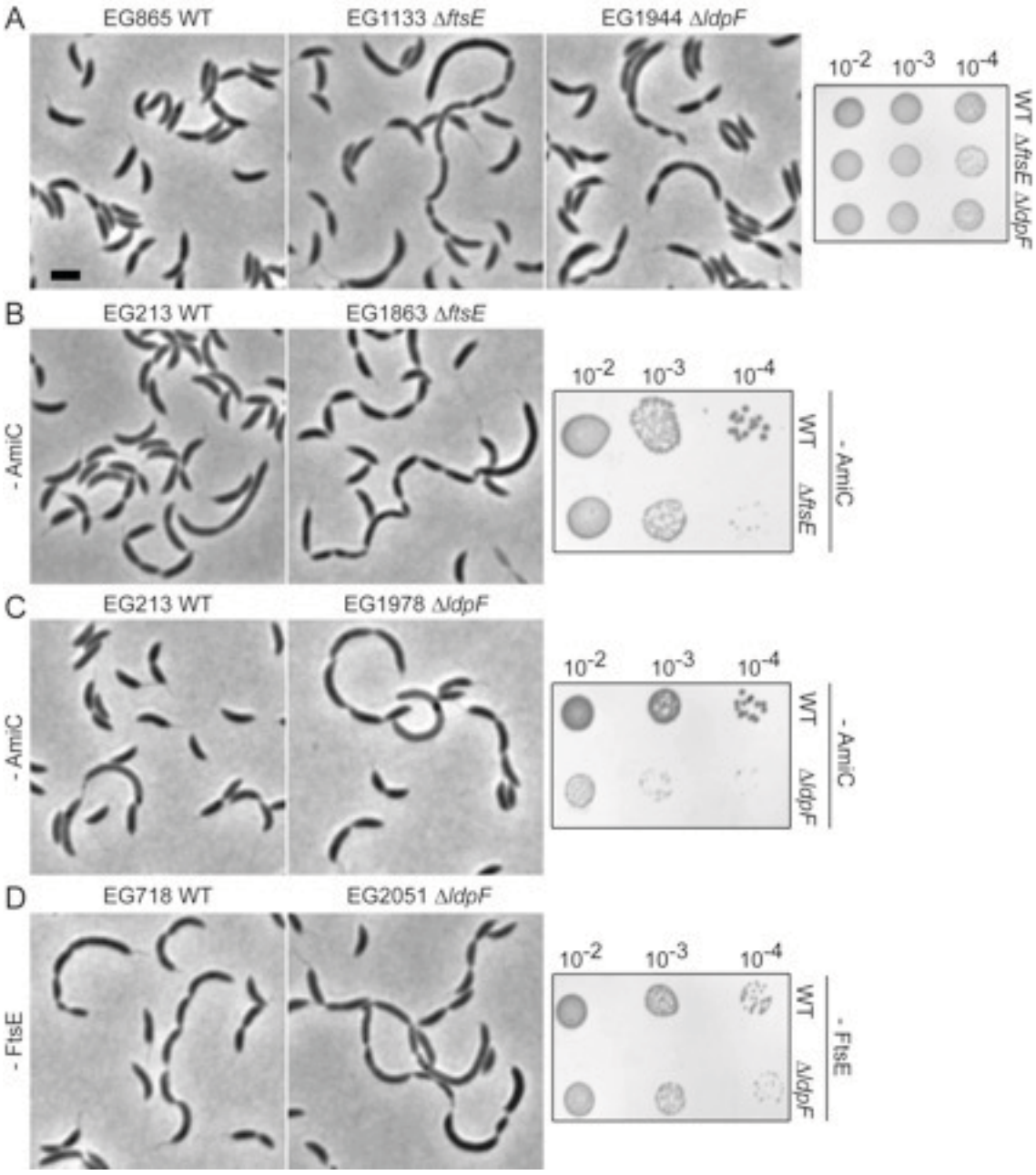

E. coli cells lacking EnvC depend on NlpD for cell separation: simultaneous inactivation of either EnvC or FtsEX and NlpD results in severe chaining, supporting the hypothesis that FtsEX activates EnvC's ability to promote septal PG cleavage (Uehara *et al*., 2009). In *C. crescentus*, the LytM protein most closely related to NlpD is DipM, which has similar domain organization to NlpD but differs in that it is not associated with the outer membrane. Depleting AmiC in cells lacking DipM caused a moderate synthetic growth defect, whereas depletion of DipM in Δ*ftsE* or Δ*ldpF* cells was synthetic lethal (Fig. 3.6). The synthetic defects associated with loss of DipM with FtsE, LdpF, or AmiC as well as the distinct morphology of Δ*dipM* cells (Goley *et al*., 2010a; Moll *et al*., 2010; Pogglio *et al*., 2010) suggests that DipM operates in a non-redundant, parallel hydrolytic pathway. We also hypothesize, based on the strong synthetic interactions between AmiC and FtsE or LdpF but only mild synthetic defects associated with loss of FtsE and LdpF, that AmiC operates in a hydrolytic pathway separate from FtsE and LdpF. However, it is apparent that all three putative PG hydrolytic pathways contribute to the efficiency of cell separation in *C. crescentus*.

Interestingly, in a transposon deep-sequencing analysis to uncover transposon insertions that alter the competitive fitness of Δ*spmX* cells, the *ftsE* and *ldpF* loci were the first and second least favored insertion sites, respectively, in Δ*spmX* cells as compared to WT (Janakiraman *et al*., 2016). We therefore tested for synthetic interactions between *ftsE* and *spmX*, which encodes a muramidase homolog that localizes to the stalked cell pole and controls the swarmer-to-stalk cell transition (Radhakrishnan *et al*., 2008). Consistent with the Δ*spmX* transposon deep-sequencing results, we observed severe synthetic growth and

morphological defects for Δ*ftsE*Δ*spmX* cells, implicating FtsE and LdpF in the stalked pole development pathway, likely through a connection to cell wall remodeling (Fig. 3.6E).

Figure 3.6. Synthetic genetic interactions between *dipM* and *amiC*, *ftsE*, or *ldpF* and between *ftsE* and *spmX*. Phase contrast micrographs and serial spot dilutions of (A) WT, Δ*ftsE*, and Δ*dipM*; (B) WT and Δ*dipM* cells depleted for AmiC for 24 h; (C) WT and Δ*ftsE* cells depleted for DipM for 24 h; (D) WT and Δ*ldpF* cells depleted for DipM for 24 h; (E) Δ*spmX* and Δ*ftsE*Δ*spmX*. Scale bar = 2 μm.

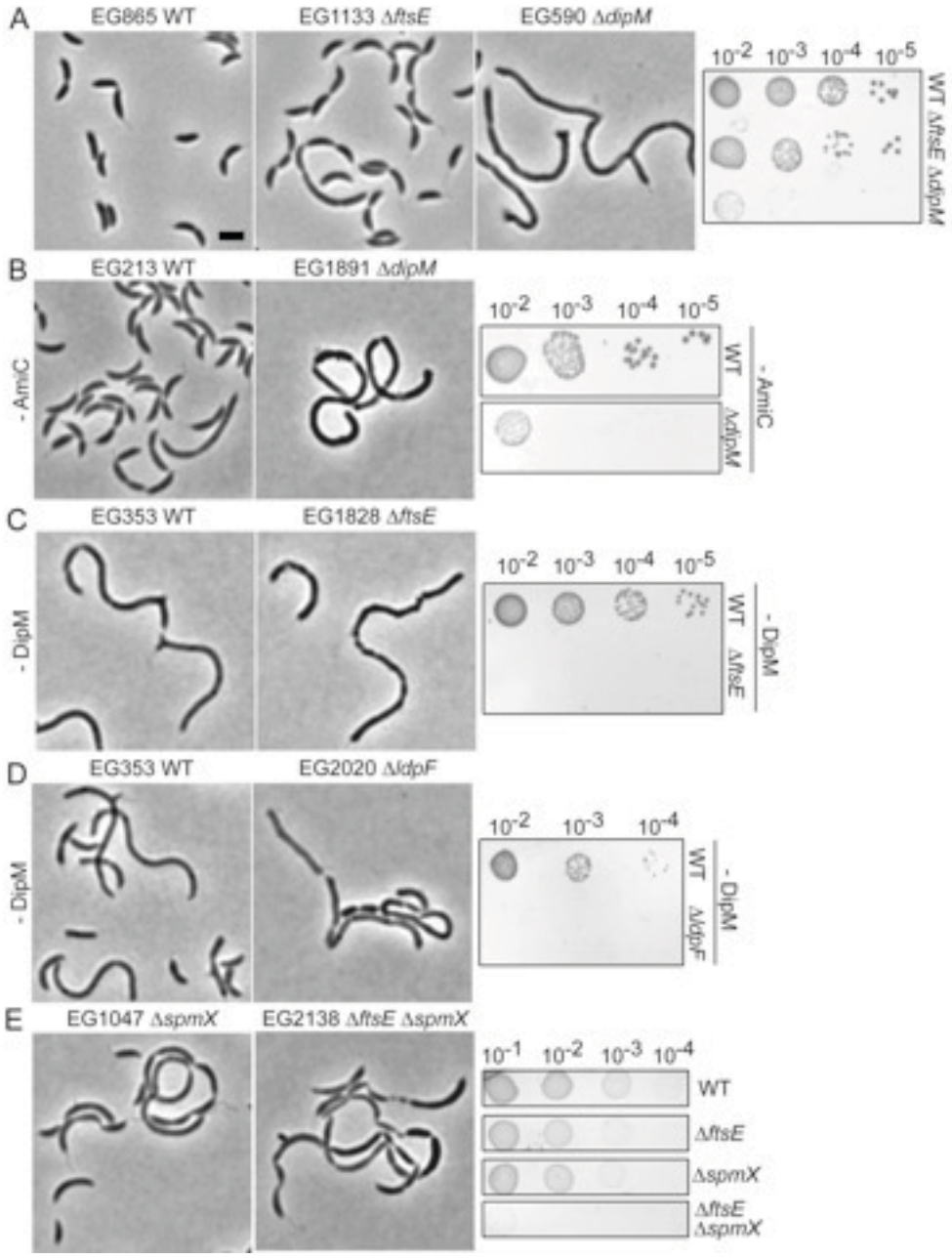

The CC domain of LdpF interacts with the ECL of FtsX, but LdpF does not activate AmiC PG hydrolysis *in vitro*

To provide biochemical support for our *in vivo* findings, we purified LdpF, AmiC, DipM, and the ECL of FtsX, and monitored PG degradation using an *in vitro* dye release assay (Zhou *et al*., 1988; Uehara *et al*., 2010). Although bacterial two hybrid showed a positive interaction for the ECL of FtsX and the CC domain of LdpF, we did not observe LdpF-activated AmiC PG hydrolysis *in vitro* (Fig. 3.7). Interestingly, the LytM domain of DipM was sufficient to mildly stimulate AmiC hydrolase activity *in vitro* (Fig. 3.7C). However, as *C. crescentus* DipM and AmiC are most similar to the *E. coli* activator-amidase pair, NlpD and AmiC, perhaps this result is unsurprising. In light of the distinct phenotypes of cells lacking DipM and AmiC, however, we suspect that DipM has activities in addition to the regulation of AmiC. Collectively, our genetic and biochemical evidence indicate at least three hydrolytic pathways in *C. crescentus* and implicate a yet unidentified downstream target of FtsEX-LdpF in the regulation of PG metabolism.

Figure 3.7. LdpF binds the extracellular loop (ECL) of FtsX but does not activate AmiC *in vitro*. (A) Bacterial two-hybrid of T18 and T25 fusions to the ECL of FtsX, the coiled coil domain (CC) of LdpF, and the CC cytoplasmic protein ZauP, which was used as a negative control. (B,C) Dye release assay with RBB-labeled sacculi and purified variants of AmiC, LdpF, DipM, and the ECL of FtsX. Each protein was used at 4 μM and reactions were incubated at 30°C for 3 h. Reactions were performed in triplicate. *** = $p < 0.0001$ by one-way ANOVA.

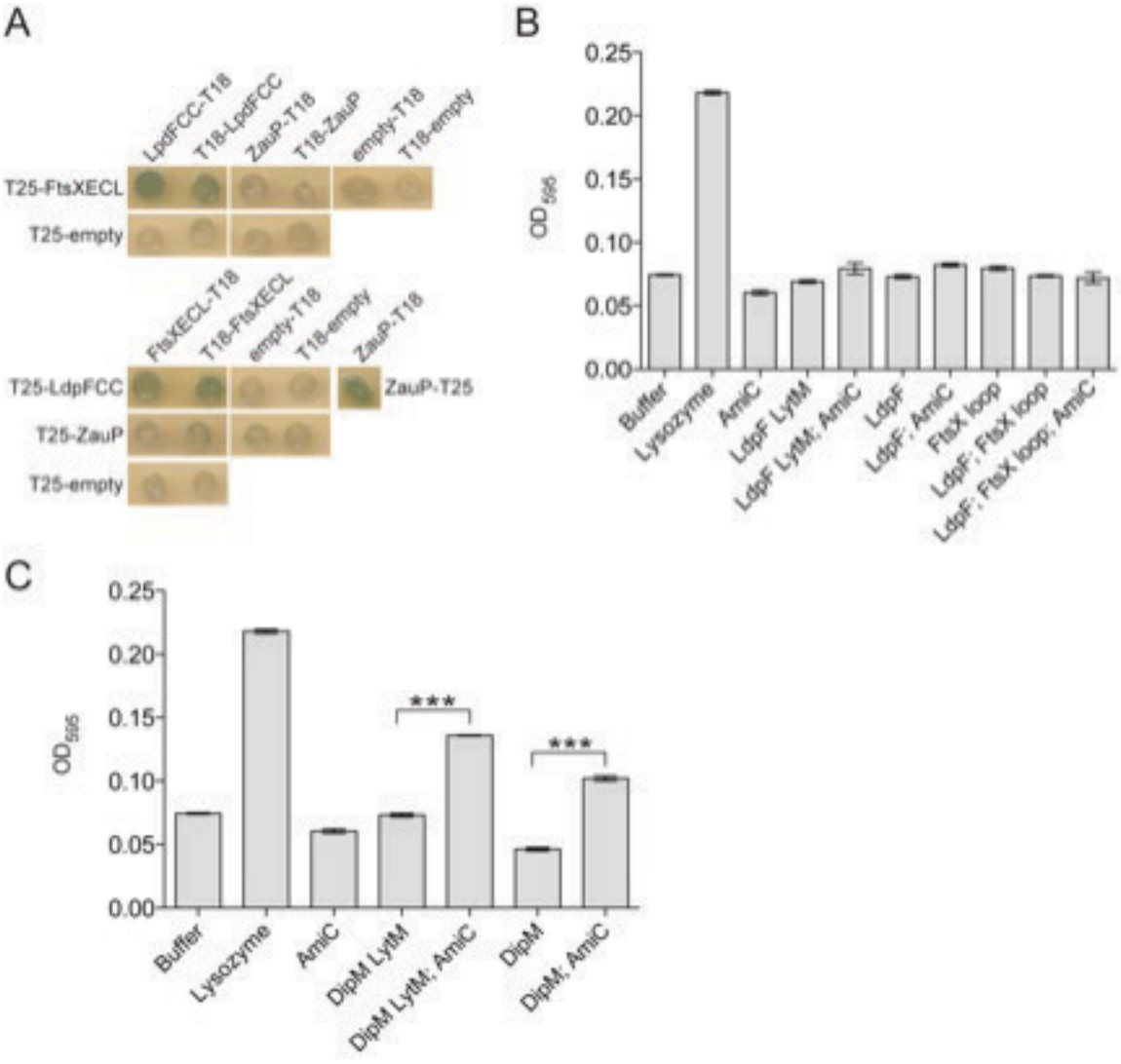

Electron cryotomography reveals unique cell envelope organization at chaining sites

Our genetic evidence is consistent with a role for FtsEX in regulating cell wall hydrolysis for cell separation. Although TEM highlighted the general cell separation defects of Δ*ftsE* cells (Fig. 3.1), electron cryotomography (ECT) allowed us to dissect the exact stages at which these cells are blocked during division (Fig. 3.8). To capture the cell envelope organization at the skinny cell-cell connections, we imaged cells lacking both FtsE and AmiC since loss of AmiC exacerbates the Δ*ftsE* chaining phenotype (Fig. 3.5). In five out of six tomograms, we could identify with certainty the presence of all layers of the cell envelope in the skinny connections between chained cell bodies (Fig. 3.8). Four of these had obvious cytoplasmic volume between the unfused inner membranes. In at least one example, however, the inner membranes were closely stacked on top of each other, but not fused (Fig. 3.8).

In WT *C. crescentus*, the final stages of inner membrane fission are rapid, and the smallest diameter for inner membrane connections that have been captured by ECT are ~60 nm (Judd *et al*., 2005). In cells lacking FtsE and AmiC with fairly uniform connections (Fig. 3.8B, D), we observed inner membrane diameters ranging from ~12 to 60 nm. Others were more variable and had intermittent bulging, with inner membrane diameters ranging from ~20 to 300 nm within a single cell-cell connection (Figs. 3.8C, 3.9). This organization of the cell envelope is strikingly different from other mutants deficient in cell wall hydrolysis. *E. coli* cells lacking EnvC and NlpD or all four LytM-domain containing factors complete inner membrane fusion and cytoplasmic compartmentalization, but struggle to constrict their outer membrane due to a layer of

intact PG between adjacent chained cells (Uehara *et al*., 2009). Similarly, Δ*dipM* cells form chains with fused inner membranes and thick, multilayered PG between cell bodies (Goley *et al*., 2010a; Moll *et al*., 2010). Therefore, the cell envelope organization of cells lacking FtsE and AmiC, namely the continuous cytoplasmic connections and narrow spacing between the inner membranes, represents a unique cell separation phenotype and, potentially, a novel pathway for cell separation in *C. crescentus.*

Figure 3.8. Electron cryotomography (ECT) of cells lacking FtsE and AmiC reveal stalk-like connections between cell bodies. (A) WT *C. crescentus* stalk with cross-bands. (B) *ftsE* mutants with skinny connections most similar to stalks. (C) *ftsE* mutants with skinny connections that are stalk-like, but that have regions with heterogeneous widths. (D) *ftsE* mutants with skinny connections that are fairly short with inner membranes that are close together or nearly fused. Abbreviations are as follows: OM = outer membrane, PG = peptidoglycan, IM = inner membrane. # = cross-band; * = cross-band-like structure. Scale bar (A) = 200 nm; Scale bars (B-D) = 100 nm.

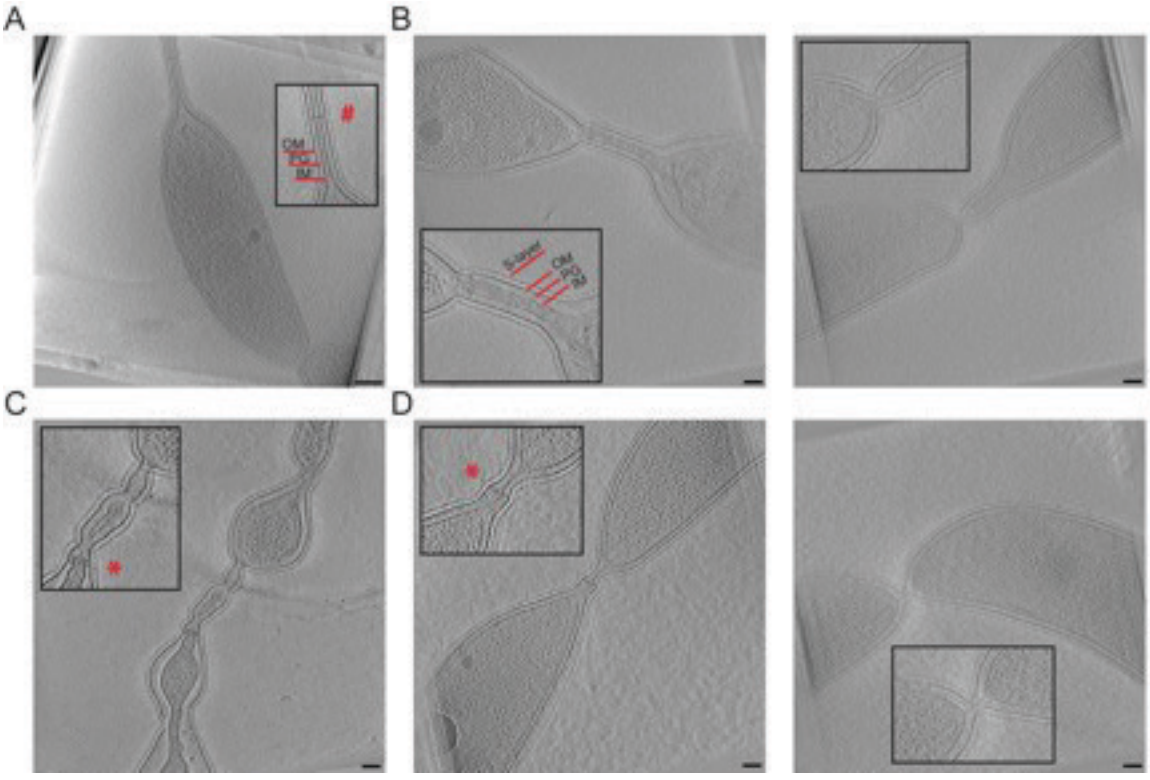

Δ*ftsE* thin connections are morphologically stalk-like and enriched for stalk proteins

During its dimorphic life cycle, *C. crescentus* elaborates a polar stalk, a tubular extension of the cell envelope important for nutrient uptake (Wagner *et al*., 2007). ECT of cells lacking FtsE and AmiC reinforced an observation we had previously made based on TEM of Δ*ftsE*, namely, the striking morphological similarities between the extended connections of *ftsE* mutants and *C. crescentus* stalks (Figs. 3.1, 3.8). In addition to sharing approximate widths (~12-300 nm inner membrane diameter for the skinny connections; ~20-40 nm inner membrane diameter for the stalks) and cell envelope organization, we occasionally observed electron dense structures that spanned the short axis of the cell envelope of the thin connections (Fig. 3.8). These structures were reminiscent of stalk cross-bands, multiprotein assemblies that transect the stalk at regular intervals and function as diffusion barriers to compartmentalize stalk and cell body periplasmic and membrane proteins (Figs. 3.8A,C,D, 3.9) (Schlimpert *et al*., 2012).

Figure 3.9. Electron cryotomography (ECT) of cells lacking FtsE and AmiC reveal stalk-like connections of heterogeneous widths. (A) *ftsE* mutant with skinny connections that are stalk-like, but have regions with heterogeneous widths. (B) WT *C. crescentus* stalks with cross-bands. # = cross-band. Scale bar (A) = 100 nm; Scale bars (B) = 200 nm.

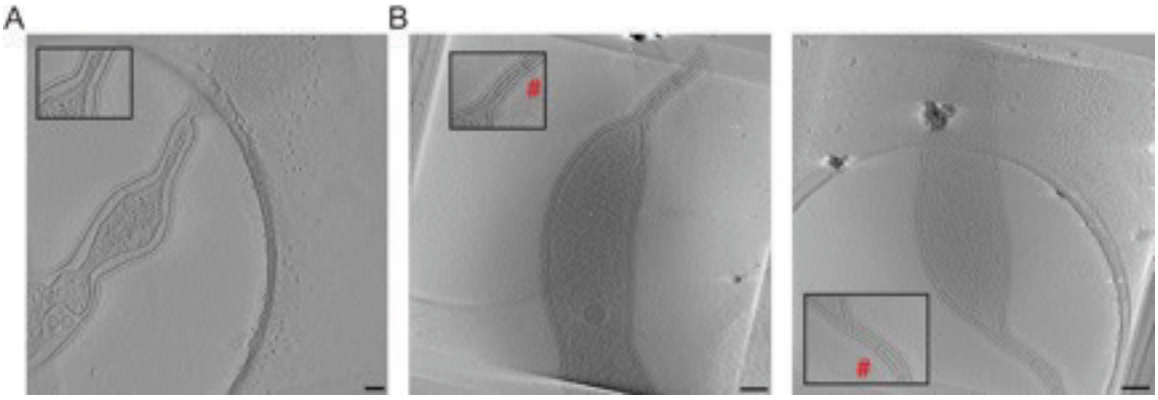

Since stalk growth occurs by incorporation of new material at the cell body-stalk junction (Wagner *et al*., 2007), we monitored HADA incorporation at the extended constrictions of *ftsE* mutants. In general, we observed incorporation of new cell wall material throughout the skinny connections (Fig. 3.10), which contrasts with the pattern of *de novo* PG synthesis only at the base of stalks. There are two modes of zonal PG synthesis in *C. crescentus*: FtsZ-independent PG incorporation at the base of the stalk and FtsZ-dependent PG incorporation at midcell (Aaron *et al*., 2007). Interestingly, in Δ*ftsE* cells, FtsZ is not enriched at the skinny connections suggesting that the new cell wall synthesis occurring throughout the skinny connections is an FtsZ-independent process similar to PG synthesis at the base of the stalk (Fig. 3.10).

Motivated by the morphological similarities between the extended constrictions in Δ*ftsE* cells and *C. crescentus* stalks, we asked if any stalk-specific proteins could localize to the skinny connections. StpX is a bitopic membrane protein enriched in the stalk that regulates stalk length (Hughes *et al*., 2010). We expressed *stpX-cfp* in WT, Δ*ftsE*, and Δ*ftsE* cells lacking AmiC: StpX-CFP localized to the stalks in all genetic backgrounds, but strikingly, was also enriched at the skinny constrictions in the *ftsE* mutant cells (Fig. 3.11A). The bifunctional penicillin binding protein, PbpC, is involved in stalk elongation (Kuhn *et al*., 2010) and is required to sequester StpX at the stalk in WT *C. crescentus* (Poindexter and Hagenzieker, 1982). To investigate the localization dependency of StpX to the skinny constrictions, we expressed *stpX-cfp* in a Δ*ftsE*Δ*pbpC* mutant background. Consistent with previous reports, StpX-CFP was not enriched in stalks in cells lacking both FtsE and PbpC. However, StpX-CFP was also not enriched at the skinny

connections between cells and instead was diffusely localized at the cell periphery (Fig. 3.11B). We also expressed *pbpC-yfp* in WT and Δ*ftsE* cells and observed enrichment at the base of stalks as well as frequent localization to the skinny connections in the *ftsE* mutant (Fig. 3.11C). Since we observe enrichment of both PbpC and StpX at the skinny connections in Δ*ftsE* cells, we hypothesize that PbpC initially recruits StpX to the skinny connections and promotes its retention at those sites.

Considering the presence of both PbpC and StpX at the skinny connections in the *ftsE* mutant, we monitored the localization of the stalk cross-band protein, StpB. StpB-mCherry localized as puncta in the stalks of WT, Δ*ftsE*, and Δ*ftsE* cells lacking AmiC, but was not enriched at the extended constriction sites (Fig. 3.11D). Consequently, the proteinaceous, envelope-spanning discs observed in the *ftsE* mutant by ECT (Fig. 3.8) may not, in fact, be cross-bands or may differ in molecular composition from stalk cross-bands. We conclude that the skinny connections share numerous morphological and molecular similarities with stalks, but the two structures are not physically or biochemically identical.

Figure 3.10. *ftsE* mutants incorporate new cell wall material throughout skinny connections between cell bodies. HADA labeling of (A) WT, (B) Δ*ftsE*, and (C) Δ*ftsE* cells depleted for AmiC for 6 h. (D) FtsZ-CFP localization after 1 h of induction in Δ*ftsE* cells. * = HADA incorporation throughout skinny connections in Δ*ftsE*; # = absence of FtsZ at skinny connections in Δ*ftsE*. Scale bars = 2 μm.

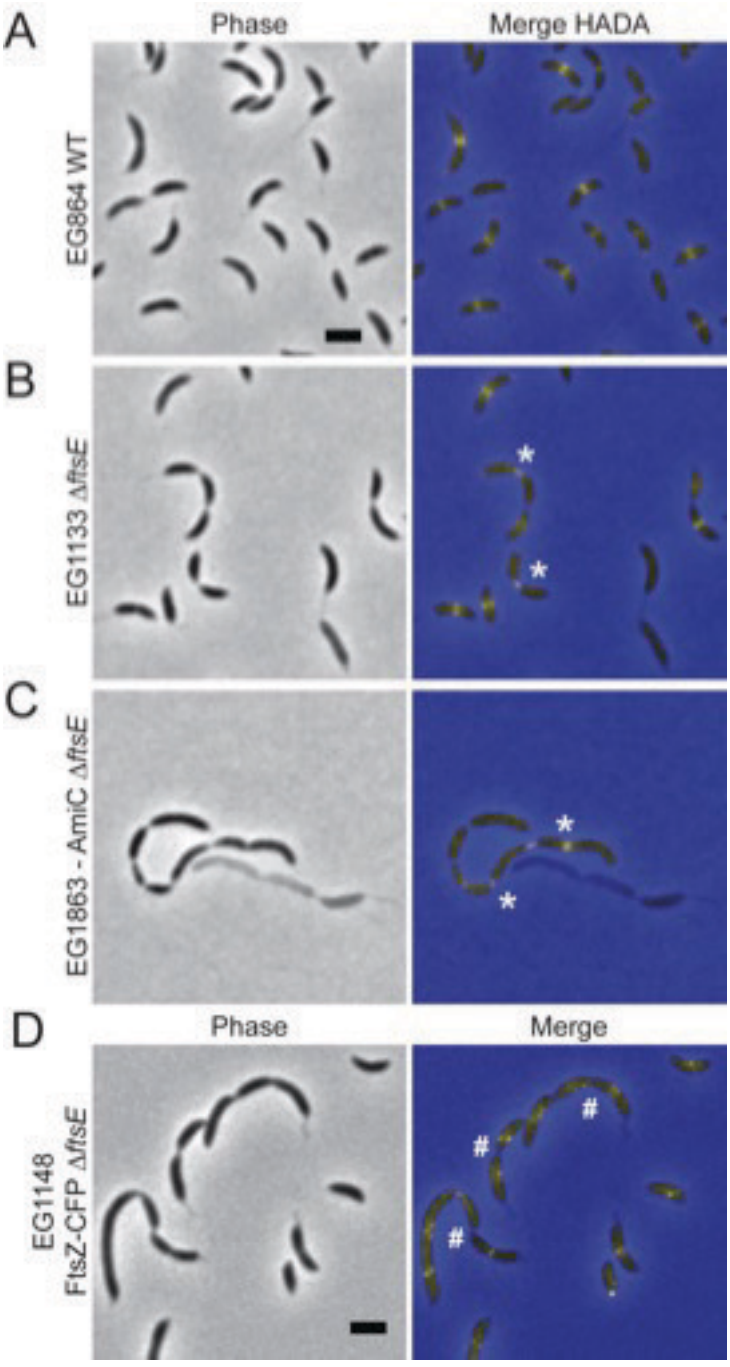

Figure 3.11. Stalk specific proteins StpX and PbpC localize to the skinny constrictions in *ftsE* mutants. (A) Localization of StpX-CFP induced for 18 h in WT, Δ*ftsE* or Δ*ftsE* cells depleted for AmiC for 18 h. (B) Localization of StpX-CFP induced for 2.75 h in Δ*ftsE*Δ*pbpC*. (C) Localization of Venus-PbpC induced for 2 h in WT or Δ*ftsE*. (D) Localization of cross-band protein StpB-mCherry induced for 18 h in WT, Δ*ftsE* or Δ*ftsE* cells depleted for AmiC for 18 h. # = stalk enrichment; * = skinny connection enrichment. Scale bars = 2 μm.

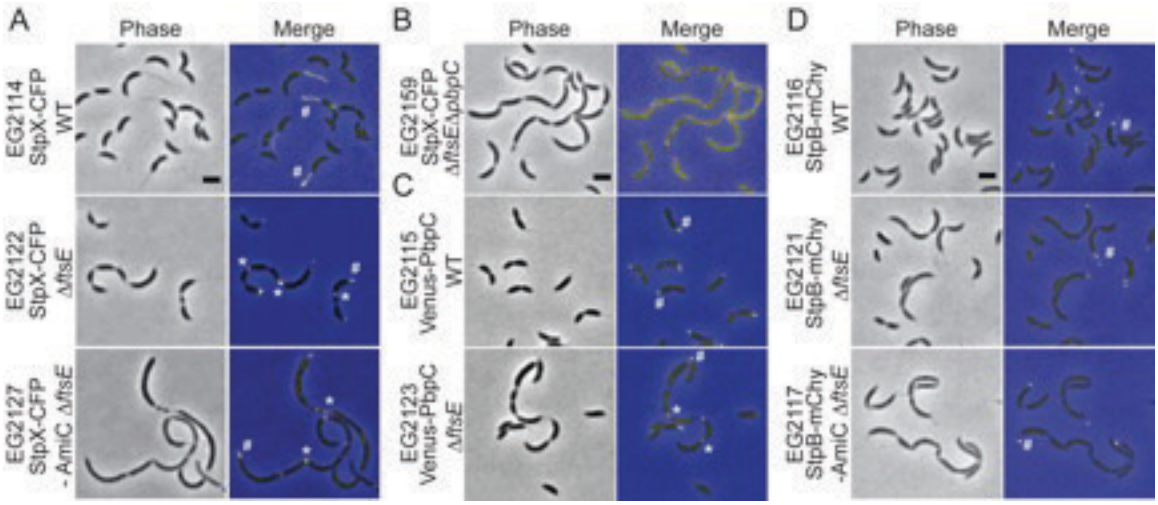

Discussion

The role of FtsEX in synchronizing PG remodeling with cell division appears to be conserved amongst distantly related bacterial species such as *E. coli*, *S. pneumoniae*, and *M. tuberculosis*, although the downstream adaptor or enzyme targets vary (Sham *et al*., 2011; Yang *et al*., 2011; Meisner *et al*., 2013; Sham *et al*., 2013; Mavrici *et al*., 2014). We provide evidence that this paradigm also extends to the α-proteobacterium *C. crescentus*. Our data indicate that FtsE is important for initial Z-ring assembly and regulates Z-ring structure in a manner dependent on its stoichiometry with FtsX (Figs. 3.2, 3.3, 3.12A). Different levels of FtsE or FtsEX not only affect FtsZ localization, but also FtsZ function, namely its ability to localize incorporation of new cell wall material (Fig. 3.3). Additionally, our data implicate FtsEX in a cell wall metabolic pathway involving LdpF and an unidentified downstream cell wall factor regulated by LdpF (Fig. 3.5, 3.12B). Thus *C. crescentus* FtsEX, similar to what has been proposed in *E. coli*, may synchronize PG remodeling with Z-ring constriction during division (Yang *et al*., 2011). ECT of the skinny connections in Δ*ftsE* revealed a cell envelope architecture remarkably distinct from *E. coli* hydrolase mutants, however, and an overall morphology that was strikingly stalk-like (Fig. 3.8). Enrichment for stalk proteins StpX and PbpC at the skinny constrictions in Δ*ftsE* and a strong genetic interaction between *ftsE* and the stalked cell fate determinant *spmX* further support mechanistic overlap between the elaboration of thin connections in *ftsE* mutants and stalk development (Figs. 3.6, 3.11, 3.12A).

Figure 3.12. FtsEX-mediated regulation of constriction initiation and final cell separation reveals morphogenetic plasticity in *C. crescentus*. (A) Cell cycle localization of FtsZ and stalk proteins in WT and Δ*ftsE* cells. (B) Three putative cell separation pathways in *C. crescentus*.

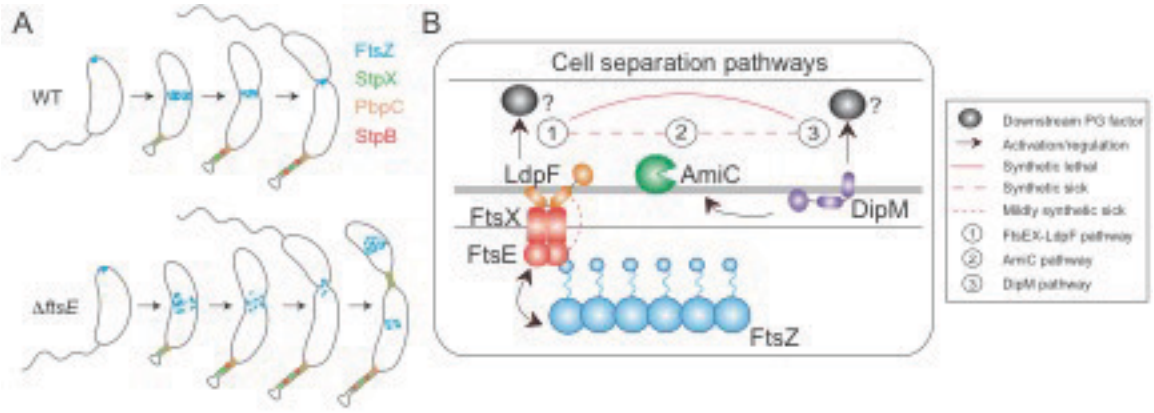

During the late stages of division in *C. crescentus*, constriction of the inner membrane proceeds until the inner membranes of the two future daughter cell compartments are connected only by a small tubular structure (Judd *et al*., 2005). Out of thousands of cells Judd and colleagues examined in their study, only five displayed inner membranes with diameters less than ~100 nm and the smallest inner membrane connection was 60 nm in diameter (Judd *et al*., 2005). ECT of cells lacking FtsE and AmiC with fairly uniform connections showed inner membrane diameters ranging from ~12 to 60 nm (Fig 3.8). Thus, the majority of cells lacking FtsE and AmiC have inner membrane diameters that fall well below the lowest threshold reported for inner membrane diameters at any stage of WT cell division. Furthermore, WT cells spend a short amount of time in these late, transitional stages, perhaps only a few seconds, and membrane topology changes very rapidly (Judd *et al*., 2005). In the case of *ftsE* mutant cells, the thin connections are abundant in a mixed cell population and, based on their nearly abutting inner membranes, are likely blocked or delayed at a terminal stage just prior to inner membrane fission. In WT *C. crescentus*, the mechanisms underlying rapid terminal constriction and membrane fusion are unknown (Judd *et al*., 2005). Our data indicate that FtsEX is important for inner membrane fusion, either directly or indirectly, and that in the absence of FtsE, inner membrane fusion frequently fails, PG synthesis continues, and cells elaborate a stalk-like structure.

Understanding how proteins are targeted specifically to the stalk is important for understanding mechanisms of subcellular organization in bacteria as well as stalk function (Hughes *et al*., 2013). We have limited knowledge about the molecular

pathways responsible for targeting proteins to the stalk; however, stalked pole geometry, membrane curvature, or unique peptidoglycan motifs are possible mechanisms for protein localization at the stalk. The observation that both StpX and PbpC localize to the skinny connections in Δ*ftsE* cells provides an experimental handle for understanding stalk biogenesis and stalk protein localization cues. In WT *C. crescentus*, the bactofilins, BacA and BacB, localize at the stalked pole and recruit PbpC during the swarmer-to-stalked cell transition (Kuhn *et al*., 2010). We have not monitored the localization of the bactofilins in Δ*ftsE* cells, but we predict that they would localize at the skinny connections upstream of PbpC, similar to the protein recruitment hierarchy observed for stalks. It has been proposed that the membrane curvature at the stalk-cell body junction drives BacAB clusters to localize there (Kuhn *et al*., 2010). These BacAB clusters could likewise recruit PbpC and StpX to the junctions between the cell bodies and skinny connections in Δ*ftsE* on the basis of shared membrane curvature with the cell body-stalk junction. Additionally, the composition of the peptidoglycan is purportedly distinct between the cell body and the stalk (Poindexter and Hagenzieker, 1982), as stalks are more resistant to lysozyme treatment (Schmidt and Stanier, 1966). PbpC may regulate the rigidity of the stalk by dictating a specific cell wall remodeling regime, which may also be active at the skinny connections (Kuhn *et al*., 2009). The periplasmic N-terminal domain of StpX is required for its stalk localization and may recognize PbpC-specific changes in PG chemistry, leading to sequestration of StpX in the stalk and the skinny constrictions of Δ*ftsE* cells (Hughes *et al*., 2010).

Within α-proteobacteria, asymmetric patterns of growth are particularly well-represented in the orders *Rhizobiales* and *Caulobacterales* (Cserti *et al*., 2016). Unlike *C. crescentus*, which divides by asymmetric binary fission, *Rhodomicrobium vannielii* and *Hyphomonas neptunium*, members of *Rhizobiales* and *Caulobacterales* respectively, use a budding mechanism whereby new offspring emerges from the tip of a stalk structure (Whittenbury and Dow, 1977; Cserti *et al*., 2016). Cell division thus occurs in an extremely asymmetric manner at the bud neck, producing a stalked mother cell and a non-stalked daughter cell (Cserti *et al*., 2016). After initially increasing in cell size by dispersed PG incorporation, *H. neptunium* displays a period of zonal growth at the new cell pole leading to the elaboration of a stalk structure (Cserti *et al*., 2016). This type of stalk outgrowth is similar to what occurs in other stalked α-proteobacteria like *C. crescentus*, which suggests conservation of core machinery. The asymmetric manner in which *H. neptunium* divides exemplifies how stalks may function not only as specialized organelles, but also as division planes, depending on the bacterial species (Cserti *et al*., 2016). The morphology of Δ*ftsE* cells, with thin, stalk-like extensions between cell bodies is reminiscent of a predivisional *H. neptunium* cell where the stalk is closely integrated within the cell division program.

While specialized protein machineries exist for cell division and cell elongation, there is no single protein, much less entire machinery, absolutely and specifically required for stalk formation. Since the elongation machinery proteins MreB and RodA contribute to stalk growth and morphogenesis, stalk synthesis has been proposed to be a specialized form of cell elongation (Wagner *et al*., 2005). Thus, it is possible that the skinny, stalk-

like connections between cell bodies in Δ*ftsE* are a result of a modified form of cell elongation, similar to what has been postulated for stalks (Wagner *et al*., 2005). Our data suggest that although the slender connections in Δ*ftsE* share certain morphological and molecular features with stalks, they are not, in actuality, ectopic stalks forming at failed division sites: the spatial pattern of PG incorporation is distinct from stalks, the diameters are not as homogeneous as for stalks, and StpB does not localize at the skinny connections (Figs 3.8, 3.9, 3.11). We instead favor the hypothesis that when Δ*ftsE* cells stall at a late stage in division, the division machinery disengages and the cell elongation machinery takes over and elaborates a thin, stalk-like connection. We interpret this phenomenon as an example of morphogenetic plasticity, whereby small changes to established morphogenetic machineries give rise to novel or, in the case of Δ*ftsE*, modified forms of preexisting structures. Overall, our findings have important implications for understanding late stage division regulation, stalk formation, and the coordination of morphogenetic events and machineries in *C. crescentus*. Loss of FtsE has revealed unexpected morphogenetic plasticity in *C. crescentus* and offers insight into the geneses of diverse morphologies in bacteria.

Materials and Methods

Growth conditions for bacterial strains

C. crescentus NA1000 strains were grown in peptone yeast extract (PYE) medium at 30^{o}C (Sundararajan *et al*., 2015). Additives and antibiotics were used at the following concentrations in liquid (solid) media for *C. crescentus*: xylose 0.3 (0.3)%, glucose 0.2 (0.2)%, vanillate 0.5 (0.5) mM, gentamycin 1 (5) μg ml^{-1}, kanamycin 5 (25) μg ml^{-1}, spectinomycin 25 (100) μg ml^{-1}, streptomycin (5 μg ml^{-1}). Before changes in induction conditions, cells were washed two to three times in plain media. Growth rate analyses were performed in 96-well plates with shaking at 30^{o}C using a Tecan Infinite 200 Pro plate reader.

Light microscopy and image analysis

Cells were imaged during the log phase of growth after immobilization on 1% agarose pads. Light microscopy was performed on a Nikon Eclipse Ti inverted microscope equipped with a Nikon Plan Fluor x 100 (numeric aperture 1.30) oil Ph3 objective and Photometrics CoolSNAP HQ cooled CCD (charge-coupled device) camera. Chroma filter cubes were used as follows: ET-EYFP for YFP and ET-ECFP for CFP, ET-dsRED for mCherry and ET-ECFP for HADA. Images were processed in Adobe Photoshop. Automated cell length analysis was performed using Oufti or MicrobeTracker (Sliusarenko *et al*., 2011). In MicrobeTracker, algorithm 4 was used for determining cell outlines, with the following parameter change: areaMin=150.

Whole cell TEM

Cells from EG864 and EG1133 were grown in PYE and prepared for whole cell TEM exactly as described (Sundararajan *et al*., 2015).

HADA labeling

Cells from strains EG213, EG379, EG864, EG930, EG1133, EG1252, EG1272, and EG1863 were grown in PYE. HADA (Kuru *et al*., 2012) was added to 0.41 mM and the cultures were returned to the shaker for 5 min. The cells were then washed twice with PBS and resuspended in PBS before imaging (Sundararajan *et al*., 2015).

Bacterial two-hybrid

The T18 and T25 plasmids were co-transformed into BTH101 (*F-, cya-99, araD139, galE15, galK16, rpsL1 (Str^r), hsdR2, mcrA1, mcrB1*; Euromedex) competent cells, plated onto LB agar with ampicillin (100 µg/µl) and kanamycin (50 µg/µl), and incubated overnight at 30^{o}C. Several colonies were inoculated into LB with ampicillin (100 µg/µl), kanamycin (50 µg/µl), and IPTG (0.5 mM) and incubated at 30^{o}C overnight. The next morning 2 µl of each culture was spotted onto plates containing ampicillin, kanamycin, X-gal (40 µg/ml), and IPTG (0.5 mM) and incubated for 1-2 days at 30^{o}C. Positive interactions were indicated by blue colonies. Every interaction was tested in triplicate.

Electron cryotomography (ECT)

For ECT imaging, strain EG1863 was grown in PYE with xylose. Once in log phase, EG1863 was washed twice with PYE and resuspended in PYE without xylose to deplete AmiC. EG1863 was then grown in PYE without xylose for ~6 h, transferred to an

eppendorf tube, and shipped on ice to Grant Jensen's lab at Caltech. The total amount of time the cells spent on ice was ~24 h. We imaged and monitored CFUs of EG1863 cells before shipment and after 24 h of incubation on ice and observed similar growth and morphology. Upon arrival, 1 ml of the EG1863 culture was centrifuged at 3000 rpm for 5 min and resuspended in fresh PYE to a final OD_{600} of ~8. This resuspension was mixed with fiducial markers (10 nm gold beads treated with bovine serum albumin to prevent aggregation) and 2 µl of the resuspension mixture was plunge-frozen on EM grids in a mixture of liquid ethane and propane (Tivol *et al*., 2008). Images were acquired using a 300 keV Polara transmission electron microscope (FEI) equipped with a GIF energy filter (Gatan) and a K2 Summit direct detector (Gatan). Tilt-series were collected from -50° to +50° in 1° increments at magnification of 22,500X using UCSF Tomography software (Zheng *et al*., 2007) with a defocus of -12 µm and total dosage of 180 $e^-/Å^2$. Tomograms were calculated using IMOD software (Kremer *et al*., 1996).

Protein purification

Rosetta pLysS *E. coli* cells containing overexpression plasmids for AmiC, LdpF, DipM, and truncated LytM domain protein variants, all with a His_6-SUMO tag fused to the N-terminus, were purified as described previously with minor changes (Meier *et al*., 2016). Rosetta cells containing the constructs were grown in 1 L of LB at 30°C to an OD_{600} of 0.4 and then induced with 1 mM IPTG for 4 h. Cells were collected by centrifugation at 6000 x g at 4°C for 10 minutes and resuspended in 40 ml Column Buffer A (CBA: 50 mM Tris-HCl pH 8.0, 300 mM NaCl, 10% glycerol, 20 mM imidazole) per 1 L of culture. Cells were snap-frozen in liquid nitrogen and stored at -80°C until use. Pellets

were thawed at 37°C and lysozyme was added to 1 µg/ml and $MgCl_2$ to 2.5 mM. Cell suspensions were left on ice for 45 minutes, then sonicated and centrifuged for 30 minutes at 15,000 x g at 4°C. The protein supernatant was filtered and loaded onto a HisTrap FF 1ml column (GE Life Sciences) pre-equilibrated with CBA. The protein was eluted with 30% Column Buffer B (same as CBA except with 1M imidazole). The protein fractions were combined and His_6-Ulp1 (SUMO protease) was added (1:500 Ulp1:protein molar ratio). The protease and protein fractions were dialyzed overnight at 4°C into CBA. Cleaved protein was run over the same HisTrap FF 1mL column equilibrated in CBA and the flow-through was collected. Flow-through fractions were dialyzed overnight at 4°C into Storage Buffer (50 mM HEPES-NaOH pH 7.2, 150 mM NaCl, 10% glycerol). Dialyzed protein was then concentrated (if needed), snap-frozen in liquid-nitrogen, and stored at -80°C.

RBB labeled sacculi preparation

Sacculi were prepared from strain EG865 as described in (Uehara *et al*., 2010). *C. crescentus* cells were grown in 1 L of PYE at 30°C, collected at an OD_{600} of 0.6 by centrifugation at 6,000 x g for 10 minutes, and resuspended in 10 ml of PBS. The cell suspension was added drop wise to 80 ml of boiling 4% sodium dodecyl sulfate (SDS) solution. Cells were boiled and mixed for 30 minutes and then incubated overnight at room temperature. Sacculi were then pelleted by ultra-centrifugation at ~80,000 x g for 60 minutes at 25°C. Pelleted sacculi were then washed four times with ultra-pure water and resuspended in 1 ml of PBS and 20 µl of 10 mg/ml amylase and incubated at 30°C overnight. The next day, sacculi were pelleted at ~400,000 x g for 15 minutes at room

temperature, washed three times with ultra-pure water, and resuspended in 1 ml of water. The sacculi suspension was labeled with 0.4 ml of 0.2 M remazol-brilliant blue (RBB), 0.3 ml 5 M NaOH, and 4.1 ml of water, and incubated at 30°C overnight. The labeled solution was neutralized with 0.4 ml of 5 M HCl and 0.75 ml of 10X PBS. Labeled sacculi were pelleted at 16,000 x g for 20 minutes at room temperature. The pellet was washed with water until the supernatant was clear. Blue-labelled sacculi were resuspended in 1 ml of 0.2% azide, incubated at 65°C for 3 hours, and then stored at 4°C.

Dye-release assay

The dye release assay was adapted from (Uehara *et al*., 2010). Briefly, 10 µl of RBB-labeled sacculi was incubated at 30°C for 3 hours with AmiC, LdpF variants, DipM variants, or FtsX ECL singly or in combination. All proteins were used at 4 µM. Total reaction volumes were brought to 100 µl with PBS. Lysozyme (4 µM) was used as a positive control. After 3 hours of incubation, reactions were heat inactivated at 95°C for 10 minutes and centrifuged for 20 minutes at 16,000 x g. Supernatants were collected and the absorbance was measured at OD_{595}.

References

Aaron M, Charbon G, Lam H, Schwarz H, Vollmer W, Jacobs-Wagner C. The tubulin homologue FtsZ contributes to cell elongation by guiding cell wall precursor synthesis in Caulobacter crescentus. Mol Microbiol. 2007;64(4):938-52.

Adams DW, Errington J. Bacterial cell division: assembly, maintenance and disassembly of the Z ring. Nat. Rev. Microbiol. 2009;7:642–653.

Allard JF, Cytrynbaum EN. Force generation by a dynamic Z-ring in Escherichia coli cell division. Proc Natl Acad Sci USA. 2009;106:145–150.

Arends SJ, Kustusch RJ, Weiss DS. ATP-binding site lesions in FtsE impair cell division. J Bacteriol. 2009;191(12):3772-84.

Arumugam S, Chwastek G, Fischer-Friedrich E, Ehrig C, Mönch I, Schwille P. Surface topology engineering of membranes for the mechanical investigation of the tubulin homologue FtsZ. Angew Chem Int Ed Engl. 2012;51(47):11858-62.

Beall B, Luktenhaus J. Impaired cell division and sporulation of a Bacillus subtilis strain with the ftsA gene deleted. J Bacteriol. 1992;174:2389-403.

Ben-Yehuda S, Losick R. Asymmetric cell division in B. subtilis involves a spiral-like intermediate of the cytokinetic protein FtsZ. Cell. 2002;109:257–266.

Beuria TK, Mullapudi S, Mileykovskaya E, Sadasivam M, Dowhan W, Margolin W. Adenine nucleotide-dependent regulation of assembly of bacterial tubulin-like FtsZ by a hypermorph of bacterial actin-like FtsA. J Biol Chem. 2009;284:14079–14086.

Biteen JS, Goley ED, Shapiro L, Moerner WE. Three-dimensional super-resolution imaging of the midplane protein FtsZ in live Caulobacter crescentus cells using astigmatism. Chemphyschem. 2012;13(4):1007-12.

Bowman GR et al. Caulobacter PopZ forms a polar subdomain dictating sequential changes in pole composition and function. Mol Microbiol. 2010;76:173-89.

Buske P, Levin PA. A flexible C-terminal linker is required for proper FtsZ assembly in vitro and cytokinetic ring formation in vivo. Mol Microbiol. 2013;89(2):249-63.

Buske PJ, Levin PA. The extreme C-terminus of the bacterial cytoskeletal protein FtsZ plays a fundamental role in assembly independent of modulatory proteins. J Biol Chem. 2012;287(14):10945-57.

Buss J, Coltharp C, Huang T, Pohlmeyer C, Hatem C, Xiao J. In vivo organization of the FtsZ-ring by ZapA and ZapB revealed by quantitative super-resolution microscopy. Mol Microbiol. 2013;89(6):1099-120.

Cabeen MT, Charbon G, Vollmer W, Born P, Ausmees N, Weibel DB, Jacobs-Wagner C. Bacterial cell curvature through mechanical control of cell growth. EMBO J. 2009;28:1208–1219.

Cabre EJ, Sanchez-Gorostiaga A, Carrara P, Ropero N, Casanova M, Palacios P, Stano P, Jiménez M, Rivas G, Vicente M. Bacterial division proteins FtsZ and ZipA induce vesicle shrinkage and cell membrane invagination. J Biol Chem. 2013;288(37):26625-34.

Christen B, Abeliuk E, Collier JM, Kalogeraki VS, Passarelli B, Coller JA, et al. The essential genome of a bacterium. Mol Syst Biol. 2011;7:528.

Christen B et al. The essential genome of a bacterium. Mol Syst Biol. 2011;7:528-34.

Contreras I, Shapiro L, Henry S. Membrane phospholipid composition of Caulobacter crescentus. J Bacteriol. 1978;135:1130-6.

Corbin BD, Wang Y, Beuria TK, Margolin W. Interaction between cell division proteins FtsE and FtsZ. J Bacteriol. 2007;189:3026-35.

Cserti E, Rosskopf S, Chang YW, Eisheuer S, Selter L, Shi J, et al. Dynamics of the peptidoglycan biosynthetic machinery in the stalked budding bacterium *Hyphomonas neptunium*. Mol Microbiol. 2016;103(5):875-895.

Curtis PD and Brun YV. Getting in the loop: regulation of development in Caulobacter crescentus. Microbiol Mol Biol Rev. 2010;74(1):13-41.

Dajkovic A, Pichoff S, Lutkenhaus J, Wirtz D. Cross-linking FtsZ polymers into coherent Z rings. Mol Microbiol. 2010;78:651–668.

Datta P, Dasgupta A, Bhakta S, Basu J. Interaction between FtsZ and FtsW of Mycobacterium tuberculosis. J Biol Chem. 2002;277:24983-7.

Din N, Quardokus EM, Sackett MJ, Brun YV. Dominant C-terminal deletions of FtsZ that affect its ability to localize in Caulobacter and its interaction with FtsA. Mol Microbiol. 1998;27:1051-63.

Domínguez-Escobar J, Chastanet A, Crevenna AH, Fromion V, Wedlich-Söldner R, Carballido-López R. Processive movement of MreB-associated cell wall biosynthetic complexes in bacteria. Science. 2011;333:225–228

Duman R et al. Structural and genetic analyses reveal the protein SepF as a new membrane anchor for the Z ring. Proc Natl Acad Sci USA. 2013;110:E4601-10.

Durand-Heredia J, Rivkin E, Fan G, Morales J, Janakiraman A. Identification of ZapD as a cell division factor that promotes the assembly of FtsZ in Escherichia coli. J. Bacteriol. 2012;194:3189–3198.

Durand-Heredia JM, Yu HH, De Carlo S, Lesser CF, Janakiraman A. Identification and characterization of ZapC, a stabilizer of the FtsZ ring in Escherichia coli. J. Bacteriol. 2011;193:1405–1413.

Ebersbach G, Galli E, Møller-Jensen J, Löwe J, Gerdes K. Novel coiled-coil cell division factor ZapB stimulates Z ring assembly and cell division. Mol Microbiol. 2008;68:720-735.

Egan AJF, Vollmer W. The physiology of bacterial cell division. Ann. N. Y. Acad. Sci. 2013;1277:8–28.

Erickson HP. FtsZ, a tubulin homologue in prokaryote cell division. Trends Cell Biol. 1997;7:362–367.

Erickson HP, Anderson DE, Osawa M. FtsZ in bacterial cytokinesis: cytoskeleton and force generator all in one. Microbiol. Mol. Biol. Rev. 2010;74:504–528.

Fenton AK, Gerdes K. Direct interaction of FtsZ and MreB is required for septum synthesis and cell division in Escherichia coli. EMBO J. 2013;32(13):1953-65.

Fu G, Huang T, Buss J, Coltharp C, Hensel Z, Xiao J. In vivo structure of the E. coli FtsZ-ring revealed by photoactivated localization microscopy (PALM). PLoS One. 2010;5(9):e12682.

Galli E, Gerdes K. Spatial resolution of two bacterial cell division proteins: ZapA recruits ZapB to the inner face of the Z-ring. Mol Microbiol. 2010;76:1514–1526.

Garner EC, Bernard R, Wang W, Zhuang X, Rudner DZ, Mitchison T. Coupled, circumferential motions of the cell wall synthesis machinery and MreB filaments in B. subtilis. Science. 2011;333:222–225.

Gardner KAJA, Moore DA, Erickson HP. The C-terminal Linker of Escherichia coli FtsZ functions as an intrinsically disordered peptide. Mol Microbiol. 2013;89(2):264-75.

Geissler B, Elraheb D, Margolin W. A gain-of-function mutation in ftsA bypasses the requirement for the essential cell division gene zipA in Escherichia coli. Proc Natl Acad Sci USA. 2003;100:4197-202.

Ghosh B, Sain A. Force generation in bacteria without nucleotide-dependent bending of cytoskeletal filaments. Phys Rev E Stat Nonlin Soft Matter Phys. 2011;83:051924.

Ghosh B, Sain A. Origin of contractile force during cell division of bacteria. Phys Rev Lett. 2008;101:178101.

Goley ED, Comolli LR, Fero KE, Downing KH, Shapiro L. DipM links peptidoglycan remodelling to outer membrane organization in Caulobacter. Mol Microbiol.

2010a;77:56-73.

Goley ED, Dye NA, Werner JN, Gitai Z, Shapiro L. Imaging-based identification of a critical regulator of FtsZ protofilament curvature in Caulobacter. Mol Cell. 2010b;39:975–987.

Goley ED, Yeh YC, Hong SH, Fero MJ, Abeliuk E, McAdams HH, Shapiro L. Assembly of the Caulobacter cell division machine. Mol Microbiol. 2011;80:1680-98.

Gueiros-Filho FJ, Losick R. A widely conserved bacterial cell division protein that promotes assembly of the tubulin-like protein FtsZ. Genes Dev. 2002;16:2544–2556.

Gündoğdu ME, Kawai Y, Pavlendova N, Ogasawara N, Errington J, Scheffers D-J, Hamoen LW. Large ring polymers align FtsZ polymers for normal septum formation. EMBO J. 2011;30:617–626.

Guo LW, Assadi-Porter FM, Grant JE, Wu H, Markley JL, Ruoho AE. One-step purification of bacterially expressed recombinant transducing α-subunit and isotopically labeled PDE6 γ-subunit for NMR analysis. Protein Expr Purif. 2007;51:187-97.
Gupta S, Banerjee SK, Chatterjee A, Sharma AK, Kundu M, Basu J. The essential protein SepF of Mycobacteria interacts with FtsZ and MurG to regulate cell growth and division. Microbiology. 2015;161:1627-1638.

Hale CA, de Boer PA. Direct binding of FtsZ to ZipA, an essential component of the septal ring structure that mediates cell division in E. coli. Cell. 1997;88:175–185.

Hale CA, Rhee AC, de Boer PA. ZipA-induced bundling of FtsZ polymers mediated by an interaction between C-terminal domains. J Bacteriol. 2000;182:5153–5166.

Hale CA, Shiomi D, Liu B, Bernhardt TG, Margolin W, Niki H, de Boer PAJ. Identification of Escherichia coli ZapC (YcbW) as a component of the division apparatus that binds and bundles FtsZ polymers. J. Bacteriol. 2011;193:1393–1404.

Heidrich C, Templin MF, Ursinus A, Merdanovic M, Berger J, Schwarz H, et al. Involvement of N-acetylmuramyl-L-alanine amidases in cell separation and antibiotic-induced autolysis of Escherichia coli. Mol Microbiol. 2001;41(1):167-78.

Hernández-Rocamora VM, García-Montañés C, Rivas G, Llorca O. Reconstitution of the Escherichia coli cell division ZipA-FtsZ complexes in nanodiscs as revealed by electron microscopy. J Struct Biol. 2012a;180(3):531-8.

Hernández-Rocamora VM, Reija B, García C, Natale P, Alfonso C, Minton AP, Zorrilla S, Rivas G, Vicente M. Dynamic Interaction of the Escherichia coli Cell Division ZipA and FtsZ Proteins Evidenced in Nanodiscs. J Biol Chem. 2012b;287:30097–30104.

Hsin J, Gopinathan A, Huang KC. Nucleotide-dependent conformations of FtsZ dimers and force generation observed through molecular dynamics simulations. Proc Natl Acad Sci USA. 2012;109:9432–9437.

Hughes HV, Huitema E, Pritchard S, Keiler KC, Brun YV, Viollier PH. Protein localization and dynamics within a bacterial organelle. Proc Natl Acad Sci USA. 2010;107(12):5599-604.

Hughes HV, Lisher JP, Hardy GG, Kysela DT, Arnold RJ, Giedroc DP, et al. Co-ordinate synthesis and protein localization in a bacterial organelle by the action of a penicillin binding-protein. Mol Microbiol. 2013;90(6):1162-77.

Janakiraman B, Mignolet J, Narayanan S, Viollier PH, Radhakrishnan SK. In-phase oscillation of global regulons is orchestrated by a pole-specific organizer. Proc Natl Acad Sci USA. 2016;113(44):12550-12555.

Jenal U, White J, Shapiro L. Caulobacter flagellar function, but not assembly, requires FliL, a non-polarly localized membrane protein present in all cell types. J Mol Biol. 1994;243:227-44.

Jennings PC, Cox GC, Monahan LG, Harry EJ. Super-resolution imaging of the bacterial cytokinetic protein FtsZ. Micron. 2010;42(4):336-41.

Jensen SO, Thompson LS, Harry EJ. Cell division in Bacillus subtilis: FtsZ and FtsA association is Z-ring independent, and FtsA is required for efficient midcell Z-ring assembly. J Bacteriol. 2005;187:6536-44.

Jiang C, Caccamo PD, Brun YV. Mechanisms of bacterial morphogenesis: evolutionary biology approaches provide new insights. Bioessays. 2015;37(4):413-25.

Jiménez M, Martos A, Vicente M, Rivas G. Reconstitution and organization of Escherichia coli proto-ring elements (FtsZ and FtsA) inside giant unilamellar vesicles obtained from bacterial inner membranes. J Biol Chem. 2011;286:11236–11241.

Judd EM, Comolli LR, Chen JC, Downing KH, Moerner WE, McAdams HH. Distinct constrictive processes, separated in time and space, divide Caulobacter inner and outer membranes. J Bacteriol. 2005;187:6874-82.

Kremer JR, Mastronarde DN, McIntosh JR. Computer visualization of three-dimensional image data using IMOD. J Struct Biol. 1996;116:71-6.

Kuhn J, Briegel A, Morschel E, Kahnt J, Leser K, Wick S, et al. Bactofilins, a ubiquitous class of cytoskeletal proteins mediating polar localization of a cell wall synthase in Caulobacter crescentus. EMBO J. 2010;29(2):327-39.

Kuru E et al. In situ probing of a newly synthesized peptidoglycan in live bacteria with fluorescent D-amino acids. Angew Chem Int Ed. 2012;51:12519-12523.

Lee TK, Huang KC. The role of hydrolases in bacterial cell-wall growth. Curr Opin Microbiol. 2013;16:760-6.

Li Y, Hsin J, Zhao L, Cheng Y, Shang W, Huang KC, Wang H-W, Ye S. FtsZ protofilaments use a hinge-opening mechanism for constrictive force generation. Science. 2013;341:392–395.

Li Z, Trimble MJ, Brun YV, Jensen GJ. The structure of FtsZ filaments in vivo suggests a force-generating role in cell division. EMBO J. 2007;26:4694–4708.

Loose M, Mitchison TJ. The bacterial cell division proteins FtsA and FtsZ self-organize into dynamic cytoskeletal patterns. Nat Cell Biol. 2014;16:38-46.

López-Montero I, López-Navajas P, Mingorance J, Vélez M, Vicente M, Monroy F. Membrane reconstitution of FtsZ-ZipA complex inside giant spherical vesicles made of E. coli lipids: large membrane dilation and analysis of membrane plasticity. Biochim Biophys Acta. 2013;1828:687–698.

Lu C, Reedy M, Erickson HP. Straight and curved conformations of FtsZ are regulated by GTP hydrolysis. J Bacteriol. 2000;182:164–170.

Luo T, Srivastava V, Ren Y, Robinson DN. Mimicking the mechanical properties of the cell cortex by the self-assembly of an actin cortex in vesicles. Appl Phys Lett. 2014;104(15):153701-5.

Ma X, Ehrhardt DW, Margolin W. Colocalization of cell division proteins FtsZ and FtsA to cytoskeletal structures in living Escherichia coli cells by using green fluorescent protein. Proc Natl Acad Sci USA. 1996;93:12998–13003.

Martin ME, Trimble MJ, Brun YV. Cell cycle-dependent abundance, stability and localization of FtsA and FtsQ in Caulobacter crescentus. Mol Microbiol. 2004;54:60-74.

Mateos-Gil P, Marquez I, López-Navajas P, Jiménez M, Vicente M, Mingorance J, Rivas G, Vélez M. FtsZ polymers bound to lipid bilayers through ZipA form dynamic two dimensional networks. Biochim Biophys Acta. 2011;1818(3):806-13.

Mavrici D et al. Mycobacterium tuberculosis FtsX extracellular domain activates the peptidoglycan hydrolase, RipC. Proc Natl Acad Sci USA. 2014;111:8037-42.

Meier EL, Goley ED. Form and function of the bacterial cytokinetic ring. Curr Opin Cell Biol. 2014; 26:19-27.

Meier EL, Razavi S, Inoue T, Goley ED. A novel membrane anchor for FtsZ is linked to cell wall hydrolysis in Caulobacter crescentus. Mol Microbiol. 2016;101(2):265-80.

Meisner J, Montero-Llopis P, Sham LT, Garner E, Bernhardt TG, Rudner DZ. FtsEX is required for CwlO peptidoglycan hydrolase activity during cell wall elongation in Bacillus subtilis. Mol Microbiol. 2013;89:1069-83.

Milam SL, Osawa M, Erickson HP. Negative-stain electron microscopy of inside-out

FtsZ rings reconstituted on artificial membrane tubules show ribbons of protofilaments. Biophys J. 2012;103:59–68.

Moll A, Schlimpert S, Briegel A, Jensen GJ, Thanbichler M. DipM, a new factor required for peptidoglycan remodeling during cell division in Caulobacter crescentus. Mol Microbiol. 2010;77:90-107.

Moll A, Thanbichler M. FtsN-like proteins are conserved components of the cell division machinery in proteobacteria. Mol Microbiol. 2009;72:1037-53.

Navajas PL, Rivas G, Mingorance J, Mateos-Gil P, Hörger I, Velasco E, Tarazona P, Vélez M. In vitro reconstitution of the initial stages of the bacterial cell division machinery. J Biol Phys 2008;34:237–247.

Nierman WC, Feldblyum TV, Laub MT, Paulsen IT, Nelson KE, Eisen JA, et al. Complete genome sequence of Caulobacter crescentus. Proc Natl Acad Sci USA. 2001;98(7):4136-41.

Ohta N, Ninfa AJ, Allaire A, Kulick L, Newton A. Identification, characterization, and chromosomal organization of cell division cycle genes in Caulobacter crescentus. J Bacteriol. 1997;179:2169-80.

Osawa M, Anderson DE, Erickson HP. Curved FtsZ protofilaments generate bending forces on liposome membranes. EMBO J. 2009;28:3476–3484.

Osawa M, Anderson DE, Erickson HP. Reconstitution of contractile FtsZ rings in liposomes. Science. 2008;320:792–794.

Osawa M, Erickson HP. Inside-out Z rings--constriction with and without GTP hydrolysis. Mol Microbiol. 2011;81:571–579.

Osawa M, Erickson HP. Liposome division by a simple bacterial division machinery. Proc Natl Acad Sci USA. 2013;110(27):11000-4.

Osley MA, Newton A. Mutational analysis and developmental control in Caulobacter crescentus. Proc Natl Acad Sci USA. 1977;74:124-8.

Pautot S, Frisken BJ, Weitz DA. Engineering asymmetric vesicles. Proc Natl Acad Sci USA. 2003;100:10718-21.

Peters PC, Migocki MD, Thoni C, Harry EJ. A new assembly pathway for the cytokinetic Z ring from a dynamic helical structure in vegetatively growing cells of Bacillus subtilis. Mol Microbiol. 2007;64:487–499.

Pichoff S, Lutkenhaus J. Tethering the Z ring to the membrane through a conserved membrane targeting sequence in FtsA. Mol Microbiol. 2005;55:1722–1734.

Pichoff S, Lutkenhaus J. Unique and overlapping roles for ZipA and FtsA in septal ring assembly in Escherichia coli. EMBO J. 2002;21:685-93.

Pichoff S, Du S, Lutkenhaus J. The bypass of ZipA by overexpression of FtsN requires a previously unknown conserved FtsN motif essential for FtsA-FtsN interaction supporting a model in which FtsA monomers recruit late cell division proteins to the Z ring. Mol Microbiol. 2015;95:971-87.

Pichoff S, Shen B, Sullivan B, Luktenhaus J. FtsA mutants impaired for self-interaction bypass ZipA suggesting a model in which FtsA's self-interaction competes with its ability to recruit downstream division proteins. Mol Microbiol. 2012;83:151-67.

Pincus Z, Theriot JA. Comparison of quantitative methods for cell-shape analysis. J Microscopy. 2007;227:140-156.

Pogglio S, Takacs CN, Vollmer W, Jacobs-Wagner C. A protein critical for cell constriction in the Gram-negative bacterium Caulobacter crescentus localizes at the division site through its peptidoglycan-binding LysM domains. Mol Microbiol. 2010;77(1):74-89.

Poindexter JS and Hagenzieker JG. Novel peptidoglycans in Caulobacter and Asticcacaulis spp. J Bacteriol. 1982;150(1):332-47.

Potluri L-P, Kannan S, Young KD. ZipA is required for FtsZ-dependent preseptal peptidoglycan synthesis prior to invagination during cell division. J Bacteriol. 2012;194:5334–5342.

Proctor SA, Minc N, Boudaoud A, Chang F. Contributions of turgor pressure, the contractile ring, and septum assembly to forces in cytokinesis in fission yeast. Curr Biol. 2012;22(17):1601-8.

Radhakrishnan SK, Thanbichler M, Viollier PH. The dynamic interplay between a cell fate determinant and a lysozyme homolog drives the asymmetric division cycle of Caulobacter crescentus. Genes Dev. 2008;22:212-25.

Reimold C, Defeu Soufo HJ, Dempwolff F, Graumann PL. Motion of variable-length MreB filaments at the bacterial cell membrane influences cell morphology. Mol Biol Cell. 2013;24:2340–2349.

Schlimpert S, Klein EA, Briegel A, Hughes V, Kahnt J, Bolte K, et al. General protein diffusion barriers create compartments within bacterial cells. Cell. 2012;151(6):1270-82.

Schmidt JM and Stanier RY. The development of cellular stalks in bacteria. J Cell Biol. 1966;28(3):423-36.

Schmidt KL, Peterson ND, Kustusch RJ, Wissel MC, Graham B, Phillips GJ, et al. A predicted ABC transporter, FtsEX, is needed for cell division in Escherichia coli. J Bacteriol. 2004;186(3):785-93.

Sham LT, Barendt SM, Kopecky KE, Winkler ME. Essential PcsB putative peptidoglycan hydrolase interacts with the essential FtsXSpn cell division protein in Streptococcus pneumonia D39. Proc Natl Acad Sci USA. 2011;108:E1061-9.

Sham LT, Jensen KR, Bruce KE, Winkler ME. Involvement of FtsE ATPase and FtsX extracellular loops 1 and 2 in FtsEX-PcsB complex function in cell division of Streptococcus pneumoniae D39. MBio. 2013;4(4). pii: e00431-13.

Singh P, Makde RD, Ghosh S, Asthana J, Kumar V, Panda D. Assembly of Bacillus subtilis FtsA: effects of pH, ionic strength and nucleotides on FtsA assembly. Int J Biol Macromol. 2013;52:170–176.

Singh JK, Makde RD, Kumar V, Panda D. A membrane protein, EzrA, regulates assembly dynamics of FtsZ by interacting with the C-terminal tail of FtsZ. Biochemistry. 2007;46:11013-22.

Sliusarenko O, Heinritz J, Emonet T, Jacobs-Wagner C. High-throughput, subpixel precision analysis of bacterial morphogenesis and intracellular spatio-temporal dynamics. Mol Microbiol. 2011;80:612-27.

Strauss MP, Liew ATF, Turnbull L, Whitchurch CB, Monahan LG, Harry EJ. 3D-SIM super resolution microscopy reveals a bead-like arrangement for FtsZ and the division machinery: implications for triggering cytokinesis. PLoS Biol. 2012;10(9):e1001389.

Stricker J, Maddox P, Salmon ED, Erickson HP. Rapid assembly dynamics of the Escherichia coli FtsZ-ring demonstrated by fluorescence recovery after photobleaching. Proc Natl Acad Sci USA. 2002;99:3171–3175.

Sun Q, Margolin W. FtsZ dynamics during the division cycle of live Escherichia coli cells. J Bacteriol. 1998;180:2050–2056.

Sundararajan K, Miguel A, Desmarais SM, Meier EL, Casey Huang K, Goley ED. The bacterial tubulin FtZ requires its intrinsically disordered linker to direct robust cell wall construction. Nat Commun. 2015;6:7281.

Sundararajan K, Goley ED. Cytoskeletal proteins in Caulobacter crescentus: Spatial orchestrators of cell cycle progression, development, and cell shape. Subcell Biochem. 2017;84:103-137.

Szwedziak P, Wang Q, Freund SM, Löwe J. FtsA forms actin-like protofilaments. EMBO J. 2012;31(10):2249-60.

Thanbichler M, Shapiro L. MipZ, a spatial regulator coordinating chromosome

segregation with cell division in Caulobacter. Cell. 2006;126:147–162.

Thanedar S, Margolin W. FtsZ exhibits rapid movement and oscillation waves in helix-like patterns in Escherichia coli. Curr Biol. 2004;14:1167–1173.

Tivol WF, Briegel A, Jensen GJ. An improved cryogen for plunge freezing. Microsc Microanal. 2008;14:375-9.

Typas A, Banzhaf M, Gross CA, Vollmer W. From the regulation of peptidoglycan synthesis to bacterial growth and morphology. Nat Rev Microbiol. 2011;10(2):123-36.

Uehara T, Dinh T, Bernhardt TG. LytM-domain factors are required for daughter cell separation and rapid ampicillin-induced lysis in Escherichia coli. J Bacteriol. 2009;191(16):5094-107.

Uehara T, Parzych KR, Dinh T, Bernhardt TG. Daughter cell separation is controlled by cytokinetic ring-activated cell wall hydrolysis. EMBO J. 2010;29:1412-22.

van Teeffelen S, Wang S, Furchtgott L, Huang KC, Wingreen NS, Shaevitz JW, Gitai Z. The bacterial actin MreB rotates, and rotation depends on cell-wall assembly. Proc Natl Acad Sci USA. 2011;108:15822–15827.

Vaughan S, Wickstead B, Gull K, Addinall SG. Molecular evolution of FtsZ protein sequences encoded within the genomes of archaea, bacteria, and eukaryote. J Mol Evol. 2004;58:19-29.

Wagner JK and Brun YV. Out on a limb: how the Caulobacter stalk can boost the study of bacterial cell shape. Mol Microbiol. 2007;64(1):28-33.

Wagner JK, Galvani CD, Brun YV. Caulobacter crescentus requires RodA and MreB for stalk synthesis and prevention of ectopic pole formation. J Bacteriol. 2005;187(2):544-53.

Woldemeskel SA and Goley ED. Shapeshifting to survive: shape determination and regulation in Caulobacter crescentus. Trends Microbiol. 2017; pii: S0966-842X(17)30058-6.

Whittenbury R and Dow CS. Morphogenesis and differentiation in Rhodomicrobium vannielii and other budding and prosthecate bacteria. Bacteriol Rev. 1977;41(3):754-808.

Yakhnina AA, Gitai Z. Diverse functions for six glycosyltransferases in Caulobacter crescentus cell wall assembly. J Bacteriol. 2013;195:4527-35.

Yang DC, Peters NT, Parzych KR, Uehara T, Markovski M, Bernhardt TG. An ATP-binding cassette transporter-like complex governs cell-wall hydrolysis at the bacterial cytokinetic ring. Proc Natl Acad Sci USA. 2011;108:E1052-60.

Zheng SQ, Keszthelyi B, Branlund E, Lyle JM, Braunfeld MB, Sedat JW, et al. UCSF tomography: an integrated software suite for real-time electron microscopic tomographic data collection, alignment, and reconstruction. J Struct Biol. 2007;157:138-47.

Zhou R, Chen S, Recsei P. A dye release assay for determination of lysostaphin activity. Anal Biochem. 1988;171(1):141-4.

Elizabeth L. Meier June 2017

Educational History:

Ph.D. expected	July 2017	Program in Biochemistry, Cellular, and Molecular Biology Mentor: Erin Goley, Ph.D.	JHSOM
B.A.	May 2011	Biology	Scripps College

Other Professional Experience

Health Security Policy Fellow	Fall 2016	Health Security Partners
Post-Graduate Summer Intern	Summer 2011	Lab of Mary Dasso, National Institutes of Health
Amgen Scholar	Summer 2010	Lab of Hannele Ruohola-Baker, Univ. of Washington

Research Travel Awards

Graduate Student Association	Dec 2013	$200	Zing Bacterial Cell Biology Conference
Graduate Student Association	June 2016	$500	ASM Microbe/ICACC Conference
American Society for Microbiology (ASM)	June 2016	$500	ASM Microbe/ICACC Conference

Academic Honors

May 2011	Graduated Summa Cum Laude with honors	Scripps College
May 2011	Inducted in the Phi Beta Kappa Honor Society	Scripps College

Peer-Reviewed Publications

Meier EL *et al*. (anticipated 2017**).** FtsEX mediated regulation of the late stages of cell division reveals morphogenetic plasticity in *Caulobacter crescentus*. (manuscript in review PLoS Genet.).

Meier EL, Razavi S, Inoue T, Goley ED. (2016) A novel membrane anchor for FtsZ is linked to cell wall hydrolysis in *Caulobacter crescentus*. Mol Microbiol. 101(2):265-80.

Sundararajan K, Miguel A, Desmarais SM, **Meier EL**, Casey Huang K, Goley ED. (2015) The bacterial tubulin FtsZ requires its intrinsically disordered linker to direct robust cell wall construction. Nat Commun. 6:7281.

Papazyan R, Voronina E, Chapman JR, Luperchio TR, Gilbert TM, **Meier E**, Mackintosh SG, Shabanowitz J, Tackett AJ, Reddy KL, Coyne RS, Hunt DF, Liu Y, Taverna SD. (2014) Methylation of histone H3K23 blocks DNA damage in pericentric heterochromatin during meiosis. Elife. 3:e02996.

Meier EL and Goley ED. (2014) Form and function of the bacterial cytokinetic ring. Curr Opin Cell Biol. 26:19-27.

Abstracts

Meier EL, Goley ED. (2016) Unique roles for FtsEX in Caulobacter crescentus: Z-ring architecture and chromosome segregation. ASM Microbe/ICACC Conference, Boston, MA, June 2016.

Meier EL, Goley ED (2015) The different modes of membrane attachment of FtsZ in Caulobacter. ASM Conference on Prokaryotic Cell Biology and Development, Washington, DC, June 2015.

Meier EL, Goley ED (2013) Investigating membrane attachment and regulation of FtsZ. Zing Bacterial Cell Biology Conference, Playa del Carmen, Mexico, December 2013.

Service and Leadership

Spring, Fall 2015	Student Director, JHSOM Directed a graduate-level course on effective science communication
Fall 2014-Spring 2015	Volunteer Contributor, ASBMB Today Wrote summaries of press releases and journal articles
Fall 2014	Teaching Assistant, JHSOM Taught a cell physiology course to medical students
Summer 2013-2016	Junior Student Mentor, JHSOM Mentored three undergraduate and two high school students